

EVALUATION OF MITOCHONDRIAL MEMBRANE
POTENTIAL ($\Delta\Psi_m$) IN ISOLATED MITOCHONDRIA,
CARDIOMYOCYTES, AND HEPATOCYTES USING NEAR-
INFRARED REGION DYE MITOFLUOR FAR RED 680

BY

HEE-JEONG KONG

A Thesis/Practicum submitted to the Faculty of Graduate Studies of The University
of

Manitoba in partial fulfillment of the requirement of the degree

OF

MASTER OF SCIENCE

Department of Biochemistry & Medical Genetics
University of Manitoba
Winnipeg

HEE-JEONG KONG © 2006

EVALUATION OF MITOCHONDRIAL MEMBRANE
POTENTIAL ($\Delta\Psi_m$) IN ISOLATED MITOCHONDRIA,
CARDIOMYOCYTES, AND HEPATOCYTES USING NEAR-
INFRARED REGION DYE MITOFLUOR FAR RED 680

by

HEE-JEONG KONG

A thesis submitted to the Faculty of Graduate Studies of
The University of Manitoba
in partial fulfilment of the requirements of the degree of

MASTER OF SCIENCE

Department of Biochemistry & Medical Genetics
University of Manitoba
Winnipeg

Copyright © 2006 by Hee-Jeong Kong

THE UNIVERSITY OF MANITOBA

FACULTY OF GRADUATE STUDIES

COPYRIGHT PERMISSION

**Evaluation of Mitochondrial Membrane Potential ($\Delta\Psi_m$) in Isolated Mitochondria,
Cardiomyocytes, and Hepatocytes Using Near-Infrared Region Dye Mitofluor Far Red 680**

BY

Hee-Jeong Kong

**A Thesis/Practicum submitted to the Faculty of Graduate Studies of The University of
Manitoba in partial fulfillment of the requirement of the degree**

OF

MASTER OF SCIENCE

Hee-Jeong Kong © 2006

Permission has been granted to the Library of the University of Manitoba to lend or sell copies of this thesis/practicum, to the National Library of Canada to microfilm this thesis and to lend or sell copies of the film, and to University Microfilms Inc. to publish an abstract of this thesis/practicum.

This reproduction or copy of this thesis has been made available by authority of the copyright owner solely for the purpose of private study and research, and may only be reproduced and copied as permitted by copyright laws or with express written authorization from the copyright owner.

TABLE OF CONTENTS

TABLE OF CONTENTS	i
ACKNOWLEDGEMENTS	iv
LIST OF FIGURES	vi
LIST OF TABLES	ix
LIST OF ABBREVIATIONS	x
ABSTRACT	xiii
CHAPTER 1. LITERATURE REVIEW	1
1.1 Introduction.....	1
1.2 Cardiac Energetics and Contractility.....	2
1.3 Mitochondria in Energy Production and Parameters Defining Energetic Status.....	5
1.3.1 Introduction.....	5
1.3.2 Mitochondrial Morphology.....	5
1.3.3 Energy Substrates.....	9
1.3.4 Tricarboxylic Acid Cycle (TCA Cycle).....	11
1.3.5 Electron Transport Chain (ETC).....	13
1.3.6 Oxidative Phosphorylation.....	17
1.3.7 Chemiosmotic Gradient.....	19
1.3.8 Inhibitors and Uncouplers of Oxidative Phosphorylation.....	19
1.4 Effects of Pathology on Mitochondria and Energy Metabolism.....	20
1.4.1 Ischemia/ Reperfusion Injury.....	21

1.4.2 Apoptosis.....	22
1.4.3 Mitochondrial Genetic Disorders.....	23
1.5 Methods for Measurements of $\Delta\Psi_m$ in Isolated Mitochondria, Cells and Intact Heart.....	24
1.5.1 Optical Methods.....	25
1.5.1.1 Spectrophotometry.....	25
1.5.1.2 Fluorescence measurements.....	25
1.5.1.3 Optical indicators of mitochondrial membrane potential	27
1.6 Mitofluor Far Red 680 (MFFR).....	33
CHAPTER 2. MATERIALS & METHODS.....	37
2.1 Materials.....	37
2.1.1 Animal Handling.....	38
2.2 Methods.....	38
2.2.1 Mitochondria Isolation.....	38
2.2.2 Protein Assay.....	39
2.2.3 Measurements of Mitochondrial Respiration.....	41
2.2.4 Isolation of Cardiomyocytes.....	42
2.2.4.1 Solutions.....	42
2.2.4.2 Isolation procedure.....	44
2.2.5 Isolation of Hepatocytes.....	45
2.2.6 Measurements of MFFR Binding in Isolated Rat Liver Mitochondria, Cardiomyocytes, and Hepatocytes.....	47
2.2.7 Measurements of MFFR Fluorescence in Isolated Rat Liver Mitochondria, Cardiomyocytes, and Hepatocytes.....	52
2.2.8 Measurement of MFFR Fluorescence at Various pH levels.....	54
2.2.9 Statistics.....	54

CHAPTER 3. RESULTS	55
3.1 Studies of MFFR Binding in Isolated Rat Liver Mitochondria, Cardiomyocytes, and Hepatocytes.....	55
3.1.1 Relationship between $\Delta\Psi_m$ and MFFR Binding.....	55
3.1.2 The MFFR Distribution in Cardiomyocytes and Hepatocytes.....	65
3.2 Influence of MFFR and P-1075 on Mitochondrial Respiration Rate.....	68
3.3 Measurements of MFFR Fluorescence in Isolated Rat Liver Mitochondria, Cardiomyocytes, and Hepatocytes.....	74
3.3.1 Dependence of MFFR Fluorescence on Its Concentration and pH.....	74
3.3.2 Changes in MFFR Fluorescence Spectra in Mitochondrial Suspensions.....	76
3.3.3 Changes in MFFR Fluorescence Spectra in Cardiomyocyte Suspensions.....	83
3.3.4 Changes in MFFR Fluorescence Spectra in Hepatocyte Suspensions.....	94
CHAPTER 4. DISCUSSION	103
4.1 Summary of Major Findings.....	103
4.2 MFFR Binding and $\Delta\Psi_m$	105
4.3 Relationships between Dye Binding and Fluorescence.....	106
4.4 Effects of Mitochondrial and Cell Concentrations on Dye Fluorescence.....	107
4.5 Conclusions.....	107
REFERENCES	109

ACKNOWLEDGEMENTS

First of all, I would like to thank my supervisor for giving me the opportunity to start on a master's degree, in which I had little background. Every piece of knowledge, support and advice given helped me to improve my research skills and accumulate knowledge and skills which I consider very valuable. Thank you Dr. Kupriyanov for putting up with me for the duration of my thesis work.

I would also like to thank my committee members Dr. Wrogemann and Dr. Jackson for giving me advice, guidance and criticism.

I would like to thank the people at the Institute for Biodiagnostics, National Research Council of Canada for providing a friendly environment. You made me feel like I was at home rather than in a work place. Special acknowledgements to the members of the Biosystem group, especially Dr. Olga Jilkina, Bozena Kuzio, Bo Xiang, and Dr. Darren Manley for their assistance with the experimental work. I want to thank the group leader Dr. Michael Jackson for his excellent leadership. Your excellent interpersonal skills made conversations flow with ease. On top of that your generosity and caring nature made you very approachable.

I would like to mention a great person, Dr Gilbert Arthur, for his tremendous generosity and support. It is difficult to find a person who is truly good in the heart. I am lucky I have had the chance to get to know him and wish him all the best. Thank you for proofreading my first draft as I know this required a lot of time, effort and patience.

Nona and Tony, my family away from home, I want to thank the both of you for your continuous support and taking me as family with your arms wide open. You both

believe in me so much, perhaps my strength is an extension of your belief in me. I love you both very much ti voglio bene.

I would like to thank my family and friends for their support and encouragement during the duration of my masters project. Especially, I want to thank my future husband Jeffrey Cheung for helping me with all his heart. He has always been there when I needed him the most. When I felt homesick, he filled my emptiness with his care and love. He helped me overcome the difficulties of writing my thesis. I could not have done this without him.

Special thanks to my mom, dad, sister, and aunt for believing in higher education and supporting me through challenging times in my transition from Korea to Canada.

LIST OF FIGURES

Figure 1-1.	Mitochondria in cardiac tissue.....	6
Figure 1-2.	The structure of mitochondrion.....	7
Figure 1-3.	The glycolysis and glycogenolysis pathways.....	10
Figure 1-4.	The TCA cycle.....	12
Figure 1-5.	The Electron Transport Chain (ETC).....	14
Figure 1-6.	Reduction potential of carriers in the ETC	15
Figure 1-7.	ATP synthase.....	18
Figure 1-8.	The ATP/ADP translocator.....	18
Figure 1-9.	Structure of MitoFluor Far Red 680 (MFFR).....	35
Figure 1-10.	Absorbance (A) and fluorescence(B) spectra of MFFR.....	36
Figure 2-1.	The BCA assay	40
Figure 2-2.	Spectrophotometric arrangement for detecting MFFR fluorescence.....	51
Figure 3-1.	Ratio of MFFR bound to free in rat liver mitochondria.....	59
Figure 3-2.	Decrease in $\Delta\Psi_m$ in rat liver mitochondrial suspension in high K^+ medium (A) and sucrose medium (B).....	60
Figure 3-3.	Effect of substrates on $\Delta\Psi_m$ in rat liver mitochondria vs. $\Delta\Psi_m$ in the FCCP uncoupled state.....	62
Figure 3-4.	Correlation between $\Delta\Psi_m$ values measured with MFFR and TMRM Binding.....	64
Figure 3-5.	Ratio of bound to free MFFR in isolated cells.....	67
Figure 3-6.	The effects of MFFR on respiration rates.....	70
Figure 3-7.	The effects of MFFR on normalized respiration rate.....	71

Figure 3-8.	The effects of P-1075 on respiration rate.....	72, 73
Figure 3-9.	The effects of pH on the fluorescence of MFFR.....	75
Figure 3-10.	MFFR fluorescence spectra in mitochondrial suspension.....	77
Figure 3-11.	Changes in MFFR fluorescence intensity in mitochondrial suspension treated with FCCP as a function of time.....	78
Figure 3-12.	Time course of normalized MFFR fluorescence at various mitochondrial concentrations.....	80
Figure 3-13.	$\Delta F/F_0$ for energized and uncoupled mitochondria as a function of protein concentration.....	82
Figure 3-14.	MFFR fluorescence spectra in cardiomyocyte suspension.....	84
Figure 3-15.	Time course of MFFR fluorescence in cardiomyocyte suspension before and after FCCP treatment.....	86
Figure 3-16.	Changes in the fluorescence ratio $\Delta F/F_0$ for energized and uncoupled cellular mitochondria in cardiomyocytes as a function of protein concentration.....	88
Figure 3-17.	The response of energized cellular mitochondria to FCCP in cardiomyocytes as a function of protein concentration.....	89
Figure 3-18.	Relationship between changes in the fluorescence ratios $\Delta F_E/F_0$ and $\Delta F_U/F_0$ and amount of MFFR bound.....	91
Figure 3-19.	The effects of the plasma membrane potential on the fluorescence of MFFR.....	93
Figure 3-20.	MFFR fluorescence spectra of hepatocyte suspension.....	95

Figure 3-21.	Time course of MFFR fluorescence in hepatocyte suspension.....	97
Figure 3-22.	$\Delta F/F_0$ for energized and uncoupled hepatocytes as a function of protein concentration.....	99
Figure 3-23.	The relationship between the amounts of MFFR bound to energized and uncoupled hepatocytes and protein concentration.....	100
Figure 3-24.	The relationship between the amounts of MFFR bound to energized and uncoupled hepatocytes and fluorescence changes.....	102

LIST OF TABLES

Table 1-1.	Absorption and emission maxima of natural chromophores in the visible range.....	30
Table 1-2.	Excitation and emission maxima of fluorescent dyes.....	33
Table 2-1.	Composition of buffers for cardiomyocyte isolation.....	43
Table 3-1.	MFFR bound and free in rat liver mitochondrial suspensions in two isolation media	56
Table 3-2.	Bound and free MFFR in cardiomyocytes and hepatocytes.....	65
Table 3-3.	The ratio of bound: free MFFR in cardiomyocytes and hepatocytes corrected for viability.....	65

LIST OF ABBREVIATIONS

Acetyl CoA : acetyl coenzyme A

ADP : adenosine diphosphate

AIF : apoptosis inducing factor

α -KG : α -Ketoglutarate

ATP : adenosine triphosphate

a.u. : arbitrary units

BCA : bicinchoninic acid

BDM : butadione monooxime

BSA : bovine serum albumin

[C] : concentration of a compound

c : speed of light

$[C]_{\text{cytosol}}$: equilibrium cytosol dye concentration

$[C]_i$: concentration of cationic dye inside mitochondria

$[C]_o$: concentration of cationic dye outside mitochondria

CK : creatine kinase

Cyt c : cytochrome c

DASPMI : N,N'-dimethylaminostyrylmethylpyridinium iodide

A : absorbance

ΔA : absorbance difference

ΔE : energy difference

DMSO : dimethyl sulfoxide

Δp : proton motive force

ΔpH : pH gradient between the matrix and cytosol

$\Delta\Psi_m$: mitochondrial membrane potential (mV)

$E^{0'}$: reduction potential (mV)

ϵ : extinction coefficient ($\text{mM}^{-1} \times \text{cm}^{-1}$)

EGTA : ethylene glycol-bis (β -aminoethyl ether) N, N, N', N'- tetraacetic acid

EDTA : ethylenediamine-tetraacetic acid

ETC : electron transport chain

F : Faraday's constant (J/V)

F_E : fluorescence intensity after the addition of energized mitochondria or cells

F_U : fluorescence intensity after the addition of FCCP

F_0 : initial fluorescence intensity

FCCP : carbonyl cyanide 4-trifluoromethoxyphenylhydrazone

Fe-S : iron-sulfur center

Glib : glibenclamide

h : Plank's constant ($\text{J} \cdot \text{s}$)

HEPES : N-2-hydroxyethylpiperazine-N'-2-ethanesulfonic acid

$^3\text{H-TPP}^+$: H^3 labeled triphenylphosphonium ion

JC-1 : 5,5',6,6'-Tetrachloro-1,1',3,3'-tetraethylbenzimidazolylcarbocyanine iodide

MDC : mitochondrial dye content

MFFR : mitofluor far red 680

Mito- K_{ATP} channel : mitochondrial ATP-sensitive potassium channel

NIR : near-infrared

OAA : oxaloacetate

λ : wavelength

P : partition coefficient between the matrix and membrane

PCr : phosphocreatine

P_i : inorganic phosphate

³¹P-NMR : phosphorus -31 nuclear magnetic resonance

PTP : permeability transition pore

R : gas constant (J/ (K· mol))

RCI : respiratory control index

Red-ox : reduced- oxidized

ROS : reactive oxygen species

SDH : succinate dehydrogenase

SR : sarcoplasmic reticulum

T : absolute temperature (K)

TCA cycle : tricarboxylic acid cycle

TMRE : tetramethylrhodamine ethyl ester

TMRM : tetramethylrhodamine methyl ester

UQ : ubiquinone

V_{matrix} : volume of matrix

V_{membrane} : volume of membrane

ABSTRACT

Mitofluor Far Red 680 (MFFR, a near-infrared (NIR) mitochondrial membrane potential ($\Delta\Psi_m$) sensitive probe), was previously used for investigating the dependence of MFFR uptake upon $\Delta\Psi_m$ in the perfused rat heart. Unexpectedly, in this study fluorescence did not change in response to a decrease in $\Delta\Psi_m$ induced by an uncoupler of oxidative phosphorylation possibly due to non specific binding to non-mitochondrial components. We therefore, investigated MFFR distribution and its optical properties in simpler systems, namely isolated mitochondria, cardiomyocytes, and hepatocytes, to evaluate the relationship between MFFR distribution and $\Delta\Psi_m$.

Mitochondria were isolated from rat liver by homogenization and differential centrifugation. Cardiomyocytes (CMC) and hepatocytes (HC) were isolated from rat heart and liver by collagenase perfusion. Viability of mitochondria as well as the toxic effects of MFFR on mitochondria were determined by measuring respiration rate. CMC and HC viability were determined by observation of cellular morphology and Evans Blue staining. Mitochondria were energized by glutamate plus succinate and ATP, CMC energized by glucose and pyruvate, and HC energized by glucose accumulated MFFR in $\Delta\Psi_m$ dependent manner. This resulted in decreases in MFFR fluorescence intensity in fluorescence assays. Addition of the uncoupler carbonyl cyanide 4-trifluoromethoxyphenyl hydrazone resulted in the dissipation of $\Delta\Psi_m$ in mitochondria, CMC and HC as evidenced by decreases in MFFR binding and increases in fluorescence intensity.

We conclude that MFFR distribution and changes in fluorescence intensity are dependent on $\Delta\Psi_m$ in isolated mitochondria and cells. $\Delta\Psi_m$ was quantitatively estimated

in isolated mitochondria whereas in the cells the estimates were qualitative. MFFR binding to isolated mitochondria was significantly greater than its binding to isolated cells. This resulted in larger changes in fluorescence in mitochondrial suspensions. We concluded that MFFR is a reliable probe to measure $\Delta\Psi_m$ in isolated mitochondria quantitatively, and to monitor $\Delta\Psi_m$ changes qualitatively in cells. A probe with lower hydrophobicity would be more suitable for monitoring $\Delta\Psi_m$ in intact cells and tissues.

CHAPTER 1

LITERATURE REVIEW

1.1 Introduction

Mitochondria are crucial for maintenance of normal cell function [1]. The proper function of these organelles ultimately determines life and death of the cell [2]. It is therefore, important to monitor the activity of these organelles using reliable indices in living tissue. One such index is cardiac oxygen (O_2) consumption rate, which is the difference between arterial and venous concentrations of O_2 multiplied by coronary flow [3, 4]. This can be used as an index for mitochondrial function as O_2 is the last electron acceptor in the series of redox reactions and mitochondrial respiration rate therefore depends on O_2 concentration. Cardiac O_2 consumption rate is thus an indicator of the health of the heart. Another index of mitochondrial function is the redox states of cytochromes (electron carriers). Cytochrome optical properties, which are altered by changes in redox states, can be measured by optical spectroscopy [5, 6]. Steady-state levels of oxidative phosphorylation products such as adenosine diphosphate (ADP), inorganic phosphate (P_i), adenosine triphosphate (ATP) and phosphocreatine (PCr) are also indices for mitochondrial function [7]. In conditions of low O_2 , changes in oxidative phosphorylation products are seen as increases in ADP and P_i and decreases in ATP and PCr, which indicate compromised mitochondrial function. This can be measured non-invasively by phosphorus -31 nuclear magnetic resonance (^{31}P -NMR) spectroscopy [3, 6, 8]. It is also important to measure the mitochondrial membrane potential ($\Delta\Psi_m$) as it drives ATP synthesis [9, 10]. $\Delta\Psi_m$ can be measured using $\Delta\Psi_m$ -sensitive fluorescent

dyes. Amongst them dyes absorbing light in the near-infrared (NIR) region are the most interesting due to weak absorbance of natural chromophores (haemoglobin and myoglobin) and high depth of light penetration.

1.2 Cardiac Energetics and Contractility

The Function of the heart is to transport oxygenated blood to the whole body in order to maintain life. The heart receives deoxygenated blood from the body and sends it to the lungs to take up oxygen. The oxygenated blood is collected in left chamber of heart and the oxygenated blood is pumped out from the heart to the tissues, which require oxygen and nutrients, to keep them alive. The heart has four chambers, right atrium and ventricle that carry deoxygenated blood and left atrium and ventricle that contain oxygenated blood. The heart is a muscle tissue consisting of bundles of muscle fibers connected to each other by collagen. The muscle fibers, known as myofibers, contain contractile muscle cells known as cardiomyocytes. Cardiomyocytes have a nucleus, a cardiac cell membrane known as the sarcolemma and the sarcoplasmic reticulum (SR) (the site of calcium (Ca^{2+}) storage and release), transverse tubules (tube-like invaginations of the sarcolemma), the intercalated disk connecting cells, mitochondria, and contractile proteins responsible for muscle contractions. The contractile proteins are organized in the structure called a myofibril, composed of thin and thick filaments. The thin filaments, also known as actin filaments, are made of globular actin molecules associated with regulatory proteins (troponin and tropomyosin), held together as chains while the thick filaments, known as myosin filaments, composed of myosin molecules. Actin and myosin filaments are structured in a contractile unit called the sarcomere.

Cardiac contractions result from the sliding of two filaments over each other, and require high energy expenditure. For example, in a rat heart, approximately 2% of the total energy in the form of ATP and PCr is used in cardiomyocytes for each contraction [11, 12].

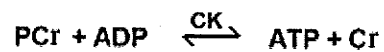
Cardiac muscle contraction results from excitation-contraction coupling. Under resting conditions, there is a membrane potential difference of about -80mV between the extra-cellular and intracellular space. When the membrane potential becomes more positive, Na^+ ions diffuse into the cells causing further membrane depolarization. This event triggers Ca^{2+} entry through the sarcolemmal Ca^{2+} channels and Ca^{2+} ions are subsequently released from the SR into the sarcoplasm. The Ca^{2+} ions then attach to binding sites on the troponin molecules, which causes a shift in the tropomyosin configuration, exposing myosin-binding sites on actin filaments. Interaction of myosin and actin filament forms cross-bridges that generate a power stroke. The energy required for this process is generated by hydrolysis of ATP to ADP and P_i by an enzyme called ATPase (on the myosin head) which causes myosin to pull along the actin filament.

Cardiomyocytes contain mitochondria that occupy approximately 30 % of their volume [13]. Ninety percent of energy produced in heart tissue comes from mitochondrial respiration [13].

ATP is produced by a process of ATP synthesis called oxidative phosphorylation in mitochondria. Mitochondria use metabolic substrates such as glucose, fatty acids, amino acids, and pyruvate to initiate oxidative phosphorylation. Hence, the heart obtains ATP through oxidation of these substrates in mitochondria. However, various other substrates can be utilised to cause cardiac contraction [14-19]. In addition, pyruvate

utilization is associated with an increase in ATP synthesis in response to an increase in cardiac work [20, 21]. It has been shown that mitochondria are better adapted to variations in ATP demand for cardiac contraction during pyruvate induced respiration than during oxidation of other substrates in the heart.

Since ATP diffusion from the mitochondria to myofibrils is slow, energy transfer systems are required. The phosphocreatine (PCr) shuttle acts as the energy transfer system that transforms ATP to PCr by an enzyme called creatine kinase (CK) inside mitochondria [22]. Once PCr is formed it can relatively easily diffuse from the mitochondria and re-synthesize ATP from PCr and ADP at the myofibrils:



This PCr shuttle can provide a strict match between ATP production and utilization for contraction [23].

ATP synthesis is well regulated and controlled by changes in ATP demand. The correlation between oxygen consumption rate and cardiac work is well known and confirms coupling of ATP production to ATP utilization [3, 24-29]. However, coupling of ATP production to contractile demand is complex. Redox state, cytosolic high energy phosphate metabolites such as ADP, P_i, ATP, and PCr, Ca²⁺, oxygen and substrate availability, and mitochondrial $\Delta\Psi_m$ may play an important role in control of cardiac energy turnover [7, 19, 30-36].

1.3 Mitochondria in Energy Production and Parameters

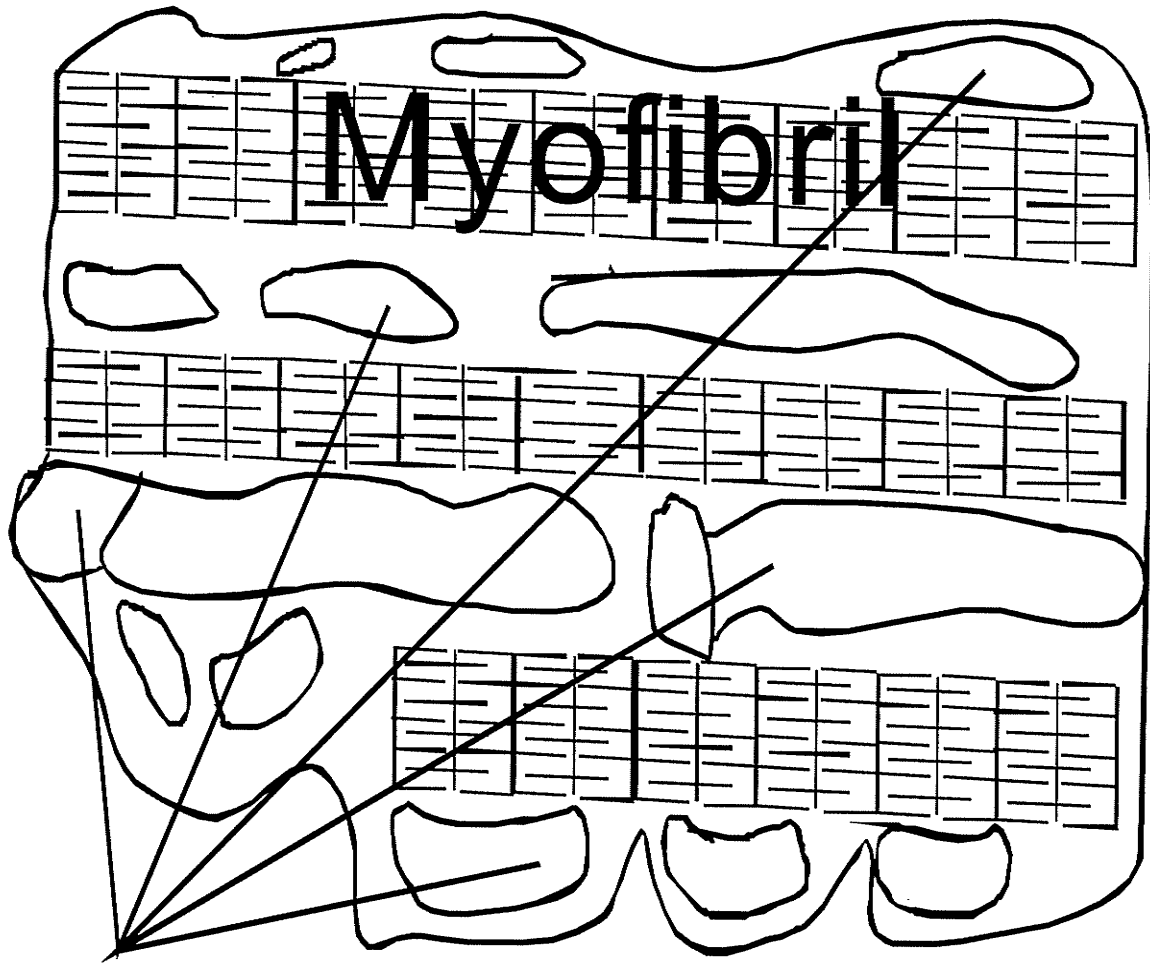
Defining Energetic Status

1.3.1 Introduction

Mitochondria are small organelles found in eukaryotic cells that generate ATP. Mitochondrial functions in the cell have been a hot area of scientific research since mitochondria were discovered by Kolliker in 1856. Scientists have come up with many hypotheses of mitochondrial functions before actual mitochondria were isolated from liver in 1940s. Following isolation of mitochondria Kennedy and Lehninger found that mitochondria are the compartment where oxidative phosphorylation occurs. Later on, it was found that oxidative phosphorylation involves electron and proton transfer through the mitochondrial membrane [37]. A large number of mitochondria are found in eukaryotic cells. For example there are approximately 1000 to 2000 mitochondria in each liver cell [38]. The distribution and arrangement of mitochondria are dynamic in each cell types. In cardiac muscle cell, mitochondria are strategically located between myofibrils to allow direct energy transfer (Figure 1-1). Normal mitochondria have a cylindrical shape and are large enough to be seen under light microscope, with a length of 0.5 to 1 μ m.

1.3.2 Mitochondrial Morphology

Mitochondria are composed of two membranes (inner and outer) and two compartments separated by the membranes, which are a major mitochondrial feature well-suited for generation of ATP (Figure 1-2).



Mitochondria

Figure 1-1. Mitochondria in cardiac tissue

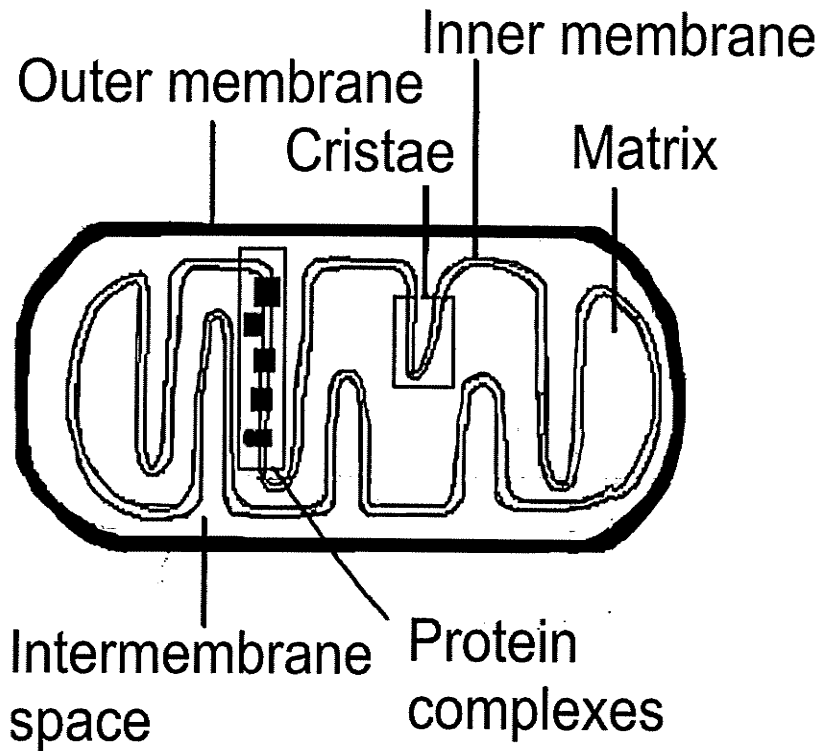


Figure 1-2. The structure of mitochondrion

Mitochondria are limited by an outer membrane consisting of a lipid bilayer, which functions as a barrier to molecules larger than 1500 dalton [39]. The outer membrane also contains proteins, called porins that allow small molecules and ions to move into the outer compartment, intermembrane space [40]. The intermembrane space separates the outer membrane from the inner membrane. Thus, the intermembrane space is analogous to the cytosol in that it is a medium through which molecules move via the outer membrane [41]. In addition, the intermembrane space has an important mitochondrial factor, cytochrome c (Cyt c) involved in electron transport for generating ATP and other enzymes such as CK, adenylate kinase, and nucleoside diphosphate kinase. The major

components of the mitochondria are the inner membrane and the matrix, which play a major role in mitochondrial energy production. The inner membrane is enriched in phospholipid and cardiolipin, which confers low membrane permeability to small molecules, ions, and metabolites [42]. Cardiolipin allows Cyt c to be localized in the intermembrane space through a direct association [39]. The inner membrane has specific electron transport proteins that help to transport H^+ across the membrane and to pass electrons from one protein to next one. The electron transport proteins in the inner membrane together function as a complex system for ATP generation and are known as the electron transport chain (ETC). The H^+ movement via the ETC is essential to the function of the mitochondria in terms of ATP synthesis. The inner membrane is highly folded. These folds are cristae increasing the surface area. The shapes of cristae folds are different in each type of cell. In addition, mitochondria in cardiac cell have three times higher cristae density than it in liver cell [38]. This is a pre-requisite for the large amount of ATP supplied to cardiac cells for muscle contraction. Contact sites where the inner membrane attaches to outer membrane contain the PCr shuttle and are a vital site for the maintenance of cytosolic ATP.

There are eight enzymes required for the tricarboxylic acid cycle (TCA cycle, also called Krebs cycle) in the matrix that are involved in the generation of reduced forms of cofactors such as NADH and $FADH_2$. NADH and $FADH_2$ provide electrons to the ETC for maintaining H^+ flow across the inner membrane. H^+ transport from the matrix to the intermembrane space generates an electro-chemical H^+ gradient across the inner membrane. The Electro-chemical H^+ gradient results in the formation of a negative charge in the matrix relative to the cytosol and a transmembrane potential, $\Delta\Psi_m$.

1.3.3 Energy Substrates

The TCA cycle requires an intermediate, acetyl coenzyme A (acetyl CoA) to produce electron donors for the ETC. Various metabolic pathways lead to production of acetyl CoA from metabolites such as carbohydrates, fat, and ketone bodies.

As a first step glucose is transported from blood to the inside of the cardiac cells. Six -carbon glucose is cleaved to two three carbons pyruvate molecules through glycolysis in the cytosol (Figure 1-3).

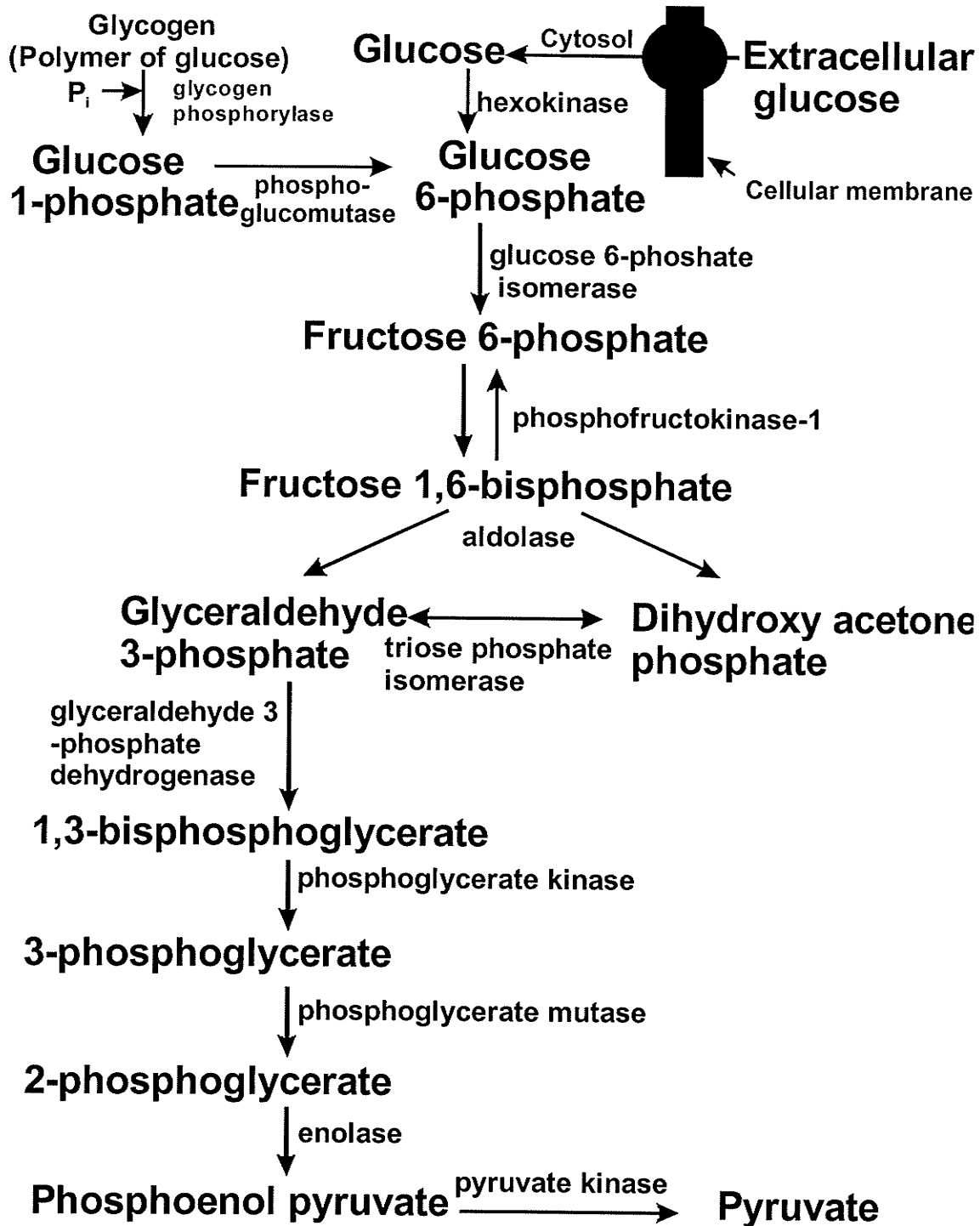


Figure 1-3. The glycolysis and glycogenolysis pathways

Pyruvate can then be used either as a source of lactate or acetyl CoA, depending on the availability of O_2 . In the absence of O_2 , lactate is generated in the cell in the lactate dehydrogenase reaction, accumulation of which can be toxic to the cells in the heart [43]. In the presence of O_2 , pyruvate generates acetyl CoA, which enters the TCA cycle leading to formation of NADH and $FADH_2$.

Fatty acids are a major energy source for the heart [44, 45]. Fat is represented by triglycerides and fatty acids. β -oxidation is involved in metabolism of fatty acid. First, long chain ($n > 12$) fatty acids are activated by conversion to fatty acyl CoA and become available for transport into the matrix in the form of acyl- carnitine. Fatty acyl-CoA goes through β -oxidation to generate NADH, $FADH_2$, and acetyl CoA which produces more NADH and $FADH_2$ in TCA cycle.

Ketone bodies are another type of metabolites involved in ATP generation. Changes in the pattern of substrate selection affect heart function and efficiency of energy utilization [14, 15]. In addition, metabolism of ketone bodies preferably occurs in the liver [46].

1.3.4 Tricarboxylic Acid Cycle (TCA Cycle)

Pyruvate forms acetyl CoA through the pyruvate dehydrogenase complex. Acetyl CoA goes to the TCA cycle to produce carbon dioxide (CO_2), NADH, and $FADH_2$. CO_2 is a waste product and NADH and $FADH_2$ are the major cofactors. Eight enzymes are involved in the TCA cycle (Figure 1-4).

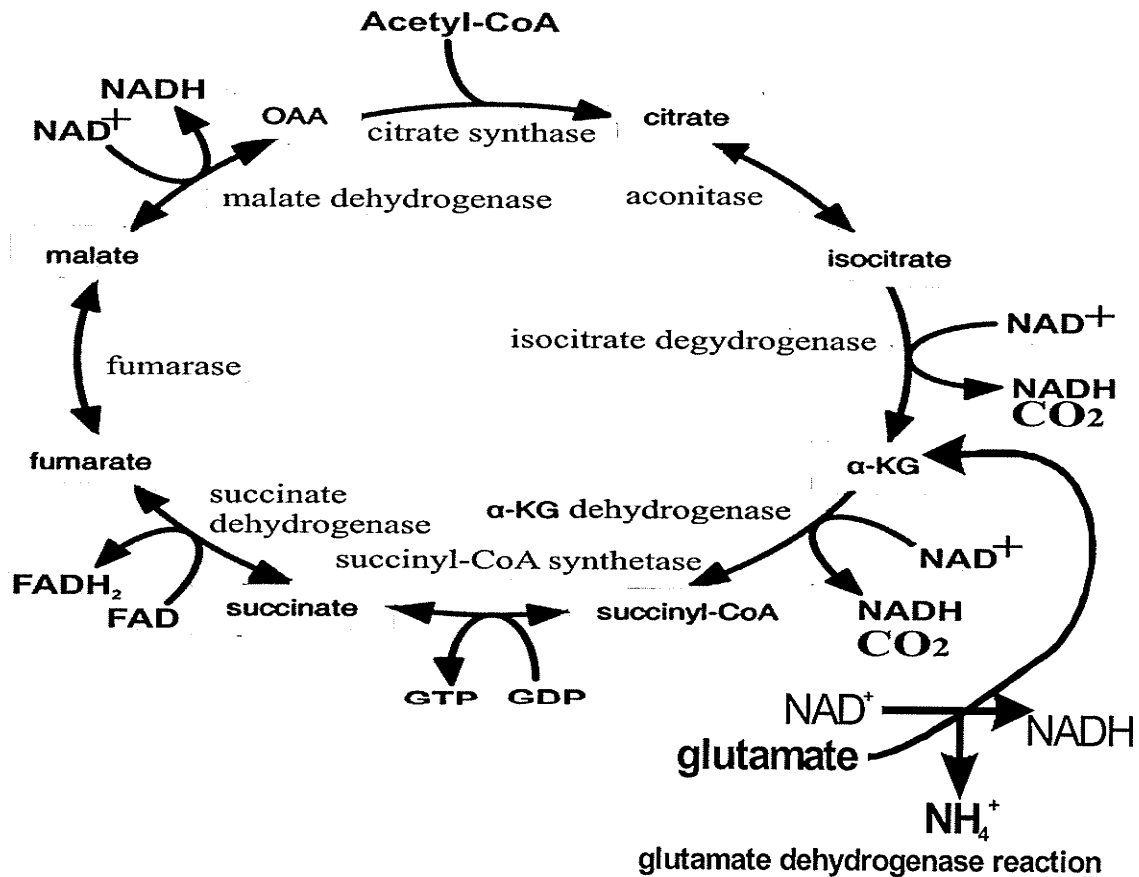


Figure 1-4. The TCA cycle

Two- carbon acetyl CoA combines with four carbon oxaloacetate (OAA) to produce six- carbon citrate. Citrate is converted to isocitrate which is metabolized by isocitrate dehydrogenase to generate one CO₂, one NADH, and α-Ketoglutarate (α-KG). α-KG can also be generated in the glutamate dehydrogenase reaction, which produces NADH and NH₄⁺. α-KG oxidation produces one more CO₂ and NADH, and succinyl CoA which is converted to succinate to produce GTP, which is equivalent to ATP . Succinate dehydrogenase, a mitochondrial membrane bound enzyme, metabolizes succinate to fumarate to generate FADH₂. Fumarate is converted to malate by fumarase.

Malate dehydrogenase oxidizes malate to produce NADH and OAA which is the end of product in TCA cycle. If acetyl CoA is available, there is one more cycle to go. Many intermediates of the TCA cycle can be supplied from outside the mitochondria and serve as oxidizable substrates (α -KG, succinate, malate, and OAA). Ca^{2+} regulates enzyme activities in the TCA cycle [46]. One round of the TCA cycle produces 2 CO_2 , 3 NADH, 1 FADH_2 and GTP. In the presence of O_2 in animal cells, NADH and FADH_2 are oxidized through the ETC by O_2 with H_2O formation, which produces the free energy required for ATP synthesis.

1.3.5 Electron Transport Chain (ETC)

ATP synthesis is achieved by an enzyme complex known as the respiratory chain or the electron transfer chain (ETC). The ETC is a series of enzyme complexes that undergo oxidation-reduction reactions to release free energy as electrons are passed down the ETC. The oxidation-reduction reactions are highly organized within the multienzyme complex. These reactions are used for ATP formation involving a multienzyme complex, ATP synthase. The entire process, called oxidative phosphorylation, is result of coupling of the ETC and ATP synthase. The ETC is composed of four complexes embedded in the inner membrane and the mobile electron carriers ubiquinone (UQ) and Cyt c (Figure 1-5).

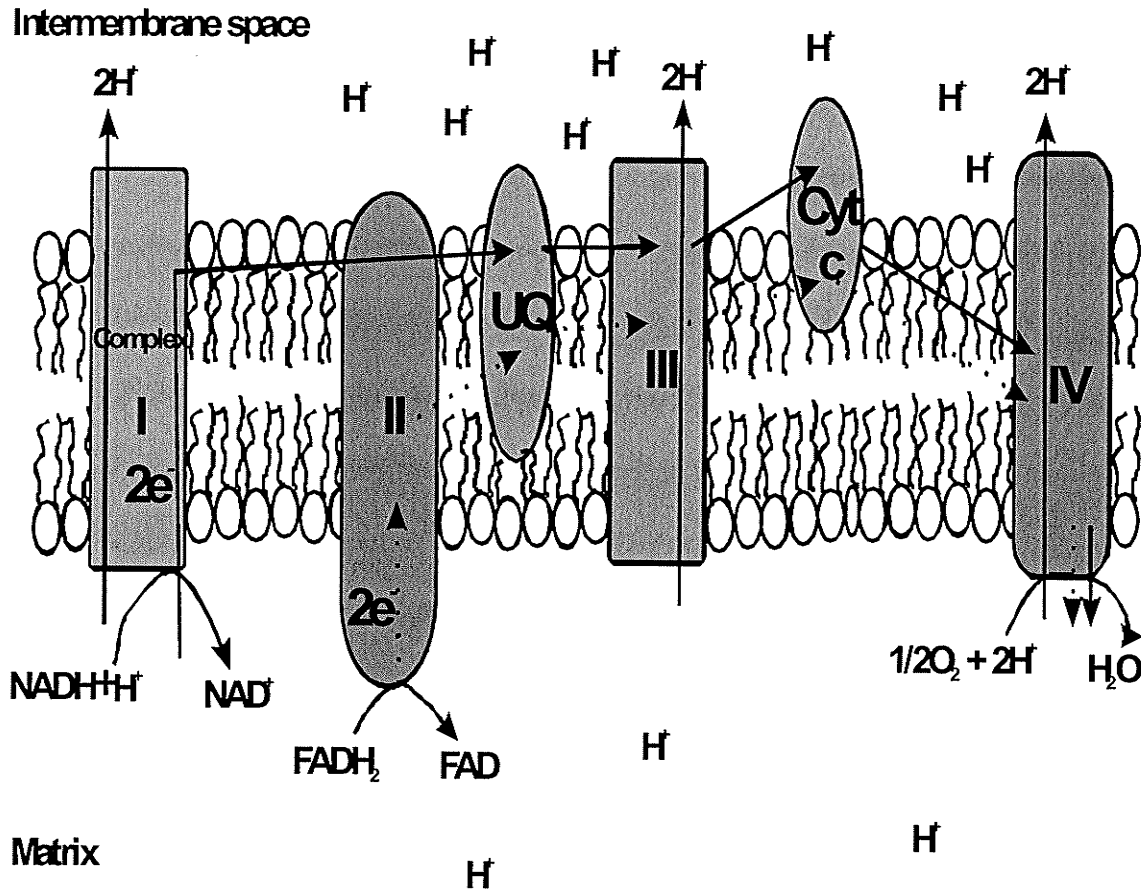
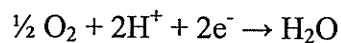


Figure 1-5. The Electron Transport Chain (ETC)

NADH passes electrons down complex I (NADH dehydrogenase) which reduces UQ. Complex III (UQ-Cyt c oxidoreductase) accepts electrons from complex I via reduced UQ. Next, complex III gives electrons to Cyt c and then to complex IV (cytochrome oxidase) to become oxidized. At the final stage, an oxygen atom receives electrons from complex IV to produce H₂O by combining with two H⁺:



The movement of electrons is coupled to H⁺ flow from the matrix to the intermembrane space through the complexes, except the complex II. In contrast, complex II (succinate

dehydrogenase (SDH)) receives electrons from succinate to form FADH_2 which reduces UQ without involving H^+ movement. Electron flows from NADH, which has a high negative reduction potential ($E^{\circ} = -0.32\text{V}$ relative to normal hydrogen electrode at pH 7.0) to the O_2 which has a high positive reduction potential ($E^{\circ} = \sim +0.82\text{V}$) (Figure 1-6) [47]. Carriers with high negative reduction potential tend to lose electron(s) easily and those with high positive E° to gain electron(s) easily.

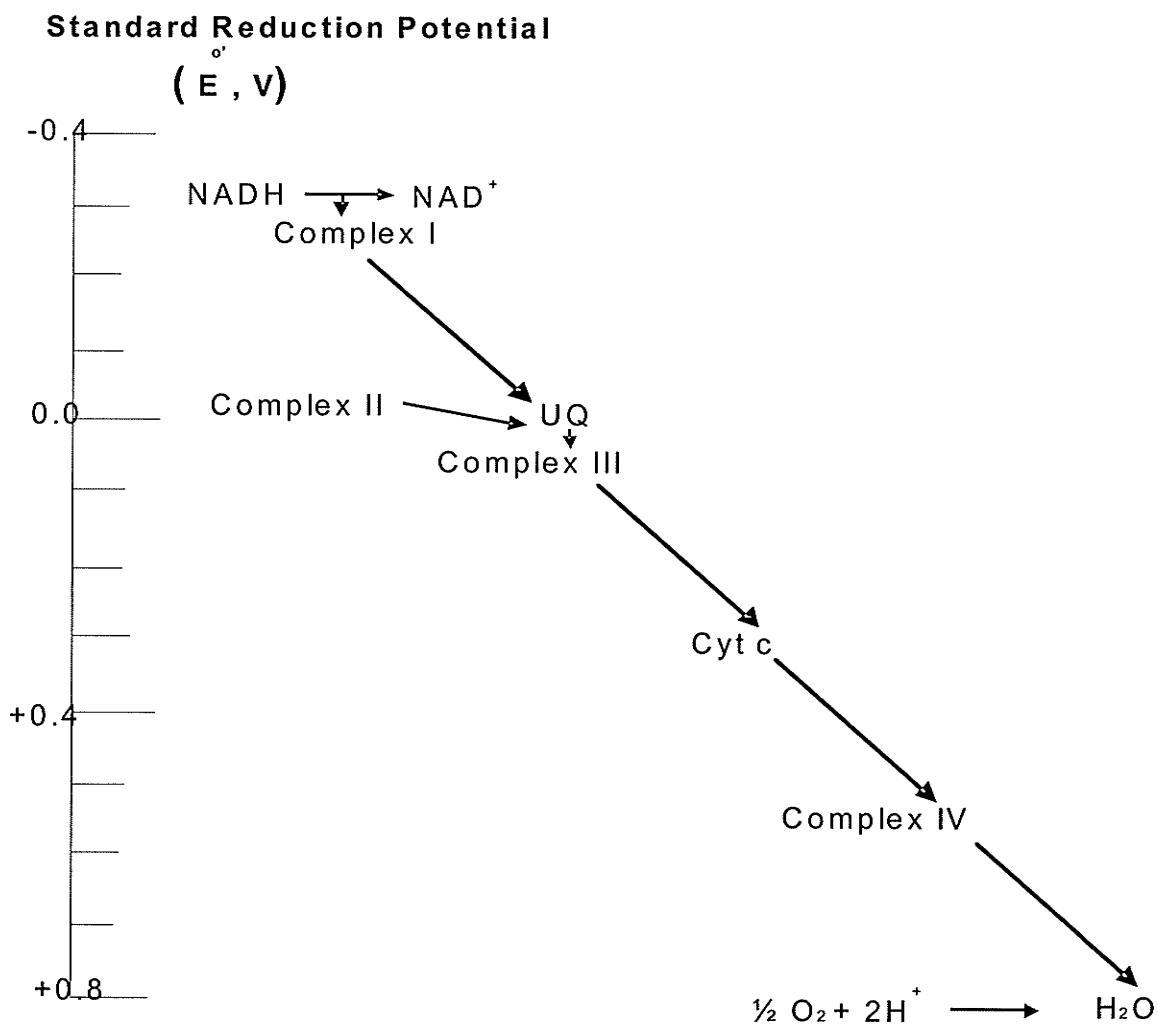
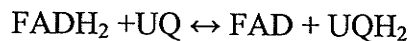


Figure 1-6. Reduction potential of carriers in the ETC

Complex I, known as NADH dehydrogenase or NADH: UQ oxidoreductase, is the largest complex in the ETC. It is composed of six iron-sulfur (Fe-S) centres and a flavin mononucleotide molecule [46]. Complex I receives two electrons from NADH and passes its electrons to the mobile electron carrier UQ. The net reaction is shown as $\text{NADH} + \text{H}^+ + \text{UQ} \leftrightarrow \text{NAD}^+ + \text{UQH}_2$. Therefore, two H^+ are pumped out from the matrix to the inter membrane space through the complex I. Study of respiratory chain activity showed that the rate of respiration is sensitive to complex I activity during aging [48] and complex I becomes a major factor in the control of mitochondrial oxidative phosphorylation [49, 50]. UQ (coenzyme Q) is lipophilic so that it can diffuse through the membrane. Ubiquinol (UQH_2) the reduced form of UQ, donates two electrons to complex III which can accept its electrons.

Complex II is SDH or succinate:UQ oxido- reductase. This is an integral membrane protein which oxidizes succinate to fumarate in the TCA cycle to reduce FAD to FADH_2 in the complex II. Complex II consists of covalently bound flavoprotein and Fe-S proteins. Transferring electrons from complex II to UQ is similar to that for complex I, except no H^+ is pumped out. The net reaction in complex II is:

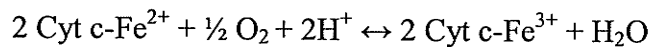


UQH_2 passes its electrons to complex III as well.

Complex III is called UQH_2 : Cyt c reductase or bc_1 complex. Complex III is composed of Cyt b, Cyt c_1 , and Fe-S protein. As complex III oxidizes UQH_2 , it transfers its electrons to Cyt c which is another mobile electron carrier. Cyt c is a peripheral membrane protein and reduced Cyt c donates its electrons to complex IV. Electron

transfer is coupled to two H^+ pumped across the complex III. Net reaction is $UQH_2 + 2 \text{cyt-Fe}^{3+} \leftrightarrow UQ + 2\text{cyt-Fe}^{2+} + 2H^+$

Complex IV is known as cytochrome oxidase or cytochrome aa_3 . Complex IV has three subunits which are composed of cytochromes (heme a and heme a_3), a Fe-S centre and copper atoms (Cu_A and Cu_B). Heme a_3 and Cu_B reduce O_2 to H_2O [46]. At the end site of complex IV, an oxygen atom receives two electrons to produce H_2O coupled with two H^+ pumped out through the complex IV. The net reaction:



1.3.6 Oxidative Phosphorylation

ATP synthase is complex V (Figure 1-7). It is composed of F_1 and F_0 proteins. F_1 is faced to the matrix and has ATP and ADP binding sites. F_0 is faced to the intermembrane space. H^+ movement via ATP synthase produces ATP from ADP and P_i . The generation of ATP is a reversible process depending on $\Delta\Psi_m$. A decrease in $\Delta\Psi_m$ drives ATP hydrolysis. Therefore, electron transfer to O_2 is necessary to maintain high $\Delta\Psi_m$ and provide ATP synthesis. Since electron transfer to O_2 through the ETC is coupled to ATP synthesis, respiration rate is controlled by ATPase substrates/ products such as ATP, ADP, P_i , as well as by PCr. The energy metabolites are in a steady- state under physiological condition (Figure 1-8). An important characteristic of mitochondrial function is an electro-chemical potential difference across the inner membrane of mitochondria which is approximately 160mV. This potential difference is dependent upon coupling between electron transport and phosphorylation as well as oxidizable substrates.

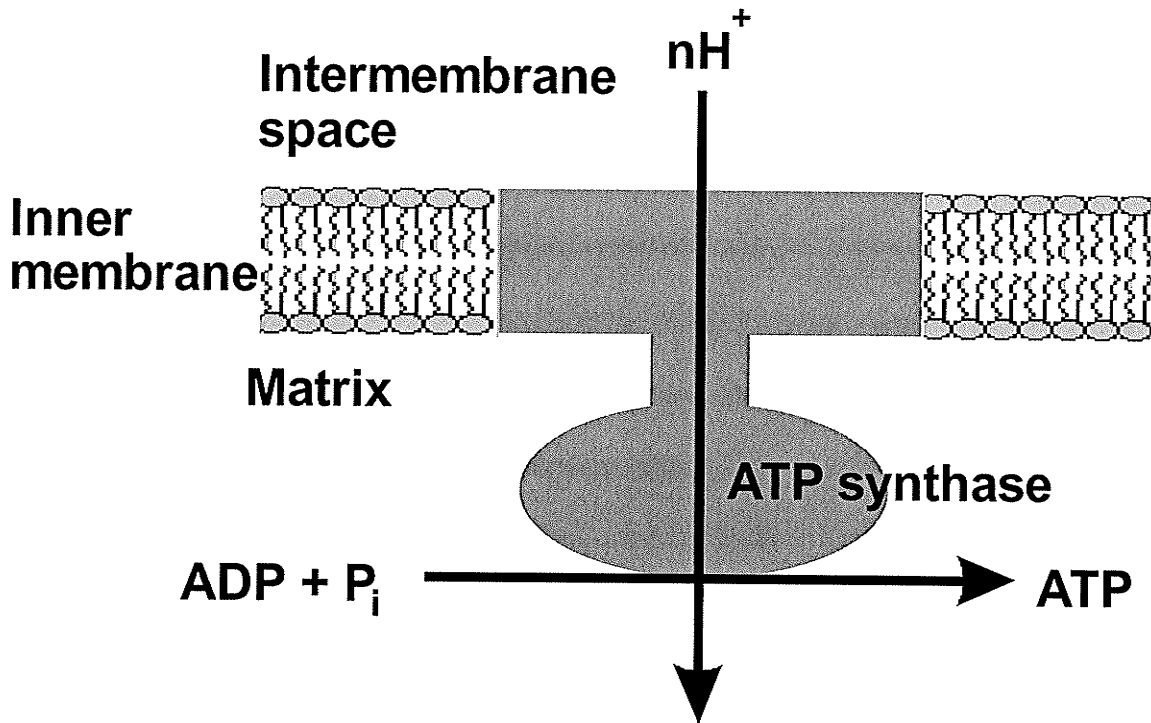


Figure 1-7. ATP synthase

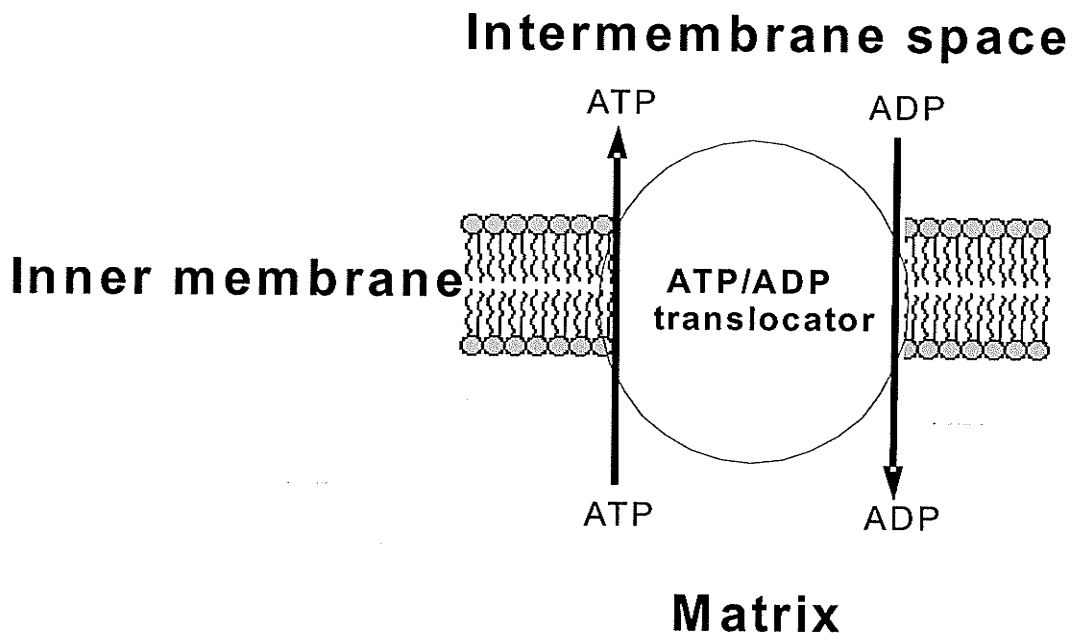


Figure 1-8. The ATP/ADP translocator

1.3.7 Chemiosmotic Gradient

Electrochemical H^+ gradient is generated by passing electrons down the ETC. The gradient forms the “energy reservoir” that allows ATP synthase to produce ATP. These events are described by the chemiosmotic theory [51]. The electrochemical H^+ gradient is composed of two components 1) a pH difference (ΔpH) between the matrix and cytosol and 2) a membrane potential difference ($\Delta\Psi_m$). ΔpH and $\Delta\Psi_m$ together influence the proton motive force (Δp) which drives H^+ flow back to the matrix through ATP synthase for ATP synthesis.

Δp is described by the following equation: $\Delta p = \Delta\Psi_m - (2.3 RT/F) \Delta pH$ (in mV) (at 37 °C, $\Delta p = \Delta\Psi_m - 60 \Delta pH$); R is the gas constant, T is absolute temperature, F is Faraday’s constant, and ΔpH is the pH gradient between the matrix and the cytosol. Δp is in the range of 200-220mV, of which 140-160mV is contributed by $\Delta\Psi_m$ and ΔpH equals typically -1 unit in mammalian cells [52]. Since $\Delta\Psi_m$ is established by the ETC through H^+ transfer across the inner mitochondrial membrane to regulate ATP synthesis, it can be used as an indicator of major mitochondrial function.

1.3.8 Inhibitors and Uncouplers of Oxidative Phosphorylation

The mechanism of electron movement and its coupling to electrochemical H^+ gradient have been investigated by using inhibitors and uncouplers of oxidative phosphorylation. The mechanisms of action of the agents are as follows. Amytal and rotenone act as inhibitors of complex I to block electron transfer from complex I to UQ [53, 54]. Antimycin A inhibits at Cyt b in the complex III [55]. Therefore, Cyt b can be reduced but can not be oxidized blocking electron transport to complex IV. Cyanide acts as inhibitor of complex IV by blocking the binding of oxygen so that electrons cannot be

passed to oxygen [56]. Oligomycin blocks ATP synthase to inhibit ATP synthesis from ADP plus P_i as well as ATP hydrolysis [57]. Atractyloside blocks ATP/ADP translocase and inhibits ATP/ADP exchange transport between matrix and cytosol [58]. Thus, oligomycin and atractyloside inhibit ATP-driven H^+ efflux causing $\Delta\Psi_m$ depolarization. The uncoupler carbonyl cyanide 4-trifluoromethoxyphenylhydrazone (FCCP) binds H^+ and thus becomes protonated [59]. FCCP in protonated form crosses the mitochondrial membrane and release H^+ in mitochondrial matrix, resulting in $\Delta\Psi_m$ depolarization. It is supposed that the opener of mitochondrial ATP-sensitive potassium (mito- K_{ATP}) channels P-1075 opens mito- K_{ATP} channels which are normally closed under physiological conditions, whereas the K_{ATP} channels blocker, glibenclamide (Glib) closes the channels opened by P-1075 [4, 60, 61]. P-1075 induced K_{ATP} opening causes influx of K^+ to the matrix down its electrochemical gradient that causes activation of the K^+/H^+ exchanger and H^+ influx resulting in partial $\Delta\Psi_m$ depolarization [62].

1.4 Effects of Pathology on Mitochondria and Energy Metabolism

The purpose of mitochondrial function is to provide ATP by oxidative phosphorylation to cells for survival and maintenance of cell function. ATP is used for regulation of cellular homeostasis in terms of controlling cell signaling pathway leading to cell survival and death. Dysfunction of mitochondria has been shown in ischemia/reperfusion injury, apoptic cells, and some hereditary diseases [2, 63].

1.4.1 Ischemia/Reperfusion Injury

The condition of inadequate blood supply to cardiomyocytes is called myocardial ischemia, and results in a deficiency of energy supply for muscle contraction. The magnitude of the energy supply cannot meet the high energy demand for the contraction in myocardial ischemia/reperfusion, which leads to cell damage and subsequent cell death. Cardiac ischemia/reperfusion injury is associated with dysfunction of mitochondria caused by defects in oxidative phosphorylation [64- 66]. The degree of damage to mitochondria is dependent on the duration and severity of ischemia [67- 69]. It has been shown that disruption of mitochondrial structure occurs in early ischemia condition [67, 70]. Consequently, disruption of mitochondria leads to further decrease in oxygen consumption rate and oxidative phosphorylation, and the changes in $\Delta\Psi_m$ seen in ischemic conditions [67, 71]. A decrease in activity of complex I and damage to ATP synthase and ATP/ADP translocase occur in early ischemia (at least up to 20 minutes) as well [69, 70, 72, 73]. For 30 minutes ischemia in the rabbit heart, Cyt c, a mobile electron carrier is released [66]. Damage of the outer membrane has been associated with release of Cyt c [74]. State 3 respiration which corresponds to O₂ utilization for synthesis of ATP from ADP and Pi with oxidizable substrates such as glutamate plus malate, recovers after the addition of Cyt c to isolated mitochondria from 30 minute ischemic heart [75]. A decrease in cardiolipin content was also observed in ischemia [76, 77]. Cardiolipin stabilizes Cyt c due to its binding to this protein [78, 79]. Cyt c release may therefore also be associated with decrease in cardiolipin content [76, 80]. Ischemia leads to an increase in generation of reactive oxygen species (ROS) due to electron leak through the ETC. In normal respiration, ROS are produced by electron flow via the ETC

[81, 82]. However, electron leak is increased in ischemia [83, 84]. Complex I and III of the ETC are the major sites for ROS generation [81, 82, 85, 86]. Since a decrease in mitochondrial respiration and complex I activity is observed in ischemia, an increase in ROS results. Further generation of ROS inhibits mitochondrial respiration by binding to various components of the ETC since ROS are very reactive [87].

Ca^{2+} accumulation by mitochondria has been shown in ischemia/reperfusion following an increase in cytosolic Ca^{2+} content [88]. Reperfusion after ischemia leads to a many -fold increase in mitochondrial Ca^{2+} uptake [40], causing opening of a permeability transition pore (PTP) which results in the release of Cyt c and activation of the cell death program [89, 90].

Since $\Delta\Psi_m$ is maintained by the ETC and used for ATP synthesis, it may be manipulated by inhibition of the ETC and ATP synthesis [2]. A decrease in $\Delta\Psi_m$ is associated with a decrease in heart performance during 35 minute ischemia [74], which agrees with the $\Delta\Psi_m$ dependence of ATP generation.

1.4.2 Apoptosis

Mitochondria play crucial roles in controlling the cell death program, called apoptosis [91- 99]. Apoptosis is a naturally occurring process in eukaryotic organisms. Apoptosis involves the activation of specific proteases named caspases [39]. The activation of caspases is interrelated with changes in mitochondrial functions. Although the general mechanisms by which mitochondria contribute to apoptosis are understood, the specific mechanisms are still unclear.

Loss of $\Delta\Psi_m$ induced by DNA damage and toxic substances cause release of Cyt c into the intermembrane space [98]. Since Cyt c is one of the electron carriers in the ETC,

its release leads to inhibition of proton and electron transport through the ETC. This results in increase in loss of $\Delta\Psi_m$, ROS production, and Ca^{2+} triggering of PTP opening, which is located in the contact sites between the outer and the inner membrane. PTP opening releases Cyt c and apoptosis inducing factor (AIF) into the cytosol [100]. Association of Cyt c with a cytosolic factor, Apaf, activates caspase 9 [101]. Activated caspase 9 activates caspase 3 and 7 [97]. Caspase 3 and 7 induce nuclear DNA condensation and fragmentation, contributing to apoptosis.

Cyt c and AIF cannot pass through the PTP unless it is associated with proapoptotic proteins (Bax and Bak) because PTP alone is too small for them [94]. Regulation of PTP with associating proapoptotic factors is controlled by antiapoptotic proteins, such as Bcl-2 and Bcl-X_L, which prevent apoptosis. Proapoptotic and antiapoptotic proteins are two groups of the Bcl-2 family. Proapoptotic proteins are Bax, Bak, Box, Bid, and Bik. Antiapoptotic proteins are Bcl-2, Bcl-X_L, Bcl-w, Mcl-1 and A-1. They all are located in the outer membrane. PTP and Bcl-2 family proteins are important factors to control cell survival and death [39].

1.4.3 Mitochondrial Genetic Disorders

Abnormal deletion and mutation of mitochondrial DNA (mtDNA) induce mitochondrial genetic disorders observed in humans [102]. The properties of mtDNA differ from those of nuclear DNA [103]. There are high risks of abnormal mitochondria induced by mutation of mtDNAs. Mitochondria do not contain reverse transcriptase, so abnormal mtDNA may not be repaired. The phenotype of mitochondria induced by mutation of mtDNA, involves abnormalities of oxidative phosphorylation. Many human mitochondrial diseases are attributed to mutations of ETC [104].

1.5 Methods for Measurements of $\Delta\Psi_m$ in Isolated Mitochondria, Cells and Intact Hearts

Two transmembrane electrical potentials normally exist in the cardiomyocyte. One of them is across the cell membrane (sarcolemma) that separates extracellular and intracellular space. This potential known as the plasma membrane potential and equal to -80mV in the resting state, is maintained and controlled by concentration gradients of Na^+ , K^+ , Cl^- , and Ca^{2+} across the cell membrane. The second potential difference is across the inner mitochondrial membrane, known as $\Delta\Psi_m$. Mitochondria are energized by substrate oxidation, which generates a potential difference of approximately -160mV across the membrane. The purpose of $\Delta\Psi_m$ generation by the ETC is to drive ATP synthesis via ATP synthase and maintain mitochondrial ion homeostasis. Several lipophilic cationic dyes ($\Delta\Psi_m$ probes), which are able to accumulate inside the mitochondria due to $\Delta\Psi_m$ have been used to study $\Delta\Psi_m$ in isolated mitochondria, cells, and intact hearts. The concentration of the probes accumulated in mitochondrial matrix can be determined to evaluate $\Delta\Psi_m$ by measuring absorbance (ΔA) with spectrophotometry. These dyes also exhibit changes in fluorescence intensity and wavelength in response to changes in $\Delta\Psi_m$, which may be assessed by fluorescence measurements.

1.5.1 Optical Methods

1.5.1.1 Spectrophotometry

Spectrophotometry is a commonly used optical technique for determination of the concentrations of compounds according to the Beer-Lambert Law: $A = \epsilon C l$,

where A is the absorbance, ϵ is a constant, the extinction coefficient of a compound ($\text{mM}^{-1}\text{cm}^{-1}$), C is the concentration of a compound (mM), and l is the path length (cm).

Spectrophotometry requires infrared, visible, or ultraviolet light as a light source to illuminate a sample. The molecules in the sample absorb the light at specific wavelengths, which are determined by energy differences between ground and excited states: $\lambda = hc / \Delta E$, where h is Plank's constant, c , speed of light and ΔE , energy difference [105]. Solvent, temperature, and pH may affect the wavelength of maximum absorption due to interaction of the molecule with an environment.

The fraction of photons that are not absorbed is exponentially related to ϵ , C , and l and defined as transmittance, the ratio of the transmitted intensity to the intensity of incident light:

$$T = I / I_0 = 10^{-\epsilon C l}; \Delta A = -\log I / I_0 = \epsilon C l$$

Transmittance is simply expressed as percent of transmission: $\% T = 100 \times I / I_0$

If ϵ of a compound is known at a specific wavelength and path length is given, the concentration of a compound can be determined by measuring the absorbance at that wavelength.

1.5.1.2 Fluorescence measurements

Fluorescence techniques require fluorescent molecules which produce fluorescence spectra at a particular wavelength through a three-stage process (Jablonski

diagram, [106]). During the first stage called excitation, a molecule absorbs the energy of a photon emitted by a light source such as laser and moves to an excited state from a ground state. The excited state is transient and unstable so that it exists for a short time. The excited state loses energy and transits to the lower energy level during the second stage, called excited-state lifetime. During the final stage of fluorescence emission, when the molecule returns to its ground state, a photon is emitted. This photon energy is lower than that of excitation due to the loss of energy in the excited-state lifetime and therefore exhibits a longer wavelength. There are particular features of fluorescence spectra. The fluorescence quantum yield which is the ratio of the number of fluorescence photons emitted to the number of photons absorbed, represents the probability of producing fluorescence by an excited fluorophore, which is a chemical group of fluorescent dye able to absorb energy. Quantum yield may be affected by environment factors such as solvent polarity, pH, temperature, and concentration. The wavelength difference between emission and absorption maxima due to the energy difference is termed as the Stokes shift. Quenching and photobleaching are factors which should be taken into consideration for fluorescence techniques [107]. Both quenching and photobleaching have the potential to produce relatively less fluorescence emission. The effects of quenching are reversible, however, the effects of photobleaching are irreversible. Quenching can reduce emission by interacting with non-fluorescent molecules. When a fluorophore is damaged by factors such as light, it loses its ability of producing emission. This is called photobleaching. Fluorescence intensity also follows the Beer-Lambert law explained in section 1.5.1.1. Fluorescence instruments include a spectrofluorometer which can be used to measure the average fluorescence of bulk samples, a fluorescence

microscope used to resolve fluorescence in two or three dimensions, and a flow cytometer used for samples such as a cell to measure fluorescence per cell. Fluorescence microscopy and flow cytometry are used to image $\Delta\Psi_m$ in isolated mitochondria [108, 109]. According to this method changes in fluorescence are correlated with alterations of $\Delta\Psi_m$.

1.5.1.3 Optical Indicators of Mitochondrial Membrane Potential

Membrane-permeable cations are driven inside the negatively charged mitochondrial matrix by electrical potential and their transmembrane distribution obeys the Nernst law. The distribution of radioactive rubidium ion (Rb^+ , K^+ congener) in the presence of valinomycin across the mitochondria has been used for measurement of $\Delta\Psi_m$ [110]. Valinomycin functions as K^+ ionophore which renders the mitochondrial membrane permeable to K^+ , so that Rb^+ is distributed at equilibrium across the mitochondria according to $\Delta\Psi_m$. However, the method requires careful handling because of the use of harmful radioactive isotopes. In addition, mitochondria have to be separated from the media after Rb^+ distribution to determine concentration of Rb^+ in mitochondria and the media separately. This method cannot monitor $\Delta\Psi_m$ in a continuous time-dependent manner. Valinomycin itself can be toxic to mitochondria, and cause dysfunction of mitochondria and change in $\Delta\Psi_m$. ^3H labeled triphenylphosphonium ion ($^3\text{H-TPP}^+$) is a lipophilic cation which can diffuse across the mitochondrial membrane and is accumulated in the matrix according to $\Delta\Psi_m$ without the presence of an ionophore [110, 111]. This also requires Rb^+ separation of mitochondria to determine concentration of $^3\text{H-TPP}^+$ in mitochondria and cytosol for calculating $\Delta\Psi_m$.

To measure or monitor $\Delta\Psi_m$ continuously, many cationic fluorescent dyes ($\Delta\Psi_m$ probes) are introduced to the mitochondria, cells, and intact hearts and their optical absorbance and fluorescence are analyzed [107, 112-116]. The dyes diffuse across the inner membrane due to their lipophilic property until an equilibrium governed by $\Delta\Psi_m$ is reached. Separating mitochondria or cells from the medium is necessary to determine intracellular dye concentration for estimating $\Delta\Psi_m$. The intracellular or intra mitochondrial dye concentration is determined either by measuring its absorbance or fluorescence. This method cannot monitor $\Delta\Psi_m$ continuously. For continuous monitoring of $\Delta\Psi_m$, mitochondria or cell suspensions are added to a cuvette with the fluorescent dye and absorbance or fluorescence are obtained. The accumulation of the positively charged dyes in the mitochondrial matrix results in a decrease in fluorescence in mitochondrial or cell suspensions due to a decrease in quantum yield induced by formation of dimers with low quantum yield or self-quenching [117, 118]. Then, dissipation of $\Delta\Psi_m$ by an uncoupler causes release of the dyes from the mitochondrial matrix into the external solution resulting in increase in fluorescence. In intact isolated hearts, the fluorescent dye is added to the perfusion medium and its absorbance and fluorescence are monitored by measurement of surface reflectance and fluorescence. Rhodamine derivatives, carbocyanines, N,N'-dimethylaminostyrylmethylpyridiniumiodide (DASPMI), and safranin are used for evaluating $\Delta\Psi_m$ in isolated mitochondria, cells, and intact hearts [119- 128]. The distribution of these cationic indicators is given by the Nernst equation:

$$\log [C]_i / [C]_o = n F / RT \times (- \Delta\Psi_m)$$

($[C]_i/[C]_o$ is the ratio of concentrations of cationic dye inside to outside of the matrix, F, Faraday's constant, R, gas constant, T,

absolute temperature, and n , ion charge usually equal to 1. Using the Nernst equation, it is possible to estimate $\Delta\Psi_m$.

Use of fluorescent dyes is limited to isolated mitochondria, cells, and intact hearts. Changes in absorbance and fluorescence should be dependent on changes in $\Delta\Psi_m$. However, it is more difficult to interpret the absorbance and fluorescence changes in cells and intact heart than in isolated mitochondria due to the complexity of their structures including sarcolemmal membrane and its potential and other membranes, organelles, and macromolecules. These factors may affect dye accumulation independent of $\Delta\Psi_m$. In addition, interactions between cellular structures and dye may result in changes in absorbance and fluorescence. Fluorescent dyes may affect cellular functions, including mitochondrial function. The intact heart is the most complicated system, containing vessels, an extracellular matrix and myocytes in which natural chromophores such as cytochromes, myoglobin, NADH, and FADH₂ are present. These chromophores exhibit absorptions at specific wavelengths and they are dependent on the redox and energy states (Table 1-1) [43, 129]. Light emitted by visible range probes (540-600nm) is absorbed partially by the endogenous chromophores. The chromophores may interact with fluorescent dyes leading to changes in fluorescent dye optical properties. Therefore, use of fluorescent dyes requires careful consideration. In addition, they should not inhibit mitochondrial electron transport, H⁺ permeability, and ATP synthesis. Since these processes determine $\Delta\Psi_m$, their inhibition and uncoupling by these probes may affect $\Delta\Psi_m$. These probes are lipophilic so that they may bind to mitochondrial membranes and other molecules. This implies that there is non-specific binding to mitochondria which may cause inaccurate quantitation of $\Delta\Psi_m$ if not taken into account. Using these probes

in optical measurements requires extra care. For example, they may be self-quenching at high concentration and sensitive to light [107].

Table 1-1. Absorption and emission maxima of natural chromophores in the visible range

Fluorescence	Endogenous Chromophore	Absorption wavelength (nm)	Emission wavelength (nm)
No	Oxygenated Myoglobin	560 and 580	n/a
No	Deoxygenated Myoglobin	570	n/a
No	Cytochrome oxidase [reduced- oxidized]	603	n/a
No	Cytochrome b [red-ox]	562-565	n/a
No	Cytochrome c and c ₁ [red-ox]	550-554	n/a
Yes	FAD [red-ox]	480	520
No	NAD	n/a	n/a
Yes	NADH	340	450

Rhodamine derivatives including rhodamine 123, tetramethylrhodamine methyl ester (TMRM) and tetramethylrhodamine ethyl ester (TMRE) have been used to estimate $\Delta\Psi_m$ in isolated mitochondria and cells [114, 130- 138]. They display emission spectra at green or red wavelengths in suspensions of mitochondria (Table 1-2). It was shown that their accumulation in mitochondria is $\Delta\Psi_m$ dependent. The probes show high nonspecific binding to mitochondria [131]. Although use of these dyes is successful in isolated mitochondria, their nonspecific binding is problematic in cells. Accumulation of these dyes in cells may be partially independent on $\Delta\Psi_m$ due to existence of the plasma

membrane potential, and binding to cell membranes and cellular components. Indeed, rhodamine 123 uptake by mitochondria in living cells could be affected by the plasma membrane potential [139]. High concentrations of rhodamine 123, TMRM, and TMRE are toxic to mitochondria [131]. Rhodamine 123 inhibits ATP synthase [140, 141]. TMRE at high concentrations generates toxic reactive oxygen species [141]. TMRE inhibits the mitochondrial respiration to a greater extent than rhodamine 123, while TMRM is less effective in inhibition of mitochondrial respiration [131]. High concentrations of these dyes also exhibit extensive self-quenching leading to loss of fluorescence signal [110, 114, 131, 141, 143]. TMRM shows photobleaching at concentrations above 200 nM [133]. Rhodamine 123 requires long incubation times with cells due to a slower release of rhodamine 123 in response to addition of uncoupler [144]. TMRM cannot be used in intact rat hearts to detect $\Delta\Psi_m$ by measuring surface fluorescence. The TMRM loaded rat heart did not show spectral changes in response to addition of an uncoupler [131]. The addition of dinitrophenol did not change the excitation spectra at 537 and 582 nm and fluorescence emission spectra at 610nm.

5,5', 6, 6'-Tetrachloro-1,1', 3, 3'-tetraethylbenzimidazolylcarbocyanine iodide (JC-1) is a cyanine family dye which exhibits two different states with different emission spectra [116, 145] (Table1-2). At low concentrations, JC-1 exists as monomer which has green fluorescence whereas at high concentrations, JC-1 forms aggregates that exhibit red fluorescence. This optical property gives a useful ratiometric method according to which the ratio of red to green fluorescence is determined to estimate $\Delta\Psi_m$. JC-1 uptake by mitochondria shows spectral shift from green to red fluorescence upon aggregate formation [145]. Theoretically, decrease in $\Delta\Psi_m$ is followed by increase in the green

fluorescence and decrease in the red fluorescence and vice versa. However, the increase in green fluorescence is only significant in response to a decrease in $\Delta\Psi_m$ [146]. The red fluorescence is more sensitive to photobleaching than green fluorescence, leading to a decrease in emission at red wavelength with prolonged excitation [147]. JC-1 fluorescence is dependent on pH and is not quenched at any concentrations [145]. Red fluorescence is linearly proportional to an increase in $\Delta\Psi_m$ over the range of 30-180mV [145]. JC-1 shows very slow uptake and extremely photosensitive [141].

The visible range dye safranin (Table 1-2) has been used for estimating $\Delta\Psi_m$ in isolated mitochondria, cells, and intact hearts [148-150]. Safranin exhibit shifts of absorbance maxima in response to changes in $\Delta\Psi_m$ in mitochondria and the shifts are linearly proportional to $\Delta\Psi_m$ over the range -40 to -170mV [151]. Safranin was also employed in the Langendorff perfused rat heart to monitor $\Delta\Psi_m$ on the surface of the perfused rat hearts [148]. Safranin fluorescence is sensitive to $\Delta\Psi_m$ but not to plasma membrane potential. However, changes in $\Delta\Psi_m$ fail to cause changes in the absorbance spectrum of safranin. It is possible that high concentration of intrinsic chromophores in the heart overwhelms the absorbance changes of safranin [148]. High concentrations of safranin are toxic to mitochondria [150]. Safranin appears to be slowly redistributed within cells [119].

DASPMI has been successfully used to monitor $\Delta\Psi_m$ in situ [127, 152]. Upon addition of 0.33 μ M DASPMI, the fluorescence intensity of DASPMI increased steadily during 45 minutes loading, and then an uncoupler reduced the fluorescence intensity [128]. High concentrations of DASPMI inhibit mitochondrial respiration [153]. Since

DASPMI is a visible range dye (Table 1-2), its fluorescence and absorbance can be modified by intrinsic chromophores.

Table 1-2. Excitation and emission maxima of fluorescent dyes

Fluorescent Dye	Fluorescence Excitation Maximum (nm)	Fluorescence Emission Maximum (nm)
Rhodamine 123	507	529
Tetramethylrhodamine methyl ester (TMRM)	549	573
Tetramethylrhodamine ethyl ester (TMRE)	549	574
5,5',6,6'-Tetrachloro-1,1',3,3'-tetraethylbenzimidazolylcarbocyanine iodide (JC-1)	514	529 and 590
Safranin	530	590
N,N''-dimethylaminostyrylmethylpyridinium iodide (DASPMI)	490	> 520

1.6 MITOFLUOR FAR RED 680 (MFFR)

The lipophilic cationic dye, Mitofluor Far Red 680 (MFFR), which is also known as rhodamine 800, has optical properties such that it absorbs and emits light in the near-infrared range (680-730nm) with absorption and emission maxima at 681 and 702nm in ethanol, respectively [154]. MFFR is a near-infrared (NIR) probe which allows for it to be used to measure polarization to determine its concentrations in samples and has the potential to measure concentrations of components in whole blood [156, 157]. In

addition, the application of MFFR in flow cytometry has been used to measure DNA content in ethanol-fixed or detergent-permeabilized cells using an inexpensive helium-neon laser [158]. MFFR appears to stain DNA bases, the composition of which influences MFFR fluorescence characteristics [157]. MFFR has a planar structure (Figure 1-9) which contributes to a small Stokes shift between excitation and emission maxima relative to that of rhodamine 123 [158, 159]. The magnitude of the red shift and amplitudes of MFFR optical spectra change with changes in mitochondrial energy states in isolated rat liver mitochondria and hepatocytes [158]. $\Delta\Psi_m$ drives positively charged dye such as MFFR to accumulate inside the mitochondria. The concentration and hence amount of MFFR that accumulates inside the mitochondria should depend on $\Delta\Psi_m$. Therefore, measurement of MFFR accumulation should allow us to determine the $\Delta\Psi_m$. Similar to rhodamine 123, TMRE, and TMRM, MFFR absorbance and fluorescence changes in rat liver mitochondria are linearly proportional to the $\Delta\Psi_m$ generated by K^+ diffusion potential with valinomycin, a lipophilic K^+ -selective ionophore which allows K^+ to flow to the mitochondria down its electrochemical gradient [158]. However, the actual dye distribution was not measured. MFFR has some benefits compared to rhodamine 123 and derivatives. Absorptions of natural chromophores may overlap with the peaks of the probe spectra in the visible range. Use of MFFR allows us to solve this problem. MFFR is a NIR optical probe which displays absorption and fluorescence maxima at longer wavelength away from natural chromophores. Moreover, the fluorescence of MFFR can be measured in relatively thick tissue layers and blood due to deeper light penetration through the tissue to excite the probe [155, 156]. Therefore, MFFR may be used for a non - invasive measurement of $\Delta\Psi_m$ in the heart without

interfering with natural chromophores such as oxy and deoxy- myoglobin and cytochromes. Our preliminary data showed that MFFR accumulates in the heart yielding absorbance and fluorescence spectra in the near-infrared region ([160], Figure 1-10). After MFFR loading, the heart was treated with an uncoupler, 2, 4 dinitrophenol which depolarizes $\Delta\Psi_m$ and washout showed that only a small amount of MFFR was released from the rat perfused heart, contrary to expectations. This means that predominant fraction of MFFR may have $\Delta\Psi_m$ - independent binding. The heart has a complex structure including the extra-cellular matrix, cell membranes, and DNA/RNA that may explain considerable passive binding of MFFR. Therefore, a study of the optical properties of MFFR incorporated in isolated mitochondria and cells and its binding properties may help us to understand such dye behaviour in intact cardiac tissue.

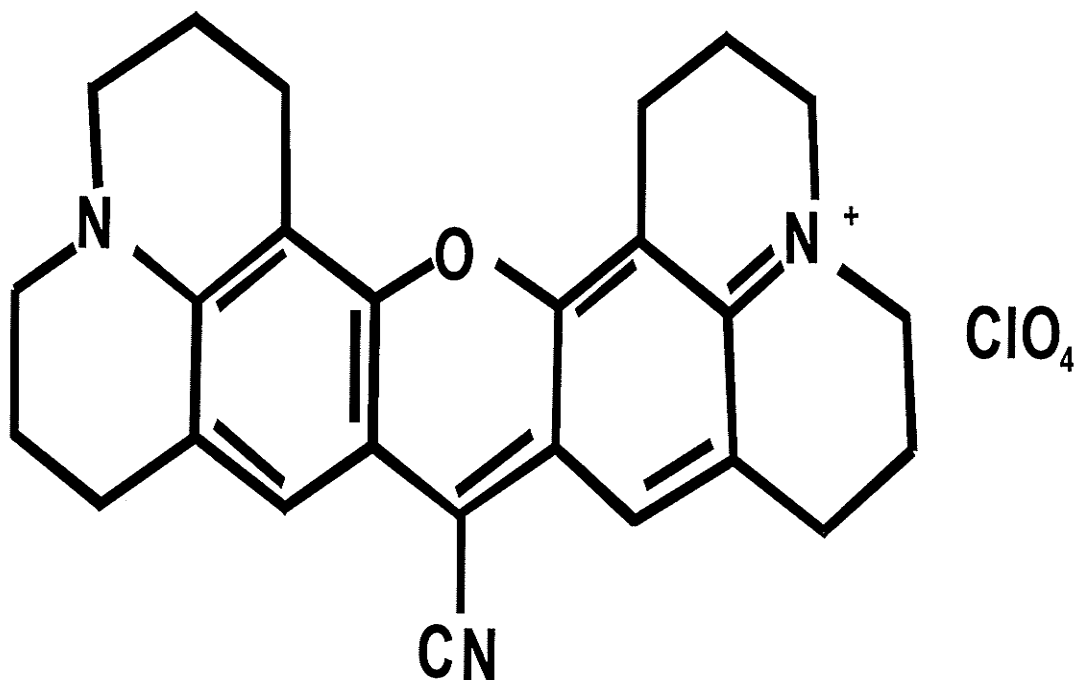


Figure 1-9. Structure of MitoFluor Far Red 680

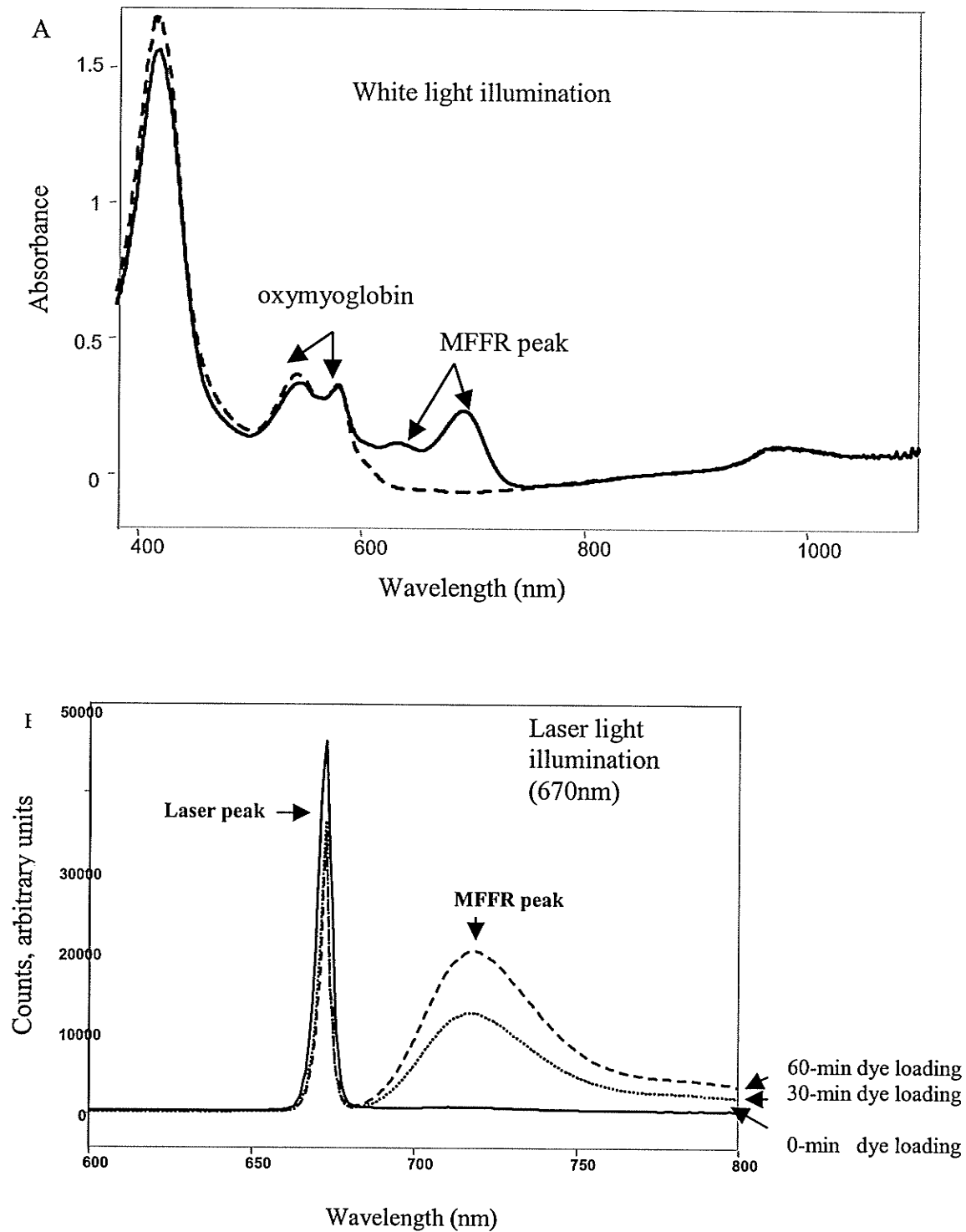


Figure 1-10. Absorbance (A) and fluorescence (B) spectra of MFFR

(Taken from reference 160)

CHAPTER 2

MATERIALS & METHODS

2.1 Materials

Carbonyl cyanide 4-trifluoromethoxyphenylhydrazone (FCCP), glibenclamide (Glib), dimethyl sulfoxide (DMSO), oligomycin, atractyloside, N-2-hydroxyethylpiperazine-N'-2-ethanesulfonic acid (HEPES), ethylenediamine-tetraacetic acid (EDTA), ethylene glycol-bis (β -aminoethyl ether) N, N, N', N'- tetraacetic acid (EGTA), K- gluconate, KH_2PO_4 , NaCl, Na_2SO_4 , Mg-ATP, Mg-ADP, L-glutamate-Na, succinate-Na, carnitine, taurine, creatine, butadione monooxime (BDM), bovine serum albumin (BSA), sodium pyruvate, sodium malate, 0.6% Evans blue solution, and Bicinchoninic Acid (BCA) Protein Assay Kit were purchased from Sigma (St Louis, MO, USA). Sucrose, $\text{MgCl}_2 \cdot 6\text{H}_2\text{O}$ and $\text{CaCl}_2 \cdot 2\text{H}_2\text{O}$ were purchased from BDH (Toronto, ON, Canada). Glucose, KCl, and MgSO_4 were purchased from EM Science (Darmstadt, Germany). Type II collagenase was purchased from Worthington Biochemical Diagnostics (Lakewood, NJ, USA). P-1075 was obtained from Bristol-Myers Squibb (BMS) Pharmaceutical Research Institute laboratories. MitoFluor Far Red 680 (MFFR) and tetramethylrhodamine methyl ester (TMRM) were purchased from Molecular Probes (Eugene, OR, USA). P-1075, Glibenclamide (Glib), MFFR, and TMRM were dissolved in DMSO and diluted in distilled water.

2.1.1 Animal Handling

Male Sprague-Dawley rats weighing 280-320 g were obtained from Charles River (Wilmington, MA, USA). Rats with final weight of 320-370g were used in our experiments after one week quarantine at the NRC animal care facility. Rats were anesthetized by administering pentobarbital (120mg/kg of body weight) and heparin into the cavity of the abdomen. After 2-4 minutes, a toe pinch test was performed to ensure full anesthesia.

2.2 Methods

2.2.1 Mitochondria Isolation

Mitochondria were isolated from the liver of anesthetized male Sprague-Dawley rats by the procedure described by Sordahl, L.A. et al. [161]. Rat liver was quickly removed and rinsed with ice-cold mitochondria isolation buffer containing (in mM) sucrose (250), HEPES-Na (2), and EDTA (1) (pH 7.2-7.4 adjusted with 6M NaOH) in a beaker to remove blood. The liver was weighed after blotting with tissue. Blotted liver was transferred to a petri dish with 10 volumes of fresh ice-cold isolation buffer per gram of tissue and was minced well with surgical scissors. Minced liver was transferred in a teflon-glass homogenizer (inside diameter: 24.89 mm, clearance: 0.18 mm) and homogenized using a pestle pushed back and forth manually. The homogenizer was immersed in ice all the time during homogenization. The homogenate was transferred to centrifuge tubes and was centrifuged at 600 x g for 10 minutes at 0°C in a Sorvall RC-5B Refrigerated Superspeed Centrifuge (DuPont Instruments, DE, USA). The supernatant

was collected and the pellet was discarded. The supernatant was transferred to a centrifuge tube and centrifuged at 8500 x g for 12 minutes at 0°C. The resulting pellet was resuspended with half the volume of ice-cold isolation buffer containing 1mg/ml BSA (washing solution) and centrifuged at 8500 x g for 10 minutes. The supernatant was discarded and the pellet was kept for another washing step. This procedure was performed once more to remove broken mitochondria and undesired cellular micro-debris. 2mL of the ice-cold isolation buffer was added to the resulting pellet to remove the light fluffy layer surrounding the pellet by gentle shaking. The final mitochondrial pellet was resuspended with one volume of resuspension buffer containing (in mM) KCl (120), HEPES-Na (20) (pH 7.2), EGTA (5), and MgSO₄ (1) per gram of initial tissue to yield 30 to 60 mg of protein per 1 mL in a centrifuge tube and stored on ice for protein assay, mitochondrial respiration assay, and MFFR binding and fluorescence assays. Mitochondrial suspensions were used for all measurements immediately except for the protein assay, which was performed later.

2.2.2 Protein Assay

Mitochondrial protein was determined by the Sigma BCA (bicinchoninic acid) Protein Assay Kit. Known concentrations of BSA standards were prepared in the range of 0 to 1000 μ g/mL with 200 μ g intervals by diluting the BSA standards to 100 μ l with distilled water in each tube. Unknown concentrations of mitochondrial protein were prepared in the same manner as BSA standard preparation to determine its concentrations from BSA standard calibration graph. The mixture of reagent A and reagent B containing BCA solution and copper (II) (Cu²⁺) sulfate solution, respectively was prepared as BCA working reagent. 2mL BCA working reagent was added to each tube to

bring total volume to 2.1mL. All tubes were incubated in a water bath for 30 minute periods at 37°C to develop a purple colour. The colour development was the result of the formation of Cu⁺-BCA complex, following reduction of the Cu²⁺ to Cu⁺ in the presence of protein under alkaline condition (Figure 2-1).

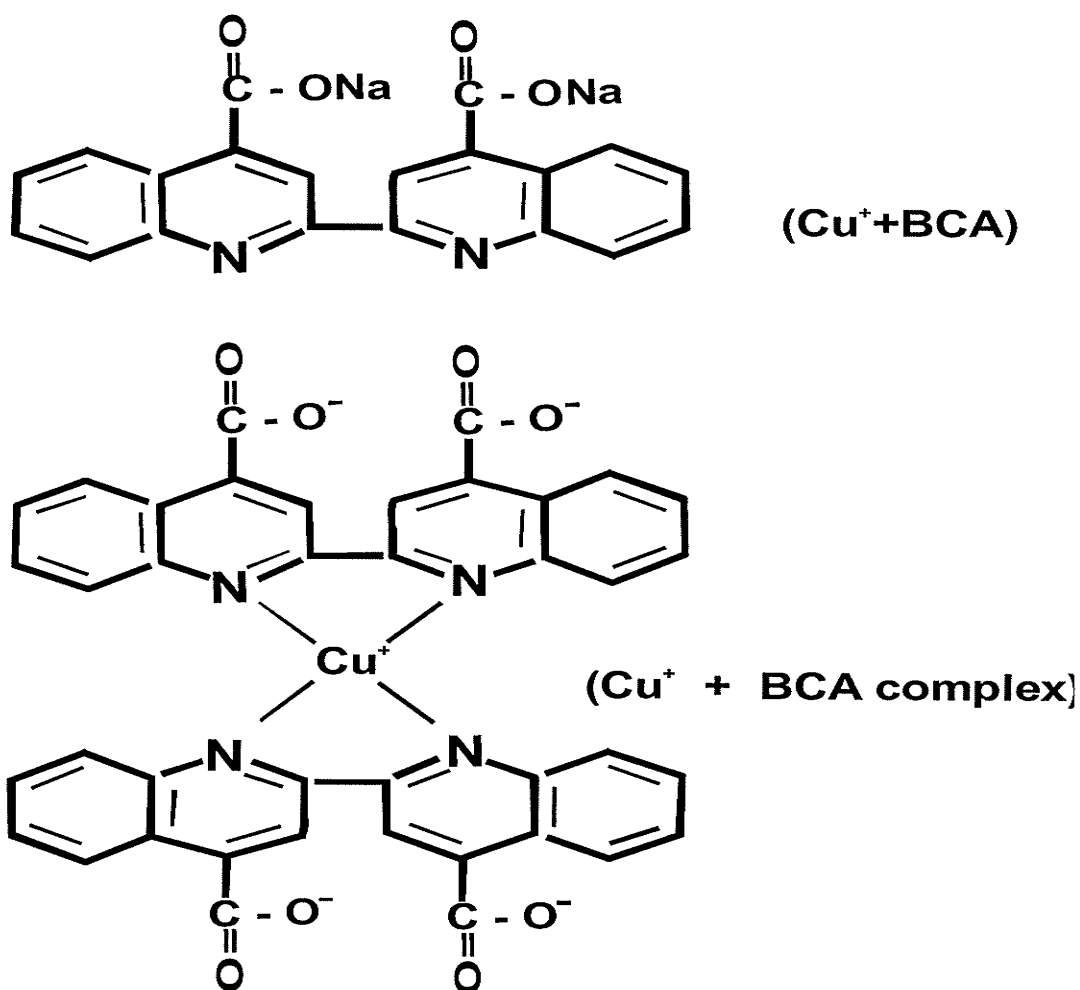
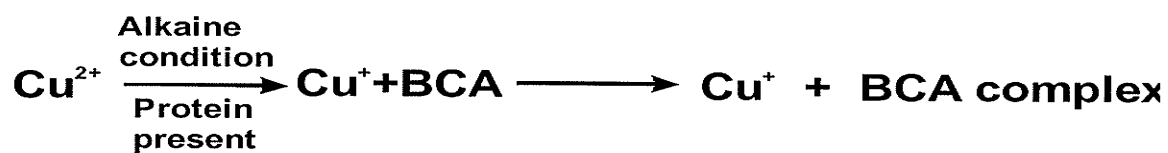


Figure 2-1. The BCA assay. Cu²⁺ sulphate solution contains 4% (w/v) concentration of Cu²⁺ sulphate pentahydrate and BCA solution contains BCA, sodium carbonate, sodium tartarate, and sodium bicarbonate in 0.1 N NaOH. The first reaction is related to the amount of reduction of Cu²⁺ to Cu⁺ proportional to protein present. Cu⁺ binds to four nitrogens (N) of BCA to form the complex which is detected by its purple colour measured spectrophotometrically at 562nm.

A Beckman DU-650 spectrophotometer (Beckman Instruments Inc, ON, Canada) was used to measure absorbance after cooling down tubes to room temperature. A BSA standard curve was obtained by plotting concentration versus absorbance. The unknown concentrations of samples were determined by comparison with the BSA standard curve (straight line). The final concentration of sample was calculated by averaging concentrations of replicate samples.

2.2.3 Measurements of Mitochondrial Respiration

Mitochondrial oxygen consumption was measured using a Clark-type oxygen electrode (Yellow Springs Instruments, OH, USA) at 30°C in the mitochondrial respiration solution containing (in mM) HEPES-Na (20) (pH 7.2), K-gluconate (100), KCl (20), EGTA (1), and KH_2PO_4 (2). 5mM glutamate-Na plus 5mM malate or 10 mM succinate were used as substrates for mitochondrial oxidation. Briefly, a Clark-type oxygen electrode, referred as the oxygen probe, was capped with a membrane permeable to oxygen (O_2), which diffuses to a platinum cathode where it is reduced, generating a current which is proportional to O_2 concentration. The electrode was immersed in a chamber containing a magnetic stirring bar, medium, and mitochondrial sample. The oxygen probe was connected to an oxygen monitor interfaced with a linear recorder, which provided oxygen consumption graphs. The O_2 concentration present in the sample is proportional to atmospheric O_2 partial pressure, which was monitored. The system was calibrated using a $\text{Na}_2\text{S}_2\text{O}_5$ solution with 0% O_2 content and 100% dissolved oxygen content in the mitochondrial respiration solution. Respiration measurements began in 100% saturated mitochondrial respiration solution containing oxidizable substrates, followed by the addition of 0.5mg/mL of mitochondria, which caused slow O_2 uptake

(state 2). Subsequently, the addition of 0.3mM Mg-ADP was used to initiate state 3 respiration which corresponds to O₂ utilization for synthesis of ATP from ADP and P_i. State 3 respiration is typically much faster than state 2 respiration. After conversion of all ADP into ATP, respiration returned to the level of state 2 (called state 4) which slowed down O₂ utilization. At the end of the assay, 1μM FCCP was added to obtain uncoupled respiration and completely deplete O₂. The respiration rates were calculated from O₂ content of 200nmol O₂/mL in 100% oxygen saturated solution (at 30°C and 760mmHg barometric pressure) and expressed in nmol O₂/min/mg. The respiratory control index (RCI) was calculated as a ratio of state 3 to state 2 respiration rates and mitochondria with RCI above 4 were used for all experiments.

To determine the toxic effect of MFFR on mitochondrial respiration, the respiration rate was measured in the presence of varying concentrations of MFFR with 5mM glutamate plus 5mM malate or 10mM succinate as oxidizable substrates to assess NAD⁺-dependent and independent (complex I and II, respectively) respiration. In addition, varying concentrations of P-1075, a mitochondrial ATP-sensitive potassium (mito- K_{ATP}) channel opener were used to assess its effect on mitochondrial respiration and coupling since it was known to affect $\Delta\Psi_m$ [4].

2.2.4 Isolation of Cardiomyocytes

2.2.4.1 Solutions

Cardiomyocyte isolation required six isolation solutions for the experiment. Solution A, a basic isolation solution contained (in mM) HEPES-Na (25) (pH 7.4), NaCl (118), KCl (4.7), MgSO₄ (1.2), glucose (15), carnitine (2), taurine (5), and creatine (2). Solution E was mixture of solution A and 15mM BDM. Solution B, a collagenase

perfusion solution, contained solution E and 1mg/mL Worthington collagenase type II (240U/mg). Solution C, an incubation solution, was composed of solution B and 10mg/mL BSA. Solution D, a rinse solution, contained solution E and 10mg/mL BSA. Solution F, a second rinse solution, was composed of solution A and 10mg/mL BSA. O₂ was dissolved in all solutions by gentle bubbling for 10 minutes with a Pasteur pipette attached to an O₂ tank through a tube. Solutions were incubated at 37°C before use.

Table 2-1. Composition of buffers for cardiomyocyte isolation

Solution						
Chemicals	A	B	C	D	E	F
HEPES-Na, mM	25	→	→	→	→	→
NaCl, mM	118	→	→	→	→	→
KCl, mM	4.7	→	→	→	→	→
MgSO ₄ , mM	1.2	→	→	→	→	→
Glucose, mM	15	→	→	→	→	→
Carnitine, mM	2	→	→	→	→	→
Taurine, mM	5	→	→	→	→	→
Creatine, mM	2	→	→	→	→	→
BDM, mM	-	15	15	15	15	-
Worthington collagenase type II mg/mL	-	1.0	1.0	-	-	-
BSA, mg/mL	-	-	10	10	-	10

2.2.4.2 Isolation procedure

Cardiomyocytes were isolated from anesthetized male Sprague-Dawley rat hearts by the collagenase perfusion procedure [162-164]. Briefly, a heart excision was performed by opening the thoracic cavity. The excised heart was weighted and immersed in ice-cold solution A. The aorta was clamped to the cannula with a small clip and tied off using a ligature. Immediately, the heart was perfused in a Langendorff perfusion apparatus with 60mL solution E oxygenated with O₂ at constant pressure (60mmHg) at 37°C for 5 minutes to remove blood. Then, the heart was perfused with 50mL solution B re-circulated by peristaltic pump for 20-30 minutes at 37°C to soften tissue. The softened tissue after collagenase digestion was treated with 10mL solution C in a petri dish and cut into small pieces with surgical scissors. Minced tissue was transferred to a beaker and 20mL solution C was added. The remaining tissue was incubated at 37°C for 10 minutes, followed by shaking it on a VWR S-500 Orbital Shaker (VWR Inc., PA, USA) at 1-2 setting and gentle aspiration periodically with a pipette for cell dissociation. The resulting tissue was filtered through a nylon mesh with 60µm mesh size to separate cells from incompletely digested tissue. The cells were rinsed by centrifugation and resuspension of the pellet four times to remove collagenase from cells. Cardiomyocytes were transferred to centrifuge tubes and were centrifuged at 100 x g for 5 minutes at room temperature in a Sorvall RC-5B Refrigerated Superspeed Centrifuge. The supernatant was removed by aspiration with a water-jet vacuum pump and the pellet was resuspended with 30mL solution D by gentle shaking. The centrifugation was repeated in the same manner. Cardiomyocytes were resuspended with solution F (30mL) and A (10mL) and centrifuged twice, respectively. Finally cardiomyocytes were resuspended in

10mL solution D. A 300 μ L pellet suspension in solution A was collected for protein assay performed by BCA. Final solution D suspensions were stored in a water incubator at 37°C under conditions of gentle shaking on a VWR S-500 Orbital Shaker and periodic aeration with a pipette. Aliquotes of this suspension were used for all measurements.

Viability of cardiomyocytes was determined by observation of cellular morphology. Cells were counted for cell viability using a hemocytometer and a light microscope. Cells were placed under the light microscope with 10x magnification and counted in three out of the nine squares in the hemocytometer. Living and dead cells were shaped as rods and spheres respectively. Samples were taken three times for averaging cell count. Cell yield and viability were expressed in number of total cells /mg protein and as a percentage of a number of living cell to the total cell number, respectively.

2.2.5 Isolation of Hepatocytes

Hepatocytes were isolated from livers of anesthetized male Sprague-Dawley rats by the cannulation of the hepatic portal vein and a collagenase perfusion procedure [165-167]. After anesthetizing the rat and opening the abdomen, the hepatic portal vein was marked with a ligature and the liver was excised with surgical scissors. Excised liver was placed in a petri dish and excess blood was removed from the liver with gauze. The vein was cut halfway *in situ* to open for cannulation. The liver was trimmed by removing undesired connective tissue and immersed in a cold-ice hepatocyte basic buffer containing (in mM) NaCl (140), KCl (6.7), and HEPES-Na (3) (pH 7.4). The liver was cannulated and tied off using a ligature. Immediately, the liver was perfused in a Langendorff - perfusion apparatus with 150 mL oxygenated hepatocytes basic buffer at

25mL/min constant flow for 5-6 minutes at 37°C to remove blood. The liver was perfused for collagenase digestion with 50mL collagenase buffer containing (in mM) NaCl (117.7), KCl (6.7), HEPES-Na (30) (pH 7.6), CaCl₂· 2H₂O (4.8), and 0.5 mg/mL Worthington collagenase type II (240U/mg) re-circulated by peristaltic pump for 10 minutes at 37°C to digest tissue. Poorly perfused liver was trimmed away and the rest of the tissue was weighed. The softened liver was transferred to a petri dish and immersed in 20mL HC washing/resuspension buffer containing (in mM) NaCl (130), KCl (5.4), HEPES-Na (30) (pH 7.4), CaCl₂· 2H₂O (1.2), MgCl₂· 6H₂O (0.6), KH₂PO₄ (1.1), Na₂SO₄ (0.7), and glucose (5.5). The tissue was gently shaken with forceps and minced with surgical scissors. Minced tissue was transferred to a beaker and treated further with 20mL HC washing/resuspension buffer. The resulting tissue was incubated at 37°C for 15 minutes, followed by shaking on a VWR S-500 Orbital Shaker at 1-2 setting and aspiration with a pipette periodically for cell dissociation. The sample was placed on ice at 4°C, shaken for 5 minutes, and filtered through a nylon mesh with 60µm pore size to separate cells from incompletely digested tissue. The bottom of the beaker was rinsed with 10mL hepatocyte washing/resuspension buffer which was then poured through the nylon mesh. The cell purification process was performed as a series of centrifugations and resuspensions of pellet. Hepatocytes were transferred to centrifuge tubes and were centrifuged at 50 x g for 5 minutes at 4°C in a Sorvall RC-5B Refrigerated Superspeed Centrifuge. The supernatant was removed by aspiration with a water-jet vacuum pump and the pellet was resuspended with 40mL hepatocytes washing/resuspension buffer by gentle shaking. The sample was centrifuged and resuspended three more times. After the last resuspension, the resulting pellet was resuspended in 50mL hepatocyte

washing/resuspension buffer and transferred to a beaker. A 0.2mL sample was collected for protein assay performed by BCA. Hepatocyte suspensions were stored in a water incubator at 37°C under conditions of gentle shaking on a VWR S-500 Orbital Shaker and periodic aeration with a pipette. Samples were used immediately for all measurements.

Cell viability was determined using the Evans blue exclusion test. 100 μ L of cell sample was mixed with 300 μ L 0.6% Evans blue solution in saline (0.9%) to bring concentration of Evan blue solution to 0.45%. Cells were counted for cell viability using a hemocytometer and a light microscope. Cells were placed under the light microscope with magnification (10x) and counted in three out of the nine squares in the hemocytometer. Non-viable cells were colored blue and viable cells were not stained. Samples were taken three times for averaging cell count. Cell yield and viability were expressed as a number of total cells /mg protein and as a percentage of a number of living cell to the total number, respectively.

2.2.6 Measurements of MFFR Binding in Isolated Rat Liver

Mitochondria, Cardiomyocytes, and Hepatocytes

MFFR binding to freshly isolated mitochondria was performed by incubation, separation by centrifugation, and determination of absorbance difference (ΔA) to evaluate $\Delta\Psi_m$. Mitochondria (0.2 mg/mL) were incubated both in 1mL of high K^+ (120mM) incubation buffer analogous to intracellular medium, containing (in mM) 20 HEPES-Na (pH 7.2), 20 KCl, 100 K-gluconate, 1 EGTA, and 1 $MgSO_4$ and in 1mL of sucrose incubation iso-osmotic buffer containing (in mM) 240 Sucrose, 20 HEPES-Na (pH 7.2), 1 EGTA, and 1 $MgSO_4$ with final concentrations of 1 or 5 μ M of MFFR for 5 minutes at

30°C with 5mM Mg-ATP in the presence or absence of 5mM glutamate-Na plus 5mM succinate-Na as substrates for mitochondrial energization. In addition, incubations were performed in the presence or absence of 1 μ M FCCP (mitochondrial uncoupler depolarizing $\Delta\Psi_m$), 20 μ M P-1075 (mito- K_{ATP} opener depolarizing $\Delta\Psi_m$), 5 μ M Glib (mito- K_{ATP} blocker), 20 μ M P-1075 plus 5 μ M Glib, 2 μ g/mL oligomycin (ATP synthase inhibitor), 10 μ M atractyloside (ATP/ADP translocase inhibitor), and 5 μ L/mL DMSO (0.5%) used for preparation of stock solutions of MFFR.

All samples were prepared in 25 mm diameter open scintillation vials which were shaken on a VWR S-500 Orbital Shaker at 1-2 setting to supply oxygen to mitochondrial samples during incubation. The samples were rapidly cooled and transferred to 1.5mL Eppendorf micro-centrifuge tubes. The samples were centrifuged at 10,000 x g for 5 minutes in a Micromax RF micro-centrifuge (ThermoIEC, FL, USA) at 0°C. Supernatant was transferred to a new Eppendorf micro-centrifuge tube using a 100-1000 μ l Eppendorf pipette. MFFR in the mitochondrial pellet was extracted in 1 mL 95% ethanol (EtOH) and kept in a dark room (due to its photosensitivity) for 30 minutes. The MFFR extract was transferred to a new Eppendorf micro-centrifuge tube. Each sample was transferred to a plastic spectrophotometer cuvette and placed into a cuvette holder in Beckman DU-650 spectrophotometer (Beckman Instruments, ON, Canada). Beckman DU-650 spectrophotometer was turned on for 30 minutes to warm up before use. One mL of mitochondrial incubation buffer and 1mL of 95% EtOH were used as a blank to get zero absorbance (A) for supernatant and MFFR extract respectively. ΔA values of MFFR were measured in mitochondrial extract at 683nm and the supernatant at 696nm. The

MFFR concentration (C) was calculated by dividing A by the MFFR extinction coefficient ϵ ($99 \text{ mM}^{-1} \text{ cm}^{-1}$), and path-length (1cm) according to the Beer-Lambert law

$$C = A / (\epsilon \times l) \quad (1)$$

and expressed in $\mu\text{mole/L}$ (μM). It is assumed that there is equilibrium distribution of MFFR between intra and extra-mitochondria spaces, governed by the Nernst equation. A correction for membrane binding introduced into the Nernst equation allowed us to calculate $\Delta\Psi_m$ in isolated rat mitochondria using a ratio of MFFR bound (nmol/mg) to free (nmol/mL) in the presence of agents such as FCCP, P-1075, Glib, oligomycin, atractyloside, or DMSO shown as:

$$(\text{bound/free})_{\text{agent}} = (V_{\text{matrix}} + P \times V_{\text{membrane}}) \times \exp(-\Delta\Psi_m \times F/RT), \quad (2)$$

where V_{matrix} and V_{membrane} are volumes of matrix and membrane, respectively, P is a partition coefficient between the matrix and membrane, F, Faraday constant, R, gas constant and T, absolute temperature.

Thus,

$$(\Delta\Psi_m)_{\text{agent}} - (\Delta\Psi_m)_{\text{control}} = 59 \times (\log ([\text{bound/free}]_{\text{control}} / [\text{bound/free}]_{\text{agent}})) \quad (3)$$

We assume that there are no significant changes in V_{matrix} and P, upon binding of these agents.

To compare MFFR to a dye commonly used for $\Delta\Psi_m$ measurements in mitochondria, mitochondria were energized with 5mM glutamate plus 5mM succinate and 5mM Mg-ATP plus 10mM PCr plus 2U/mL creatine kinase in the presence of both,

TMRM (0 to 20 μ M) and MFFR (20 to 0 μ M) in 1mL of high K⁺ incubation buffer +/- 1 μ M FCCP.

TMRM (μ M)	0	5	10	15	20
MFFR (μ M)	20	15	10	5	0

ΔA for TMRM was determined in supernatant and extract at 554 and 551 nm ($\epsilon = 107$ mM⁻¹cm⁻¹), respectively, simultaneously with ΔA for MFFR determined at 696 and 683nm in the same manner. TMRM and MFFR contents were calculated using equation 1. $\Delta\Psi_m$ was calculated both from TMRM and MFFR distributions in the same manner as for MFFR alone using equation 3:

$$(\Delta\Psi_m)_{+FCCP} - (\Delta\Psi_m)_{control} = 59 \times (\log ((\text{bound/free})_{control}) / (\text{bound/free})_{+FCCP})$$

where $(\Delta\Psi_m)_{+FCCP}$ is 0 mitochondrial membrane potential in the presence of FCCP and $(\Delta\Psi_m)_{control}$ is a control value in the absence of FCCP.

MFFR binding to cardiomyocytes and hepatocytes was performed in a similar manner to that described for mitochondria although in different media. Cardiomyocytes (0.2-0.9 mg protein/mL) were incubated with 10mM glucose plus 1mM pyruvate by shaking on a VWR S-500 Orbital Shaker at 1-2 setting for 5 minutes at 35°C both in 1mL of CMC high K⁺ incubation buffer containing (in mM) 120 KCl, 20 HEPES-Na (pH 7.4), 1 EGTA, and 1 MgSO₄ and 1mL of cardiomyocyte low K⁺ incubation buffer containing (in mM) 4.7 KCl, 118 NaCl, 25 HEPES-Na (pH 7.4), and 1.2 MgSO₄ in the presence or absence of 1 μ M FCCP. Hepatocytes (0.2- 0.9 mg/mL) were incubated with 11 mM glucose in the same manner both in hepatocyte washing/respiration buffer (low

K⁺ buffer) and in cardiomyocyte high K⁺ incubation buffer. The high K⁺ incubation buffer allowed isolated cells to depolarize and bring the plasma membrane potential to near zero. Simultaneously, MFFR was added to bring the MFFR concentration to 1 μ M and then the samples were incubated for 5 minutes to equilibrate with MFFR. Then, samples were centrifuged at 100 x g for 5 minutes at 0°C in a Micromax RF micro-centrifuge to separate supernatant from cells. MFFR bound to the cells was extracted with 1mL 95% EtOH for 30 minutes and the cells were centrifuged to separate MFFR extract from the cells. Supernatant and MFFR extract were taken for measurement of MFFR fluorescence intensity at 708-720nm wavelength using a spectrophotometric arrangement developed in our laboratory for detecting low concentration of MFFR in sample (Figure 2-2).

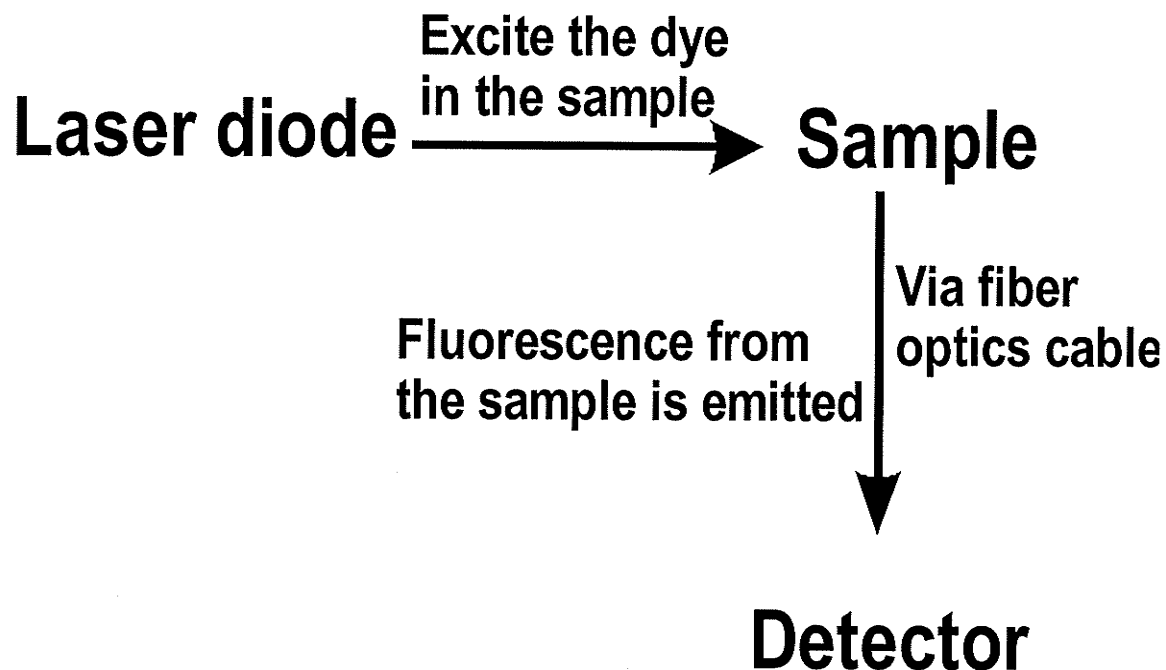


Figure 2-2. Spectrophotometric arrangement for detecting MFFR fluorescence. A laser diode is used to excite MFFR in the sample at 670nm. Fluorescence from the sample is emitted, which is detected at 90° by detector via a fiber optic cable at appropriate wavelength, (708-720nm).

To calculate MFFR content in the samples, MFFR standards were prepared in the range of 0 to $1\mu\text{M}$ by diluting the MFFR standards to 3mL of cell incubation buffer and 3mL 95%EtOH in a cuvette. MFFR content in sample was calculated using a MFFR standard calibration curve plotted as MFFR fluorescence intensity versus MFFR concentration. The ratio of bound to free MFFR in energized (E) and uncoupled (U) samples was used to determine the distribution of MFFR governed by $\Delta\Psi_m$ in cells with correction for cell viability. Binding ratios for viable cells were calculated assuming that non-viable cells were uncoupled, using equation 4, which was rearranged to equation 5. If we assume that non-viable cells were uncoupled, then

$$(\text{bound /free})_E = (\text{bound /free})_{\text{viable}} \cdot X + (\text{bound /free})_U \cdot (1 -X) \quad (4)$$

where $(\text{bound/free})_E$ and $(\text{bound/free})_U$ were obtained in the experiment. Hence, the ratio for actual viable cells was defined as:

$$(\text{bound /free})_{\text{viable}} = ((\text{bound /free})_E - (\text{bound /free})_U \cdot (1 -X)) / X \quad (5)$$

2.2.7 Measurements of MFFR Fluorescence in Isolated Rat Liver

Mitochondria, Cardiomyocytes, and Hepatocytes

MFFR fluorescence was determined in mitochondria, cardiomyocytes, and hepatocytes using the same spectrophotometric arrangement as for the MFFR binding by cardiomyocytes and hepatocytes samples. To measure MFFR fluorescence in mitochondria, cardiomyocyte, and hepatocyte as a function of $\Delta\Psi_m$, incubation buffers were prepared for mitochondria, cardiomyocytes, and hepatocytes in a disposable plastic cuvette (1cm x 1cm x 4cm) placed in a cuvette holder: mitochondrial high K^+ incubation

buffer with 5mM glutamate plus 5mM succinate was used for mitochondria.

Cardiomyocyte high K^+ incubation buffer or low K^+ incubation buffer with 11mM glucose plus 1mM pyruvate were used for cardiomyocytes. Cardiomyocyte high K^+ and low K^+ buffer or incubation buffer with 11 mM glucose were used for hepatocytes.

Freshly isolated mitochondria, cardiomyocytes, and hepatocytes were diluted 10 fold in a cuvette containing 3mL of high or low K^+ buffers, followed by continuous gentle stirring with magnetic stir bar. Final concentrations of mitochondria, cardiomyocytes, and hepatocytes were 0.03-0.5 mg/mL, 0.3-0.9 mg/mL, and 0.04-1.24 mg/mL, respectively.

Measurements of MFFR fluorescence were performed by exciting the sample in the given incubation buffer containing MFFR, oxidizable substrates and mitochondria, cardiomyocytes, or hepatocytes in a cuvette using a 670 nm laser diode (3 mW, NVG Inc, GA, USA) placed in a hole on the cuvette holder and by detecting the fluorescence emission at 90° using a spectrometer (Control Development, IN, USA) via $600\mu\text{m}$ in diameter fiber optic cable (Ocean Optics Inc., FL, USA) capped with a 695 nm high pass filter (CRG 695) to minimize scattered laser light intensity and placed in the other hole perpendicular to the hole for the laser diode. Before the addition of mitochondria, cardiomyocytes, and hepatocytes, $1\mu\text{M}$ MFFR fluorescence spectrum was obtained as a reference using the CDI Spectrograph software (Control Development, IN, USA) with an integration time 1.0 second and averaging 20 measurements. Additional MFFR was added after the addition of mitochondria, cardiomyocytes, or hepatocytes to maintain $1\mu\text{M}$ of MFFR concentration in the cuvette. Fluorescence spectra were saved every 20 seconds for 5 minutes. After 5 minute recording, FCCP was added to a final concentration of $1\mu\text{M}$ to collapse $\Delta\Psi_m$. Measurement was performed by taking spectra

every 20 seconds for 5 minute periods in the presence of $1\mu\text{M}$ FCCP. The measurements were repeated twice with two samples and averaged. Spectra were analyzed using Grams/32 Version 4.11 computer program (Galactic Industries Corp, NH, USA) for spectral data analysis. After the fluorescence measurement, samples were taken for the determination of MFFR binding. MFFR binding protocol was the same as that described in 2.2.6 section.

2.2.8 Measurement of MFFR Fluorescence at Various pH levels

MFFR fluorescence was measured at various pH levels to test whether pH affects MFFR fluorescence spectrum. Three mL of cardiomyocyte high K^+ incubation buffer was titrated with 6M NaOH to bring pH in the range of 5.34 to 9.08 and transferred to a cuvette placed in a cuvette holder. MFFR in the range of 0 to $30\mu\text{M}$ final concentrations was added to the cuvette. MFFR fluorescence was measured using the same set up as for fluorescence measurements in mitochondria and cells. Spectral data were analyzed using Grams/32 Version 4.11.

2.2.9 Statistics

ANOVA (one-way analysis) was used for determination of statistically significant differences at $P < 0.05$. The mean \pm S.E. are shown.

CHAPTER 3

RESULTS

3.1 Studies of MFFR Binding in Isolated Rat Liver

Mitochondria, Cardiomyocytes, and Hepatocytes

3.1.1 Relationship between $\Delta\Psi_m$ and MFFR Binding

To investigate if the amount of MFFR bound to mitochondria is dependent on $\Delta\Psi_m$, isolated mitochondria were energized and incubated with 5 μM MFFR and various agents to manipulate $\Delta\Psi_m$. The studies were performed in high K^+ incubation buffer to mimic intracellular medium and also in K^+ -free sucrose incubation iso-osmotic medium which is frequently used in mitochondrial studies. The results of these studies are summarized in Table 3-1. In control experiments, the contents of MFFR inside energized rat liver mitochondria were high and similar in high K^+ and sucrose buffers. The concentrations of MFFR outside the mitochondria were low and similar in both high K^+ and sucrose buffer. The addition of FCCP (1 μM), a mitochondrial uncoupler, in the assay media resulted in a 10 fold decrease in mitochondrial contents of MFFR in the high K^+ and sucrose media. Simultaneously, there was 22- fold increase in the MFFR concentration outside the mitochondria in both media. These results indicated that the distribution of MFFR between the media and mitochondria is dependent on $\Delta\Psi_m$.

Table 3-1. MFFR bound and free in rat liver mitochondrial suspensions in two isolation media

Group	High K ⁺ (120mM) medium		Sucrose medium	
	bound ^a , nmol/mg	free ^b , nmol/mL	bound ^a , nmol/mg	free ^b , nmol/mL
Control, n = 30	26.57 ± 0.58	0.14 ± 0.01	26.64 ± 0.45	0.14 ± 0.01
FCCP, n = 30	2.20 ± 0.11	3.08 ± 0.12	2.02 ± 0.17	3.16 ± 0.13
<i>P vs. Control</i>	2.48×10^{-37}	3.58×10^{-18}	2.06×10^{-21}	7.99×10^{-15}
Oligomycin, n = 3	8.62 ± 0.90	2.67 ± 0.04	7.93 ± 1.39	2.63 ± 0.31
<i>P vs. Control</i>	2.30×10^{-9}	3.13×10^{-20}	4.45×10^{-6}	2.42×10^{-8}
Atractyloside, n = 3	10.89 ± 1.76	2.14 ± 0.26	6.68 ± 0.60	2.42 ± 0.19
<i>P vs. Control</i>	3.35×10^{-11}	2.71×10^{-10}	1.48×10^{-6}	7.61×10^{-10}
P-1075, n = 30	24.51 ± 0.42	0.33 ± 0.08	24.14 ± 0.72	0.22 ± 0.04
<i>P vs. Control</i>	0.014	0.028	0.014	0.025
<i>P vs. P-1075/Glib</i>	0.03	0.05	0.47	0.076
Glib, n = 22	25.62 ± 0.43	0.16 ± 0.02	25.01 ± 0.43	0.16 ± 0.03
P-1075/Glib, n = 21	26.01 ± 1.39	0.12 ± 0.01	25.38 ± 0.03	0.11 ± 0.02
DMSO, n = 19	24.72 ± 0.50	0.12 ± 0.01	23.89 ± 2.00	0.17 ± 0.04

Mitochondria were energized by simultaneous ATP hydrolysis (5mM ATP) and respiration (5mM glutamate and 5mM succinate).

a. Referred to the amount of MFFR accumulated in mitochondria and calculated from concentration of MFFR bound to mitochondria described in 2.2.6 of Materials and Methods section, divided by protein concentration (0.2mg/mL) used in this experiment.

b. Based on the amount of MFFR in extra-mitochondrial medium and was determined as described in 2.2.6 of Materials and Methods section.

Data are presented as means ± S.E.

Oligomycin ($2\mu\text{g/mL}$), an ATP synthase inhibitor, and atractyloside ($10\mu\text{M}$), an ATP/ADP translocase inhibitor, both resulted in a partial decrease in MFFR binding compared to the control group. These two agents caused a 3.5 fold decrease in the amount of MFFR in the mitochondria and a 20 fold increase in the media irrespective of the incubation medium. P-1075 ($20\mu\text{M}$) which opens mito- K_{ATP} and may reduce the potential difference across mitochondrial membrane did not cause changes in the MFFR binding to mitochondria both in the high K^+ and sucrose media, however, increased its concentration in the media (2.5- fold). Glibenclamide (Glib, $5\mu\text{M}$) mito- K_{ATP} blocker had no effect on MFFR distribution by itself. However, glib prevented the MFFR releasing effect of P-1075. DMSO (0.5%) that was used for preparation of stock solutions of MFFR did not affect the distribution of MFFR between mitochondria and media.

To calculate $\Delta\Psi_m$ in isolated rat liver mitochondria, the ratio of bound to free MFFR was determined in the presence of agents and subsequently used to calculate $\Delta\Psi_m$. With this purpose, MFFR bound per mg was multiplied by mitochondria concentration (0.2 mg/mL) and divided by the amount in the incubation medium ($\text{nmol/mL} \times 1\text{ mL} = \text{nmole}$): Bound x mitochondria concentration / Free = dimensionless. The average ratios of bound MFFR to free (bound/free) in energized mitochondria in high K^+ was 39.66 ± 2.08 ($n=30$) and 38.16 ± 4.66 ($n=30$) in the sucrose medium (Figure 3-1). These two ratios were not significantly different ($P>0.05$). Addition of FCCP to mitochondrial suspensions caused a decrease in ratios to 0.15 ± 0.01 and 0.18 ± 0.01 in high K^+ and sucrose media, respectively. Oligomycin, atractyloside, and P-1075 decreased the ratio to 0.65 ± 0.08 , 1.17 ± 0.25 , and 33.45 ± 2.00 in high K^+ medium respectively. In the

sucrose medium, oligomycin, atractyloside, and P-1075 decreased the ratio to 0.61 ± 0.16 , 0.56 ± 0.09 , and 32.63 ± 2.54 . The addition of Glib, P-1075 and Glib, or DMSO did not significantly change bound / free compared to the control ($P > 0.05$).

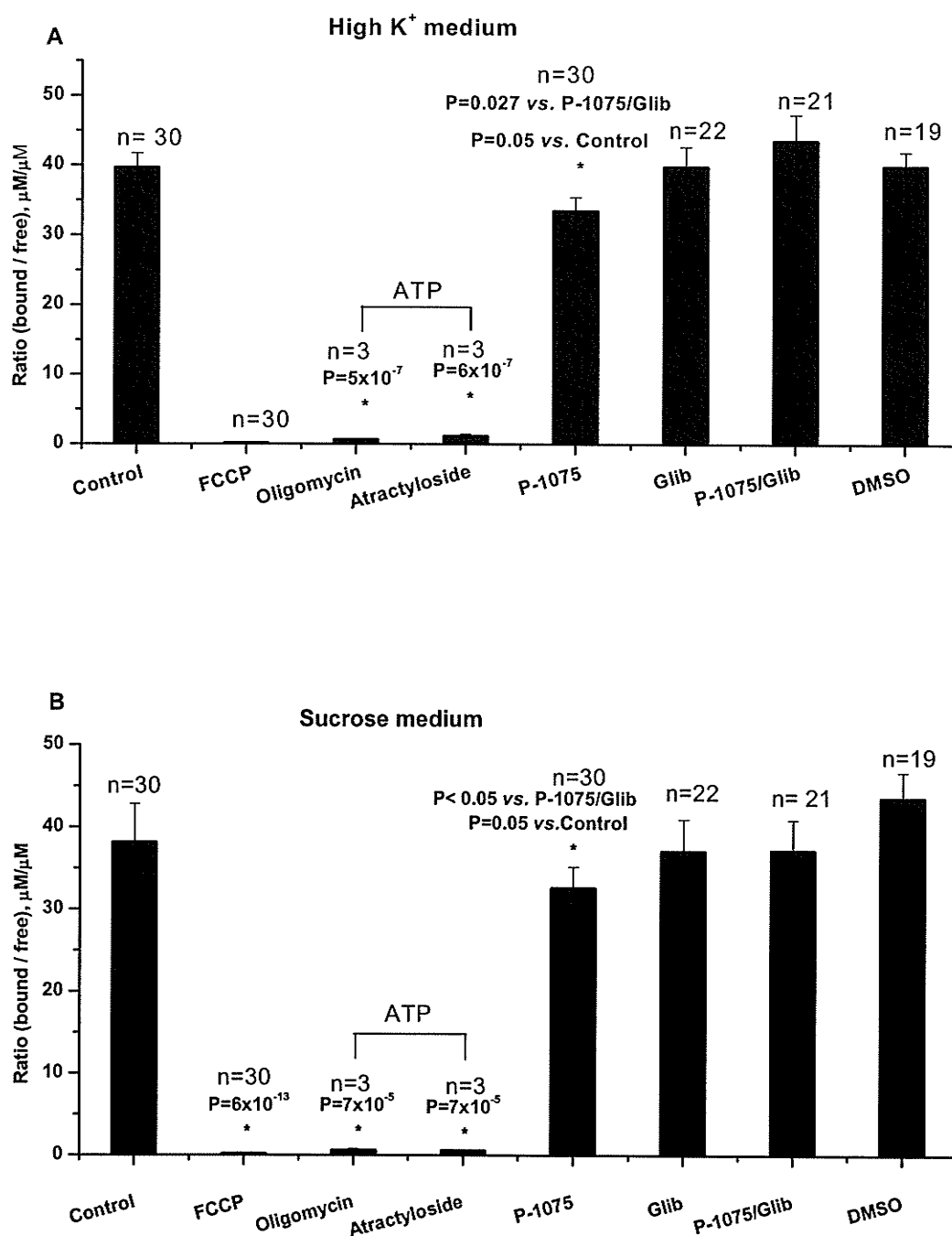


Figure 3-1. Ratio of MFFR bound to free in rat liver mitochondria (0.2mg/mL) in high K⁺ medium (A) and sucrose medium (B) at 30°C in the presence of 1 μM FCCP (n= 30), 2 $\mu\text{g}/\text{mL}$ oligomycin (n=3), 10 μM atractyloside (n=3), 20 μM P-1075 (n=30), 5 μM Glib (n=22), 20 μM P-1075 and 5 μM Glib (n=21), and 0.5% DMSO (n=19). Energized mitochondria (by 5mM ATP in the presence or absence of 5mM glutamate and 5mM succinate) were incubated with 5 μM MFFR. P is shown for data comparisons between control and a modulator. Data are presented as means \pm S.E.

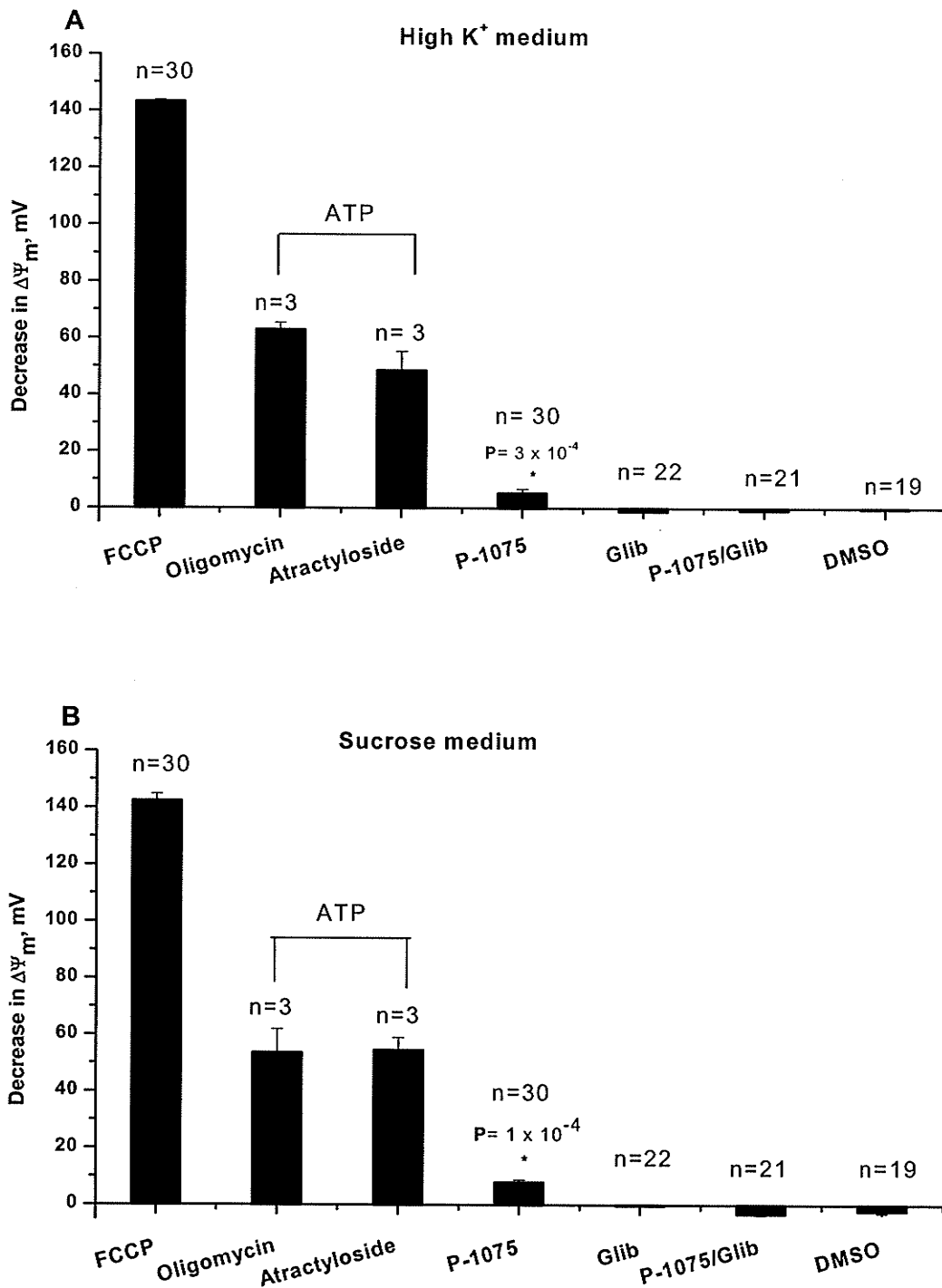


Figure 3-2. Decrease in $\Delta\Psi_m$ in rat liver mitochondrial suspension in high K⁺ medium (A) and sucrose medium (B). $\Delta\Psi_m$ was calculated as described in 2.2.6 of Materials and Methods section. Changes in $\Delta\Psi_m$ are expressed relative to the control. P values are shown for data comparison between P-1075 and P-1075 + Glib.

$\Delta\Psi_m$ was calculated from the bound/free values obtained above (Figure 3-1) according to the Nernst equation (section 2.2.6.). FCCP depolarized $\Delta\Psi_m$ by 143 ± 0.74 and 142 ± 2.55 mV in high K^+ and sucrose media, respectively (Figure 3-2). Oligomycin and atractyloside caused a less considerable decrease in $\Delta\Psi_m$ by 62.8 ± 2.62 and 48.5 ± 6.80 mV in high K^+ medium, respectively. In sucrose medium, oligomycin and atractyloside produced similar effects on decreasing $\Delta\Psi_m$ by 53.6 ± 8.42 and 54.6 ± 4.45 mV, respectively. P-1075 induced a slight depolarization of $\Delta\Psi_m$ by 5.19 ± 1.46 in high K^+ medium and 7.82 ± 0.93 mV in sucrose medium. However, Glib reversed the effects of P-1075, while Glib alone and DMSO did not change $\Delta\Psi_m$. Similar decreases in $\Delta\Psi_m$ by P-1075 both in high K^+ and sucrose (free- K^+) media indicate that P-1075 effects are K^+ -independent. Therefore, unknown mechanisms other than K_{ATP} channels are involved.

To investigate the effects of substrates on $\Delta\Psi_m$, mitochondria were energized by different substrates in the absence and presence of FCCP. ATP hydrolysis was induced by incubation with ATP, respiration induced by glutamate and succinate, and ATP hydrolysis and respiration were induced by incubation with ATP plus glutamate plus succinate. The results from this study are shown in Figure 3-3. The addition of FCCP to the mitochondria energized by ATP hydrolysis in high K^+ media decreased the $\Delta\Psi_m$ by 88.5 ± 7.77 mV. In sucrose medium, this decrease was 81.8 ± 9.80 mV. In mitochondria energized by respiration, FCCP decreased $\Delta\Psi_m$ by 104 ± 0.04 and 104 ± 5.75 mV in high K^+ and sucrose media, respectively. In mitochondria energized by both ATP hydrolysis and respiration, FCCP decreased $\Delta\Psi_m$ by 143 ± 0.74 and 142 ± 2.55 mV in high K^+ and sucrose media.

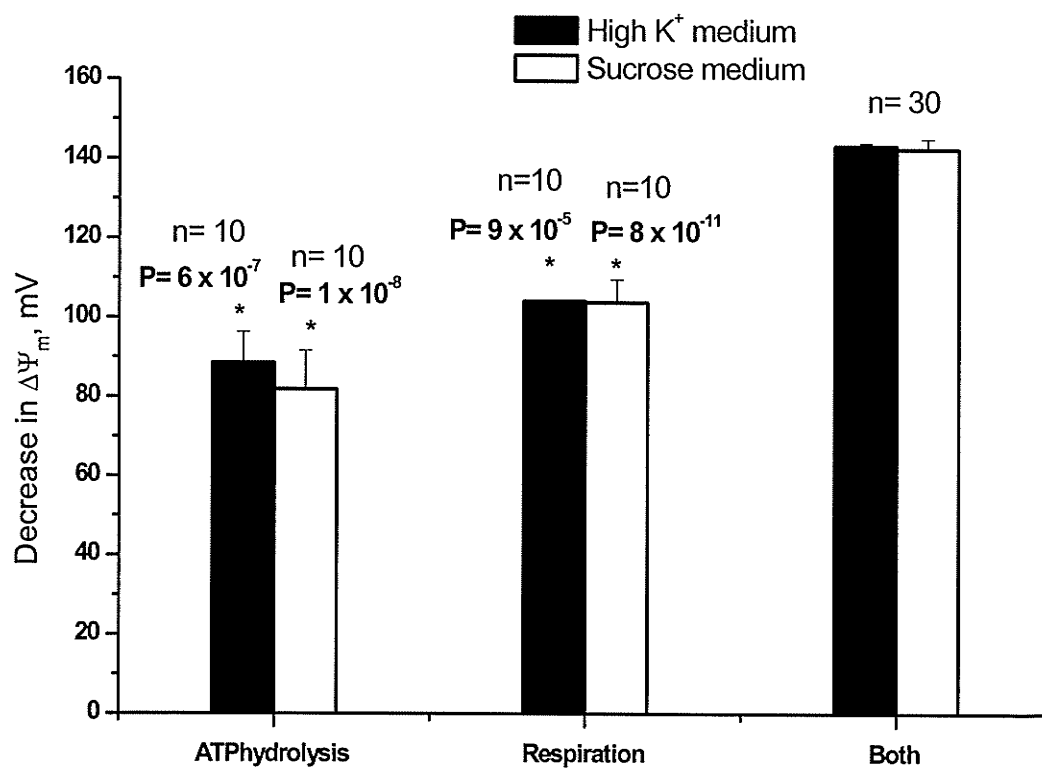


Figure 3-3. Effect of substrates on $\Delta\Psi_m$ in rat liver mitochondria vs. $\Delta\Psi_m$ in the FCCP uncoupled state. ATP hydrolysis was induced by 5mM ATP, respiration by 5mM glutamate and 5mM succinate, and both by 5mM of ATP, glutamate, and succinate. P values are shown for comparisons between ATP hydrolysis or respiration groups vs. ATP+ respiration group.

To compare MFFR to tetramethylrhodamine methylester (TMRM), a dye commonly used for $\Delta\Psi_m$ measurements in mitochondria, studies were conducted with both dyes in mitochondria energized in high K^+ medium (section 2.2.6 for details). The results of this experiment are displayed in Figure 3-4. ATP hydrolysis-dependent or respiration-dependent $\Delta\Psi_m$ values measured by both MFFR and TMRM distribution, were similar at all TMRM and MFFR concentrations (from 0 to 20 μM) and decreased as MFFR or TMRM increased to 20 μM . There was good linear correlation between $\Delta\Psi_m$ values calculated from TMRM and MFFR distribution (Figure 3-4), although slopes of the straight lines deviated from unity (0.85 and 0.73). In the presence of 5 μM of MFFR and TMRM, the ATP hydrolysis dependent average $\Delta\Psi_m$ values were -62 ± 4.75 mV and -59 ± 0.50 mV (n=4) for MFFR and TMRM binding, respectively. The maximal $\Delta\Psi_m$ values induced by respiration were -121 ± 8.22 mV and -106 ± 8.73 mV (n=4) for MFFR and TMRM binding, respectively.

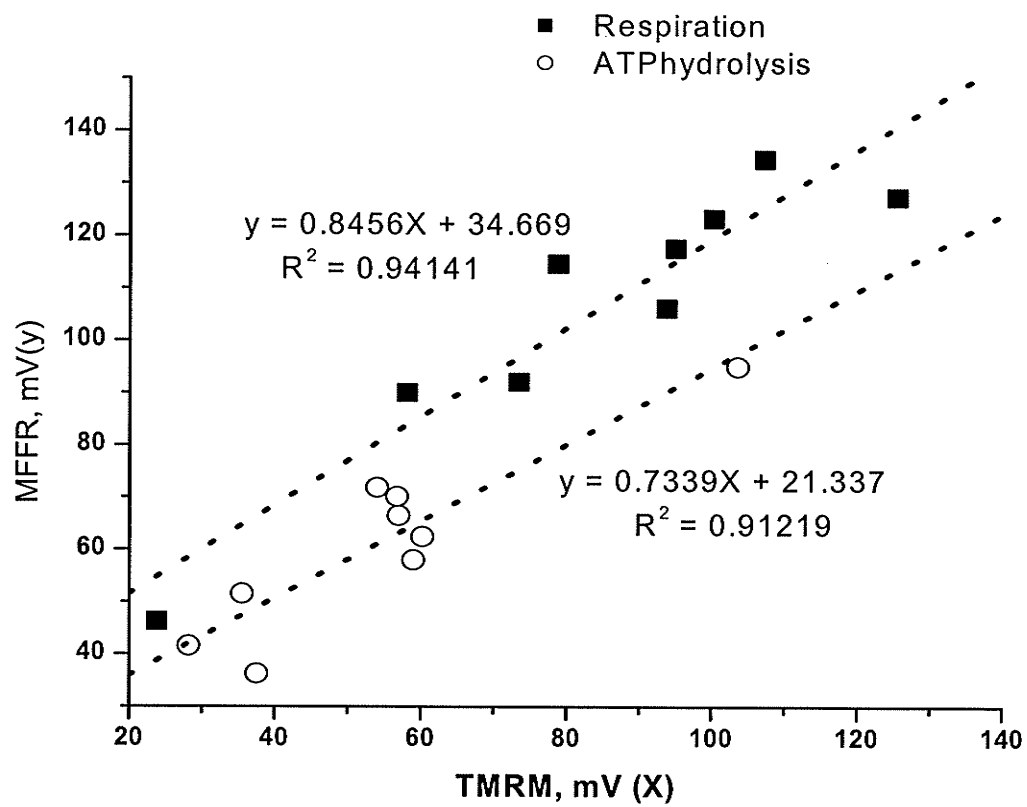


Figure 3-4. Correlation between $\Delta\Psi_m$ values measured with MFRR and TMRM binding.

3.1.2 The MFFR Distribution in Cardiomyocytes and Hepatocytes

Table 3-2. Bound and free MFFR in cardiomyocytes and hepatocytes

Group	Control		FCCP	
	bound, nmol/mg	free, nmol/mL	bound, nmol/mg	free, nmol/mL
Cardiomyocytes n= 20	1.20 ± 0.09	0.33 ± 0.02	0.91 ± 0.07	0.46 ± 0.02
<i>P vs. Control</i>			0.013	0.0001
Hepatocytes n= 20	1.34 ± 0.19	0.30 ± 0.03	1.21 ± 0.21	0.34 ± 0.03
<i>P vs. Control</i>			0.014	0.05

Cardiomyocytes and hepatocytes were energized by 10mM glucose plus 1mM pyruvate and 11mM glucose, respectively.

Cell concentrations were 0.2 – 0.9 mg protein/mL.

Data are represented as mean ± S.E.

Table 3-3. The ratio of bound : free MFFR in cardiomyocytes and hepatocytes corrected for cell viability

Group	(bound / free) _{viable} ^a
Cardiomyocytes, n=20	3.37 ± 0.37
Hepatocytes, n=20	2.99 ± 0.49

a) The ratio of bound MFFR to free MFFR corrected for cell viability and calculated by equation 5 in 2.2.6 of Materials and Methods section.

In the previous section, MFFR was used to evaluate $\Delta\Psi_m$ in isolated mitochondria. To investigate if MFFR could be used in cells to evaluate $\Delta\Psi_m$, studies were conducted with cardiomyocytes and hepatocytes. To determine the effects of FCCP on MFFR binding in isolated cells, the amounts of the dye bound to cardiomyocytes and hepatocytes and free dye in the incubation medium were determined using the procedure described in section 2.2.6. Table 3-2 shows the results obtained. The average amounts of bound MFFR were similar for cardiomyocytes and hepatocytes (Table 3-2). Similarly, the mean concentrations of free MFFR did not differ. The mitochondrial uncoupler FCCP was added to the cells in the presence of MFFR to determine whether its effects on cellular mitochondria could be detected by MFFR. The Table 3-2 shows that FCCP resulted in a modest decrease in bound MFFR and slight increase in free MFFR in cardiomyocytes and hepatocytes. The average ratios of bound / free dye with correction for cell viability were 3.37 ± 0.37 for cardiomyocytes and 2.99 ± 0.49 for hepatocytes. Without the correction for cell viability (Figure 3-5) the control ratios of were 1.87 ± 0.17 and 2.30 ± 0.32 for cardiomyocytes and hepatocytes, respectively. After addition of FCCP, the ratios were decreased to 0.90 ± 0.07 for cardiomyocytes and 1.31 ± 0.11 for hepatocytes. The ratios in the text are obtained in the following way: Bound (nmol/mg) x cell concentration (0.2-0.9 mg/mL) / Free (nmol/mL) = dimensionless, i.e. the same calculation for mitochondria.

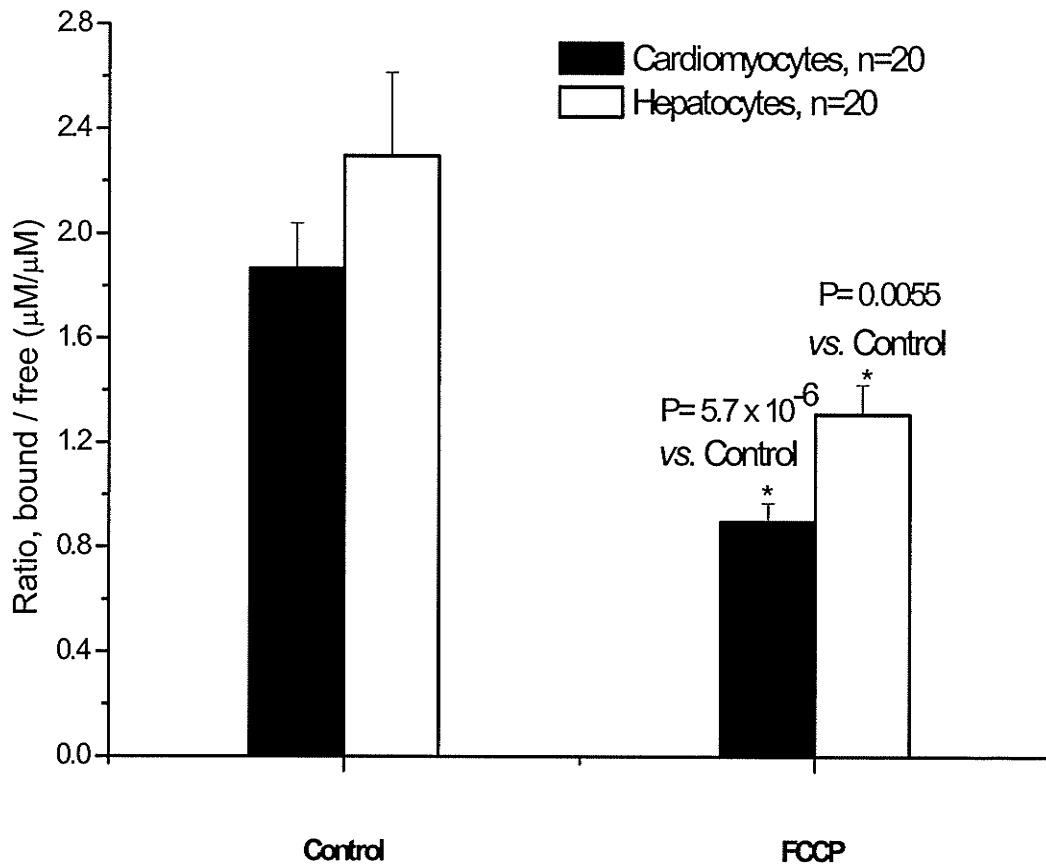


Figure 3-5. Ratio of bound to free MFFR in isolated cells. Isolated cells were incubated on a shaking water bath for 5 minutes at 35 °C in hepatocytes incubation buffer for hepatocytes and in cardiomyocytes incubation buffer for cardiomyocytes. P values correspond to comparison of FCCP to control. Data are presented as mean \pm S.E.

3.2 Influence of MFFR and P-1075 on Mitochondrial Respiration Rate

MFFR should not affect mitochondrial function and $\Delta\Psi_m$ if it is to be used for evaluation of $\Delta\Psi_m$ in mitochondria and the cells. Therefore, the toxicity of MFFR was investigated by examining its effects on two pathways of mitochondria respiration in isolated rat liver mitochondria in high K^+ buffer. Incubation with 5mM glutamate-Na plus 5mM malate (NAD^+ dependent substrates) was used to energize mitochondria via complex I while 10 mM succinate was used to energize mitochondria via complex II (section 2.2.3 for details). The results of these studies are shown in Figure 3-7.

Increasing the concentrations of MFFR significantly affected complex I dependent respiration (Figure 3-6 A and 3-7 A). However, MFFR had no effect on complex II dependent respiration (see figure 3-6 B and 3-7 B). In the complex I dependent respiration, MFFR concentrations below 0.2 μM showed a steep decrease in state 3 respiration from 66.5 ± 7.97 to 35.2 ± 4.08 nmol/min/mg and also a decrease in uncoupled respiration from 80.0 ± 7.33 to 37.0 ± 4.05 nmol/min/mg. The concentrations of MFFR above 0.2 μM changed significantly both in state 3 respiration from 35.2 ± 4.08 to 21.5 ± 1.84 nmol/min/mg and in uncoupled respiration from 37.0 ± 4.05 to 29.5 ± 2.64 nmol/min/mg. When the results were expressed as a percentage of state 3 respiration in the absence of MFFR (Figure 3-7), they showed that rates of state 3 and uncoupled respiration decreased to 56 ± 3.04 % and 59 ± 3.08 % of control value, respectively at 0.2 μM MFFR. The average rates of state 3 and uncoupled respiration were 28 ± 2.91 % and 38.5 ± 4.32 % at 1 μM MFFR, respectively. In both complex I and II dependent

mitochondrial respiration, MFFR concentrations had no effect on state 2 and 4 respiration. Figure 3-6 B and 3-7 B show that the rates of state 3 and uncoupled respiration are not affected by MFFR when complex II is involved.

Since we used P-1075 as an agent for evaluating $\Delta\Psi_m$ by MFFR binding, respiratory effects of P-1075 require consideration. High concentrations of P-1075 could have effect on mitochondrial respiration. To investigate the effects of P-1075 on mitochondrial respiration, it was measured in the presence of varying the concentrations of P-1075 in the same manner as described for the effects of MFFR. Concentrations of P-1075 below 20 μM had no effect on all states of respiration rates dependent on complex I and II (Figure 3-8). The initial respiration rates were 9.2 ± 1.23 , 66 ± 7.59 , 12 ± 0.86 , and 78 ± 5.39 nmol/min/mg protein for state 2, 3, 4, and uncoupled state for complex I dependent mitochondrial respiration, respectively. In complex II dependent respiration, the initial respiration rates were 21.3 ± 1.94 for state 2, 97.8 ± 14.5 for state 3, 21.5 ± 2.33 for state 4, and 97 ± 11.97 nmol/min/mg for the uncoupled state. The concentrations of P-1075 below 20 μM used in the experiments were not toxic to state 2, 3, 4, and the uncoupled state for both complex I and II dependent respiration.

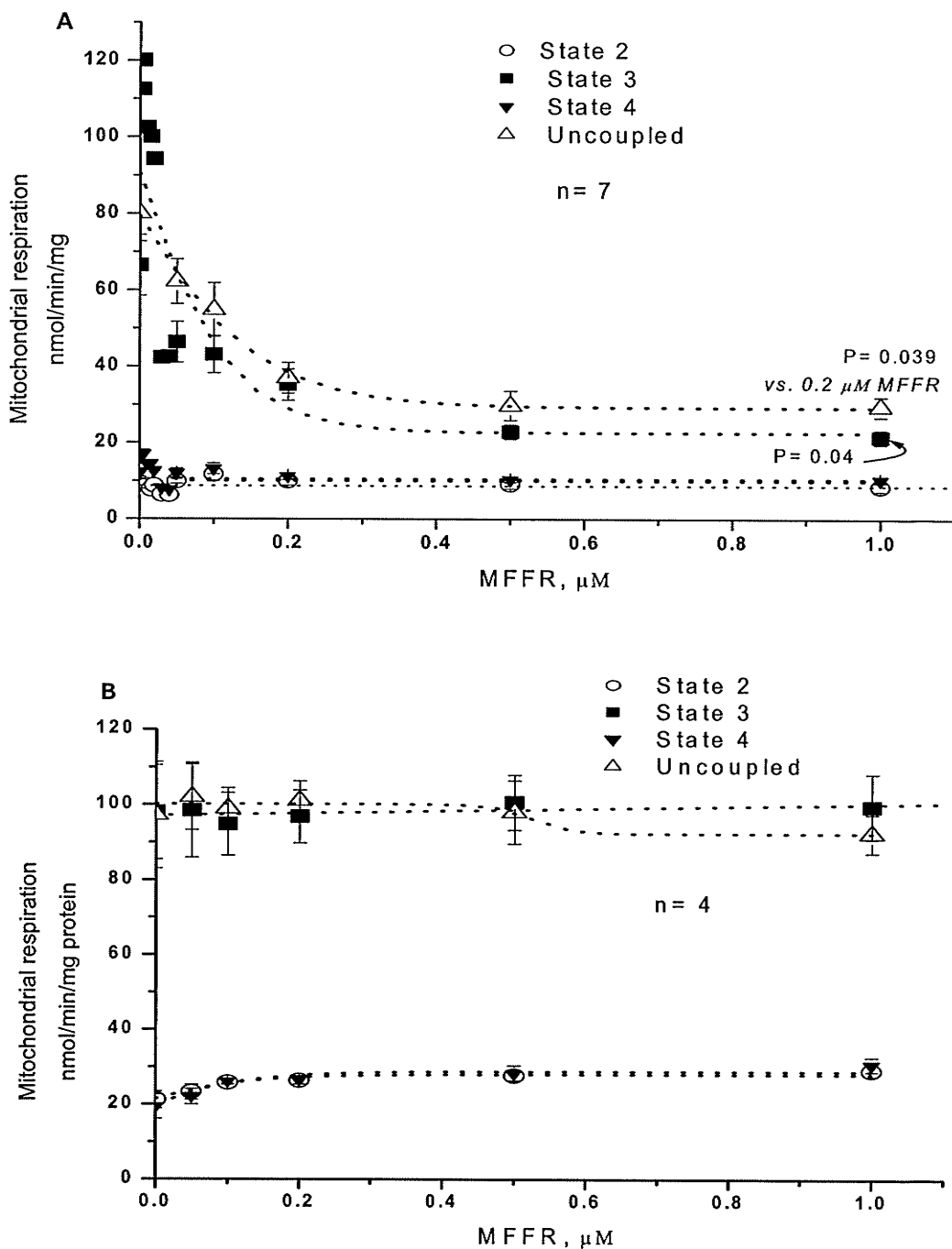


Figure 3-6. The effects of MFFR on respiration rates. Isolated liver mitochondria (0.5mg/mL) were incubated with varying concentrations of MFFR. State 2 respiration was initiated by addition of 5mM glutamate plus 5mM malate (A) energizing mitochondria through complex I or 10mM succinate (B) energizing mitochondria through complex II. Mg-ADP (0.3mM) was added to mitochondria in state 2 to initiate state 3 and state 4 was reached when ADP was used up. Uncoupled respiration was obtained by addition of 1 μM FCCP. P values are shown for data comparison between 0.2 μM and 1 μM MFFR. Data are presented as the mean \pm S.E.

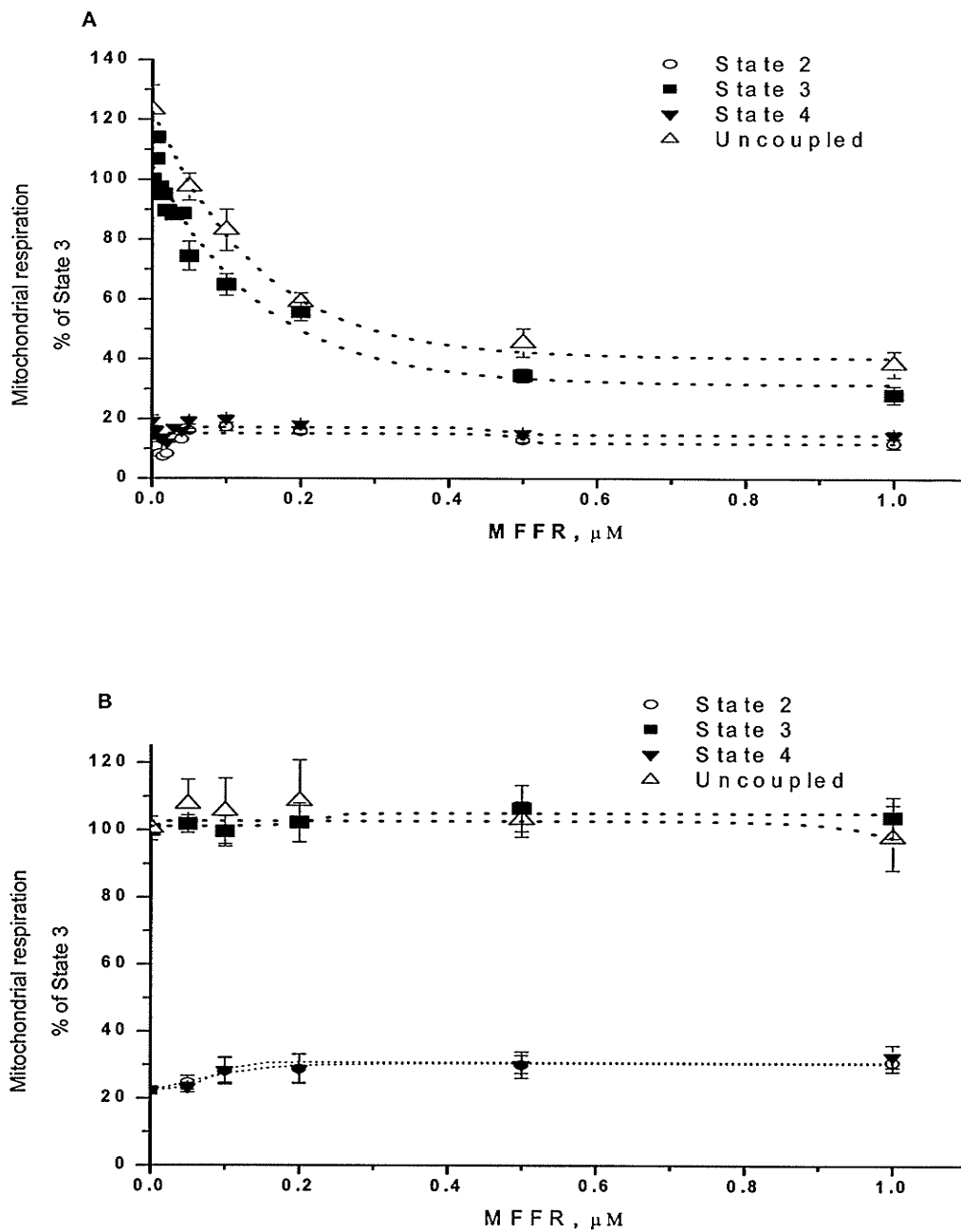
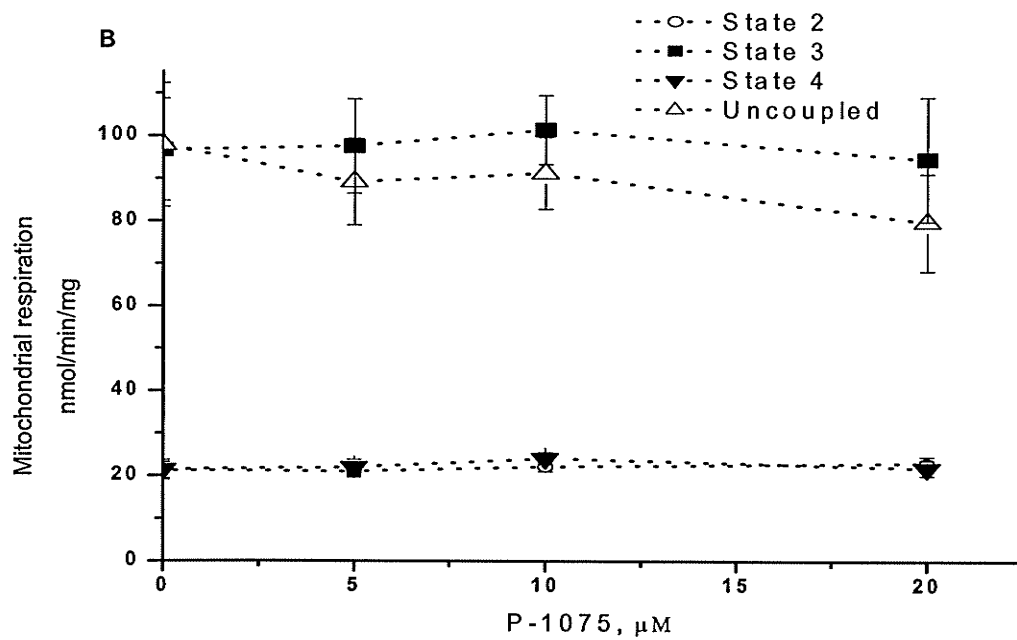
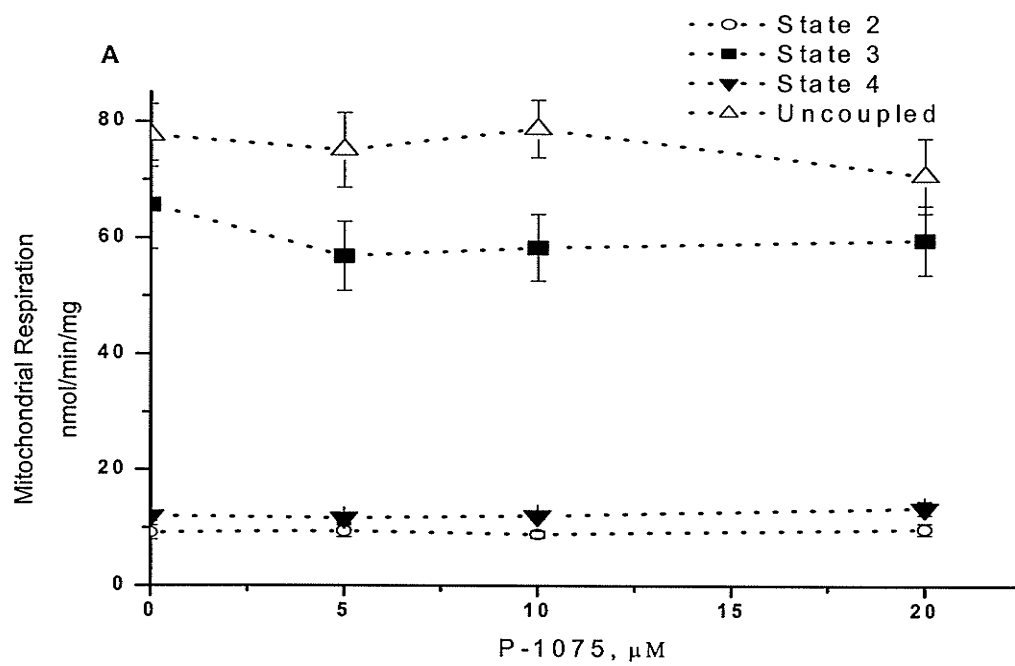


Figure 3-7. The effects of MFFR on normalized respiration rate. Data were expressed as a percentage of state 3 respiration for comparison between state 3 and uncoupled, state 2, or state 4 respiration rate. Mitochondria were energized by 5mM glutamate plus 5mM malate (A) and 10mM succinate (B).



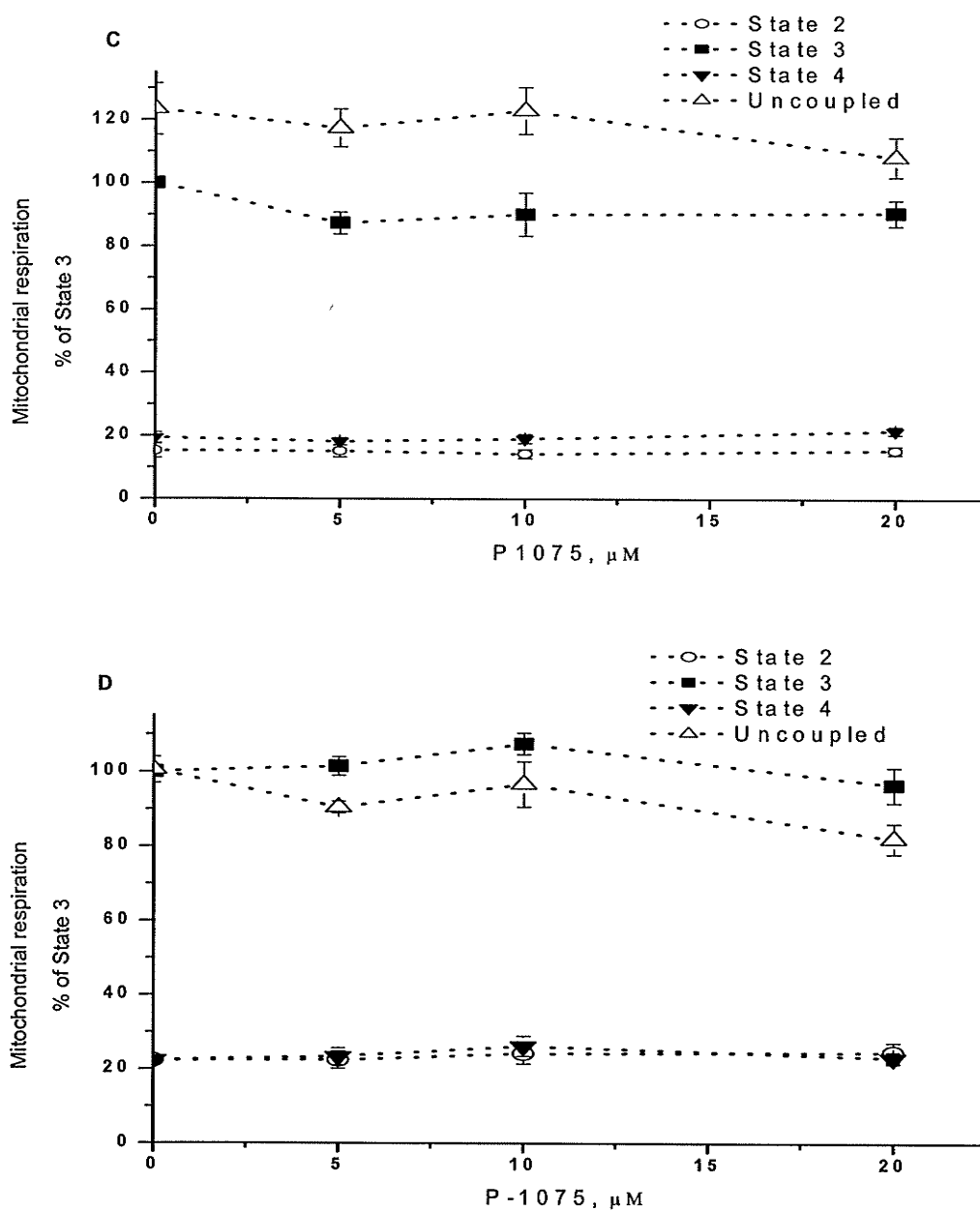


Figure 3-8. The effects of P-1075 on respiration rate. Mitochondria were energized by 5mM glutamate plus 5mM malate (**A, C**) and by 10mM succinate (**B, D**). Data in panels A and B were expressed in nmol/min/mg and data in C and D were normalized to state 3 respiration rate and expressed as percent of state 3 values.

3.3 Measurements of MFFR Fluorescence in Isolated Rat Liver Mitochondria, Cardiomyocytes, and Hepatocytes

In the previous sections, bound MFFR was physically separated from free MFFR by centrifugation. In this section, the possibility of monitoring MFFR in the absence of a separation steps was explored. It was shown that uptake of MFFR by energized mitochondria resulted in a decrease in MFFR fluorescence intensity [157]. In contrast, addition of an uncoupler, FCCP dissipates $\Delta\Psi_m$ and should result in increase MFFR fluorescence intensity as the dye is released from the mitochondria. To confirm this hypothesis and evaluate $\Delta\Psi_m$, we determined changes of MFFR fluorescence in isolated mitochondria and cells caused by changes in $\Delta\Psi_m$.

3.3.1 Dependence of MFFR Fluorescence on Its Concentration and pH

To determine the effect of pH and concentration on the fluorescence of MFFR, the pH of the high K^+ incubation buffer was varied between 5.34 to 9.08 with 6M NaOH and MFFR concentration varied between 0 to $30\mu\text{M}$. The fluorescence was measured in each buffer. The results which are shown in Figure 3- 9 revealed that MFFR fluorescence was not affected by changes in pH value. At all pH values, MFFR fluorescence increased between 0 and $5\mu\text{M}$, peaking at a value of 659 ± 3.90 arbitrary units (a.u.) before declining steadily to a value of 224 ± 8.36 a.u. at $30\mu\text{M}$. This shows that the alkaline pH of the mitochondrial matrix (pH~8.2) should not affect MFFR fluorescence. Figure 3-9 is a good demonstration of the self-quenching effect of MFFR at concentrations above $5\mu\text{M}$ ($\Delta A = 0.5$) which takes place in the mitochondrial matrix membrane where the concentration of MFFR may be as high as $\sim 200\mu\text{M}$.

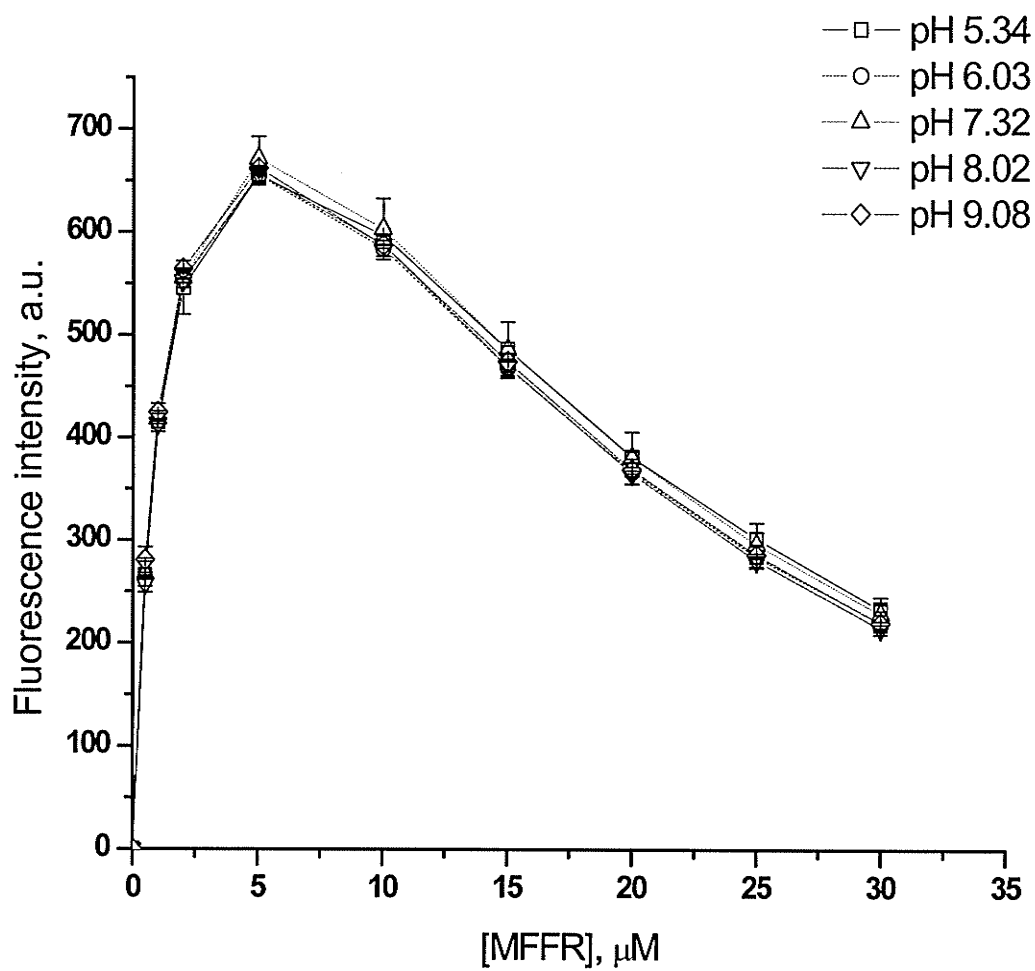
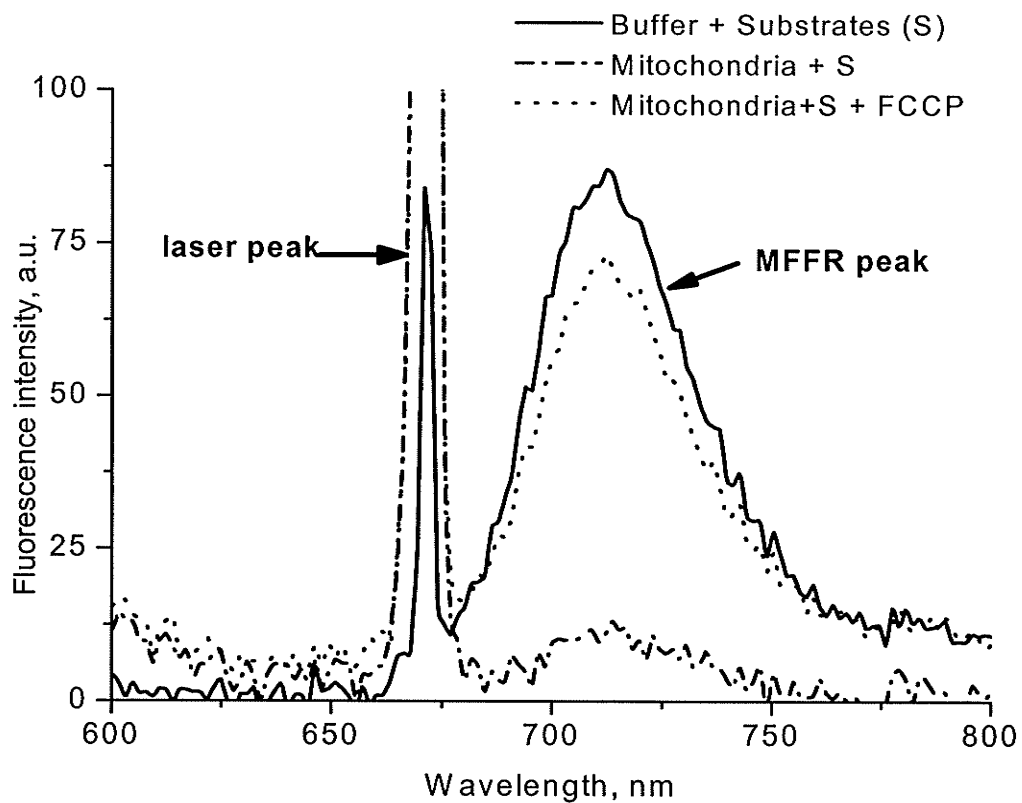


Figure 3-9. The effects of pH on the fluorescence of MFFR.
Data are presented as mean \pm S.E.

3.3.2 Changes in MFFR Fluorescence Spectra in Mitochondrial Suspensions

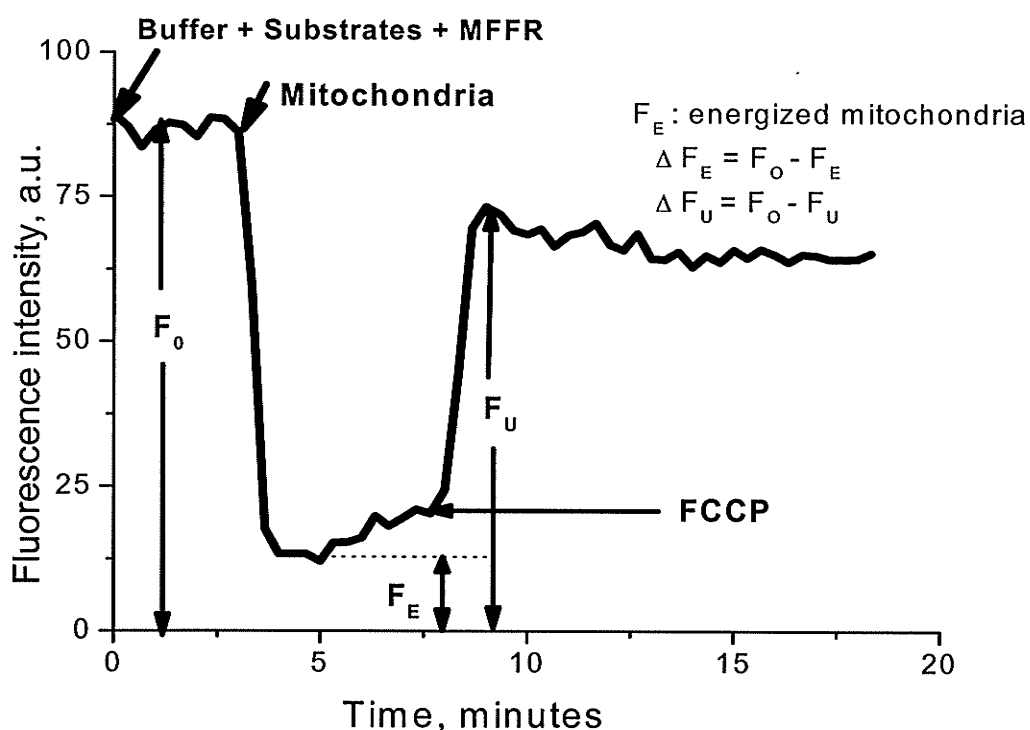
Figure 3-10 shows spectra of MFFR samples in high K^+ incubation buffer obtained by laser illumination at 670 nm. The spectra consist of two principal components: a peak of scattered excitation laser light at 670 nm and broad peak of emitted fluorescence at 712-716 nm. In the absence of mitochondria (indicated as the buffer in figure 3-10) fluorescence intensity was 87 arbitrary units (a.u.) at 712.5 nm. Accumulation of MFFR by energized mitochondria resulted in a decrease in fluorescence intensity to 12 a.u., an indication of fluorescence quenching (or decrease in quantum yield) and a shift in the fluorescence peak to 716.5 nm. The addition of FCCP to energized mitochondria caused the MFFR fluorescence intensity to shift from 716.5 back to 712.5 nm which was the same wavelength that MFFR had in high K^+ buffer. In the presence of FCCP, fluorescence intensity increased to 73 a.u. compared to that of 12.1 obtained for energized mitochondria. This increase in MFFR fluorescence intensity was presumably caused by release of MFFR from mitochondria as was shown in the previous section.



S = Substrates: glutamate + succinate

Figure 3-10. MFFR fluorescence spectra in mitochondrial suspension. Isolated rat liver mitochondria (0.082 mg/mL) were added to 1 μ M MFFR in mitochondrial high K^+ incubation buffer (described in 2.2.7 of Materials and Methods section) with 5mM glutamate plus 5mM succinate (energized state). Subsequently FCCP was added to induce uncoupled state.

3-11 shows changes in MFFR fluorescence intensity in response to mitochondria addition and FCCP treatment as a function of time. The addition of mitochondria drastically decreased fluorescence intensity within less than 1 minute from 89 to 12 a.u. After the fluorescence intensity of MFFR remained relatively stable for 5 minutes, the addition of $1\mu\text{M}$ FCCP resulted in an increase in fluorescence intensity within less than 1 minute from 12 to 73 a.u.



Substrates: glutamate + succinate

Figure 3-11. Changes in MFFR fluorescence intensity in mitochondrial suspension treated with FCCP as a function of time. Spectra were recorded every 20 seconds for 10 minutes. Five minutes after the addition of mitochondria to the substrates containing buffer, mitochondria were treated with FCCP to a final concentration of $1\mu\text{M}$. Fluorescence peak was determined between 708 and 720 nm. F_0 is the initial fluorescence intensity before the addition of mitochondria, F_E is the fluorescence intensity after the addition of mitochondria, and F_U is the fluorescence intensity after the addition of FCCP.

To determine whether the fluorescence intensity of MFFR is dependent on concentrations of mitochondrial protein, the fluorescence of MFFR was measured as a function of mitochondria concentration. In this experiment, the fluorescence peak was normalized to the initial fluorescence to calculate the ratio F_E (energized) or F_U (uncoupled) to F_O . The range of protein concentrations used was 0.03-0.17 mg/mL. Five minutes after the addition of mitochondria, FCCP was added. After an additional 5 minutes, FCCP was added again. The results shown in Figure 3-12 indicate that the protein concentration (0.03-0.17 mg/mL) did not significantly affect the ratio of F_E or F_U to F_O . The values of the ratios were approximately 0.20 for energized mitochondria and 0.86 for FCCP- treated mitochondria. The mean values of the ratio in each group were not significantly different from each other ($P>0.05$).

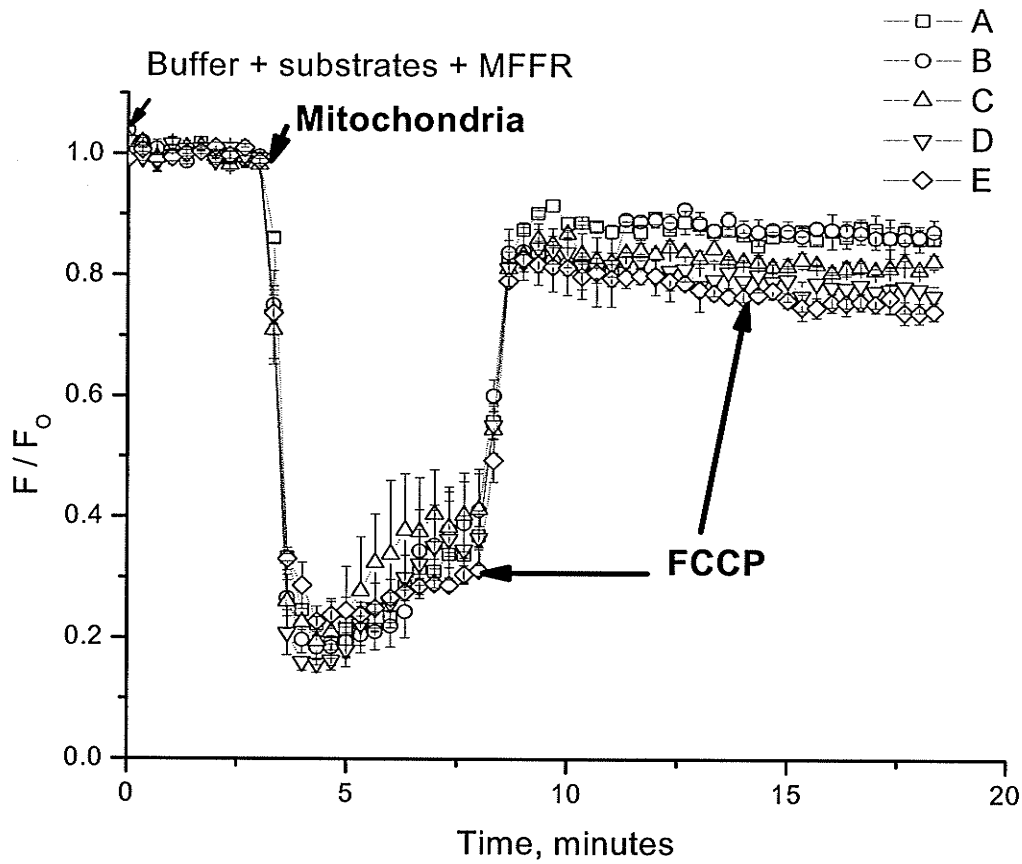
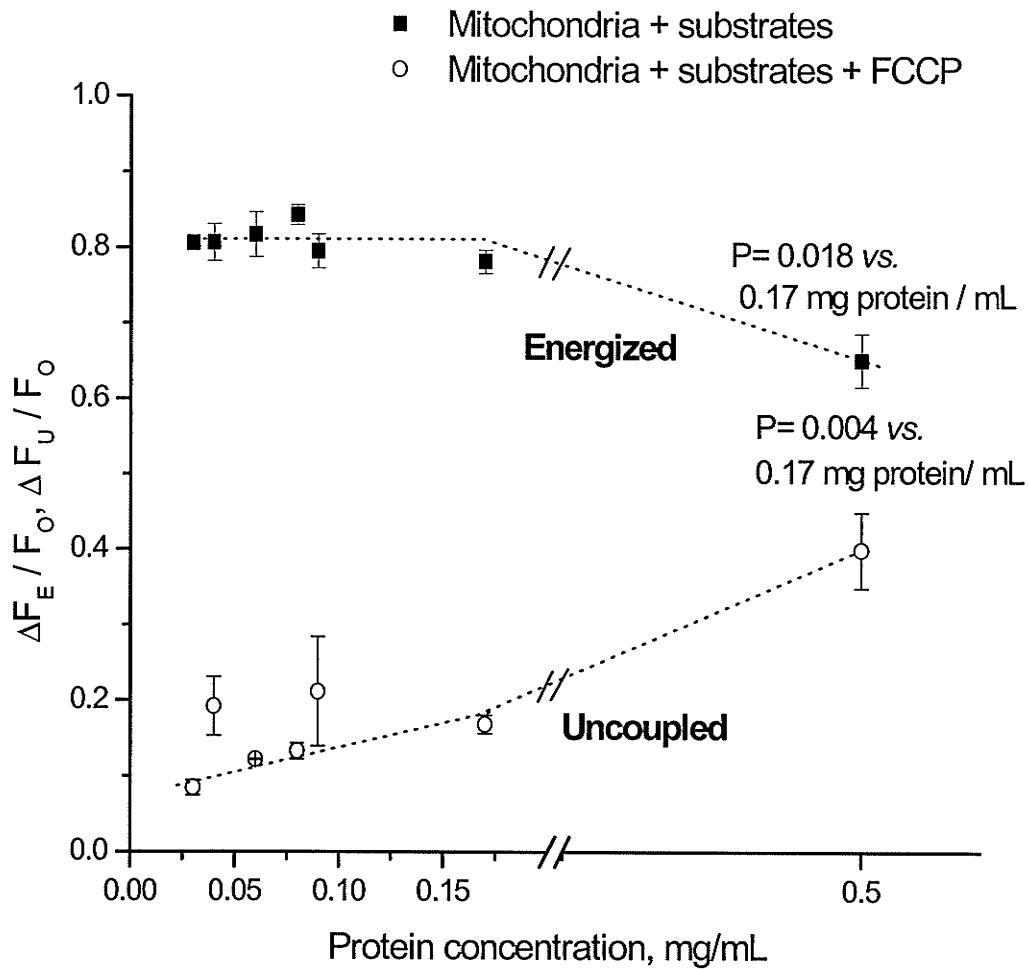


Figure 3-12. Time course of normalized MFFR fluorescence at various mitochondrial concentrations. 0.03 mg/mL of protein (A), 0.04 mg/mL of protein (B), 0.06 mg/mL of protein (C), 0.08 mg/mL of protein (D), and 0.17 mg/mL (E). F_E , F_U , and F_0 are indicated in figure 3-11. Data are presented as mean \pm S.E.

In order to better visualize the relationship between protein concentration and the change in fluorescence ratio in response to the addition of mitochondria to the substrate containing buffer and FCCP as shown in Figure 3-12, the values of the immediate changes ($\Delta F_E / F_O$) obtained after the addition of mitochondria as well as the change in the ratio ($\Delta F_U / F_O$) upon the addition of FCCP to the mitochondria were re-plotted against the protein concentration (Figure 3-13). The average values were 0.81 ± 0.01 for the addition of mitochondria and 0.17 ± 0.02 for the addition of FCCP at protein concentrations below 0.17 mg/mL. However, the change in ratio decreased in energized mitochondria and increased in de-energized mitochondria with increasing protein concentration at protein concentrations above 0.17 mg/mL. At a protein concentration of 0.5 mg/mL, the value was 0.65 ± 0.04 for energized mitochondria and 0.4 ± 0.05 for de-energized mitochondria.



$$\Delta F_E / F_0 = (F_0 - F_E) / F_0 = 1 - F_E / F_0, \quad \Delta F_U / F_0 = (F_0 - F_U) / F_0 = 1 - F_U / F_0$$

Figure 3-13. $\Delta F/F_0$ for energized (■) and uncoupled mitochondria (○) as a function of protein concentration (0.03-0.5mg/mL). Mitochondria were energized by respiration in the presence of 5mM glutamate plus 5mM succinate and de-energized (uncoupled) by subsequent addition of 1 μ M FCCP. Data are presented as mean \pm S.E.

3.3.3 Changes in MFFR Fluorescence Spectra in Cardiomyocyte

Suspensions

To determine changes in MFFR fluorescence upon binding to cardiomyocytes caused by changes in $\Delta\Psi_m$, the fluorescence spectra of $1\mu\text{M}$ MFFR were measured before and after cardiomyocytes addition followed by FCCP treatment. In the absence of cardiomyocytes, the fluorescence intensity was 310 a.u. at 712 nm in the representative experiment shown in Figure 3- 14. Accumulation of MFFR by energized cardiomyocytes (10mM glucose plus 1mM pyruvate) resulted in a decrease in the fluorescence intensity to 237 a.u. (24 % decrease) an indication of changes of MFFR fluorescent properties upon binding. The addition of FCCP to energized cardiomyocytes caused partial recovery of the MFFR fluorescence intensity to 275 a.u. (increased by 15.7 % of that in the energized state). This increase in the fluorescence intensity was presumably caused by release of MFFR from cellular mitochondria.

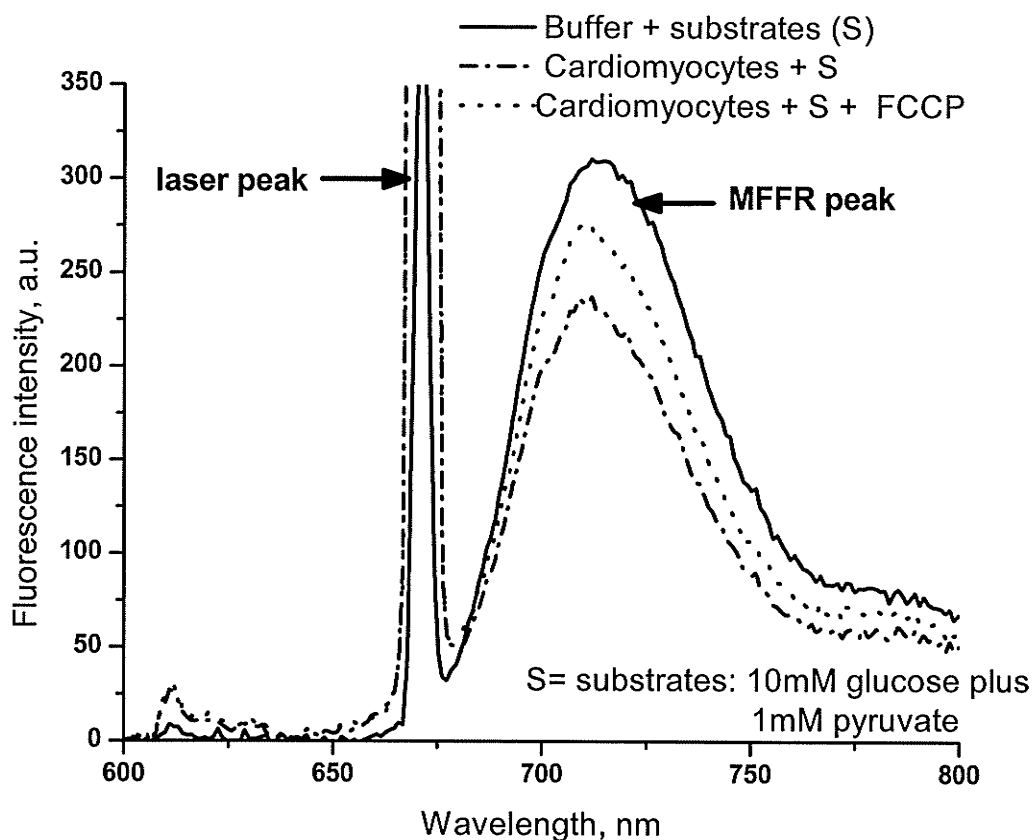


Figure 3-14. MFFR fluorescence spectra in cardiomyocyte suspension. Isolated rat heart cardiomyocytes (0.7 mg/mL) were added to 1 μ M MFFR in cardiomyocytes high K^+ incubation buffer (see for details in 2.2.7 of Materials and Methods section) with substrates (10mM glucose plus 1mM pyruvate). Subsequently FCCP was added to energized cardiomyocytes. The fluorescence maxima were determined between 708-720nm.

To determine the change in MFFR fluorescence over time, the fluorescence intensity of MFFR was measured as a function of time. Figure 3-15 shows changes in MFFR fluorescence intensity caused by cardiomyocytes addition and subsequent FCCP treatment as a function of time. Addition of cardiomyocytes slowly decreased the fluorescence intensity of MFFR within 7 minutes from 310 to 235 a.u. After the fluorescence intensity of MFFR was monitored for 5 minutes, the addition of 1 μ M FCCP resulted in a slight increase in the fluorescence intensity within 2 minutes from 235 to 276 a.u. and stopped its decline.

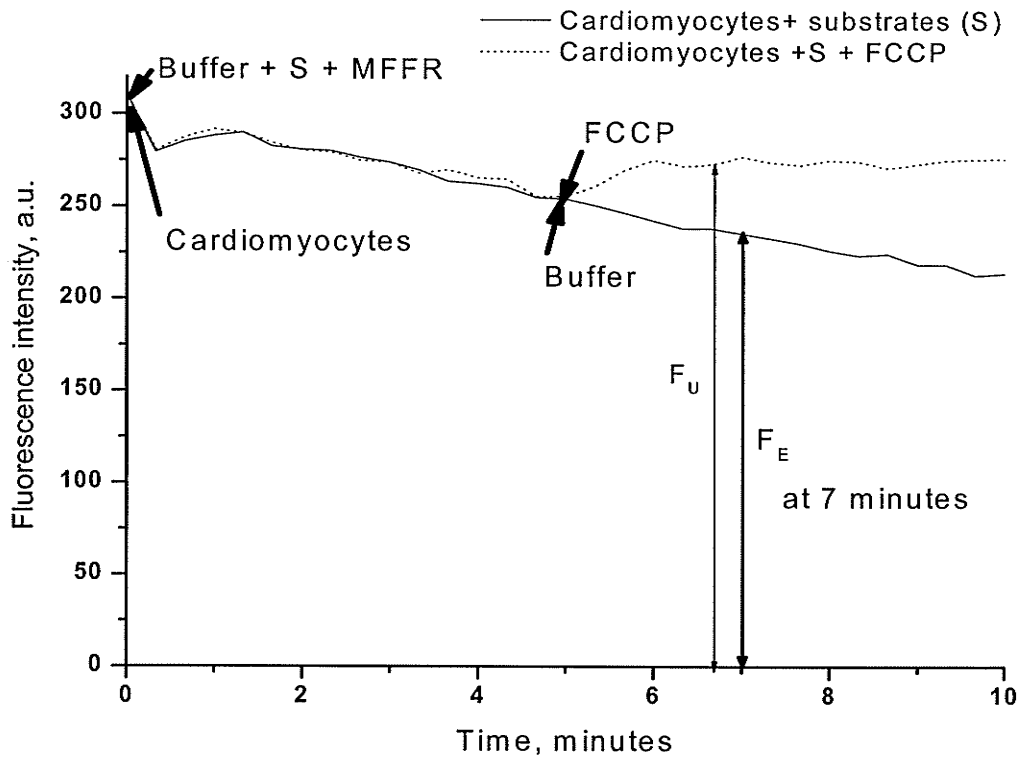


Figure 3-15. Time course of MFR fluorescence in cardiomyocyte suspension before and after FCCP treatment. Spectra were recorded every 20 seconds for 10 minutes. For the energized state, 5 minutes after the addition of cardiomyocytes, cardiomyocytes incubation buffer (the volume was the same as the amount of FCCP) was added. To induce the uncoupled state, 5 minutes after the addition of cardiomyocytes, cardiomyocytes were treated with FCCP to a final concentration of $1 \mu\text{M}$. The fluorescence peak intensity was determined between 708 and 720 nm at 7 minutes. F_O is the initial fluorescence before the addition of cardiomyocytes, F_E is the fluorescence intensity after the addition of cardiomyocytes, and F_U is the fluorescence intensity after the addition of FCCP.

To determine whether the fluorescence intensity of MFFR is dependent on the concentration of cardiomyocytes expressed as protein concentration, the fluorescence intensity was measured as a function of cardiomyocyte concentration in the time course experiments. In this experiment, the fluorescence peak was normalized to the initial fluorescence to calculate the changes in the ratios F_E / F_O and F_U / F_O . The results which are shown Figure 3-16 indicate that the protein concentration (0.3-0.9 mg/mL) did significantly affect the F_E / F_O and F_U / F_O . The values of the changes ($\Delta F_E / F_O$) obtained after the addition of cardiomyocytes as well as the changes in values ($\Delta F_U / F_O$) obtained upon the addition of FCCP to the cardiomyocytes were plotted against the protein concentration. The value for energized cardiomyocytes was increased from 0.16 ± 0.01 at protein concentration of 0.4 mg/mL to 0.22 ± 0.01 at the concentration of 0.7 mg/mL. However, at protein concentrations above 0.7 mg/mL, the change decreased with increasing protein concentration from 0.22 ± 0.01 to 0.16 ± 0.02 at protein concentration of 0.8 mg/mL.

If a part of the accumulation of MFFR is associated with MFFR binding to cellular membranes and structures, then the uncoupling of cellular mitochondria by FCCP should result in the incomplete release of the dye from the cell and fluorescence value should not return to the baseline. To investigate whether this is the case here, the ratio of change in fluorescence upon addition of FCCP (ΔF_U) to the change in response to the addition of cardiomyocytes (ΔF_E) was plotted as function of protein concentration. The results which are shown in Figure 3-17 indicate that the response of energized cellular mitochondria to FCCP was dependent on the protein concentrations below 0.7 mg/mL (0.3 mg/mL to 0.7 mg/mL). The value was increased from 0.25 ± 0.07 to 0.51 ± 0.03 (P

= 0.013). However, at protein concentrations between 0.7 mg / mL and 0.9 mg/mL, the response to FCCP was not dependent on the protein concentrations. At protein concentration of 0.9 mg/mL the value was 0.51 (n=1).

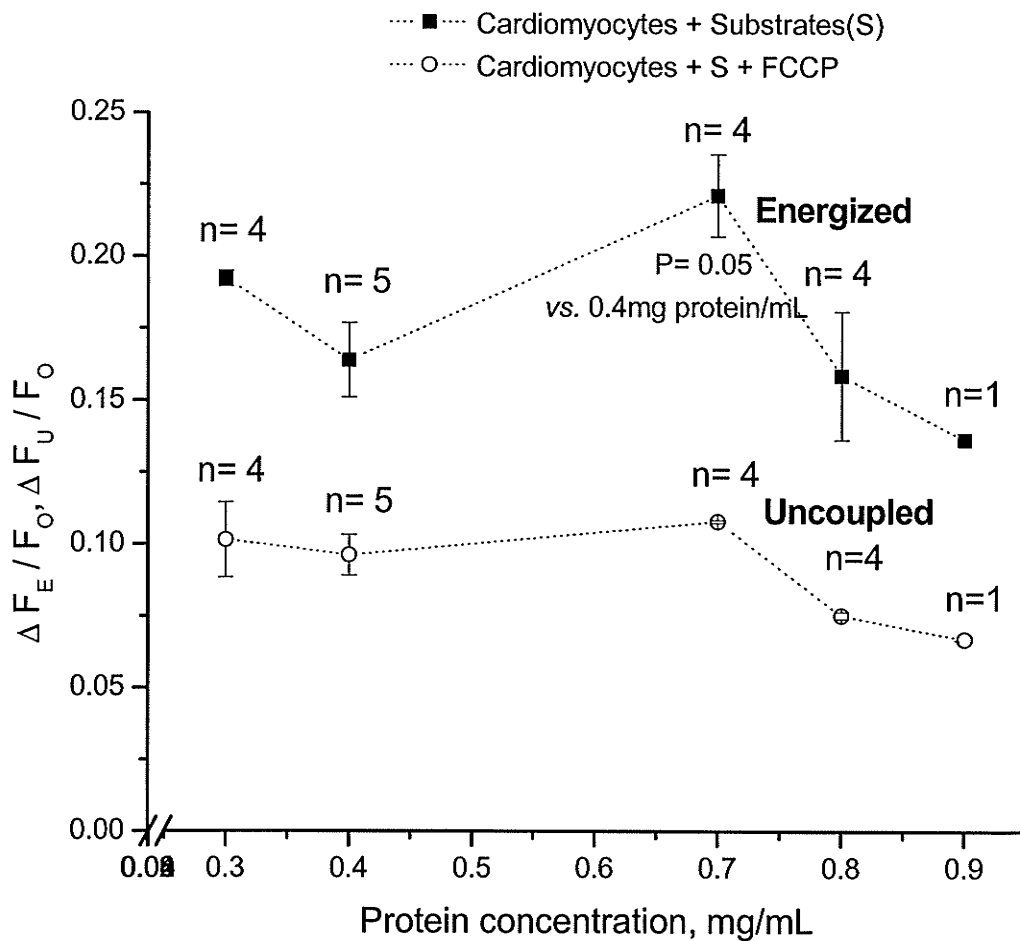


Figure 3-16. Changes in the fluorescence ratio $\Delta F/F_0$ for energized (■) and uncoupled cellular mitochondria (○) in cardiomyocytes as a function of protein concentration (0.3- 0.9mg/mL). The cellular mitochondria in cardiomyocytes were energized and uncoupled by 10mM glucose plus 1mM pyruvate and 1 μ M FCCP, respectively. Average cell viability was 40%. Data are presented as mean \pm S.E.

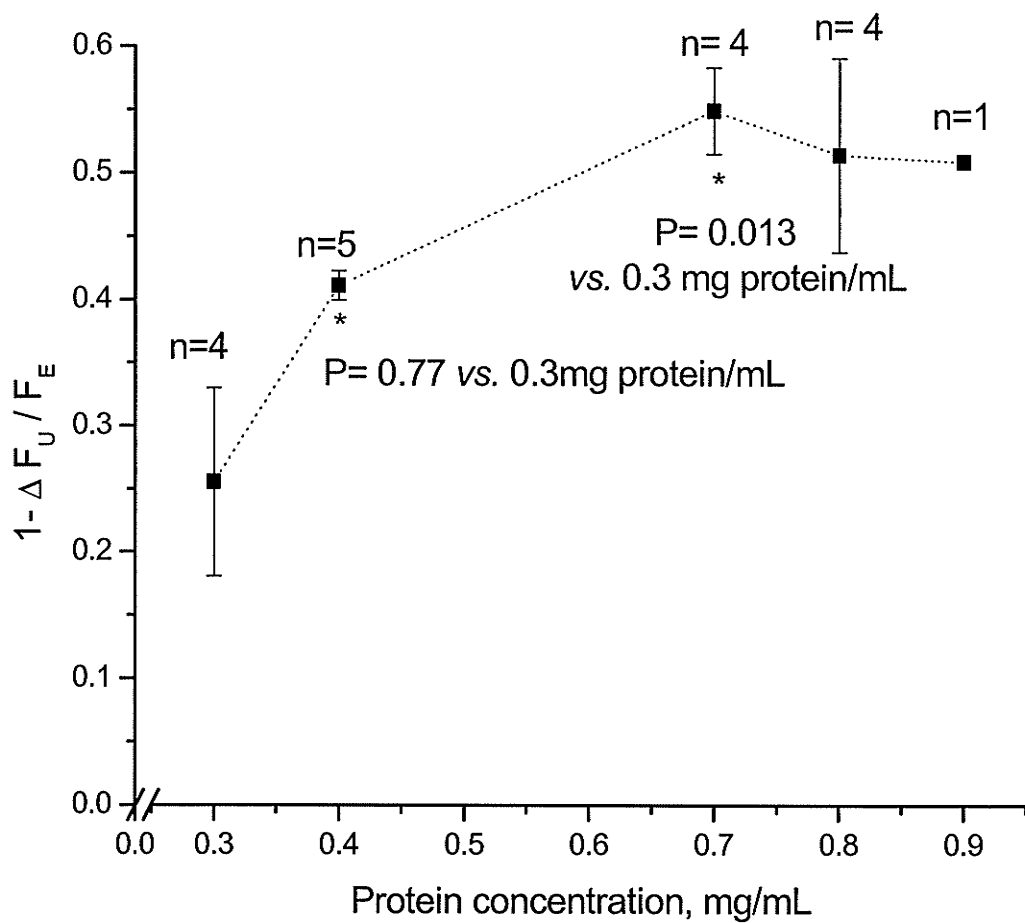


Figure 3-17. The response of energized cellular mitochondria to FCCP in cardiomyocytes as a function of protein concentration (0.3- 0.9 mg/mL). Average cell viability was 40%. Data are presented as mean \pm S.E.

To investigate the relationship between the changes in the fluorescence ratios F_E and F_U to F_O and MFFR binding, the binding was measured after fluorescence measurements by separating cardiomyocytes and free MFFR by centrifugation (section 2.2.7). The fraction of bound MFFR was increased by increasing cell concentrations in the suspension. Increase in the amount of bound MFFR from 57 ± 0.90 to 74 ± 1.25 % resulted in no significant changes in the fluorescence (Figure 3-18). Similarly, there was no correlation between the fluorescence change and the amount of MFFR bound for the uncoupled cellular mitochondria. Mean values of the fluorescence change for energized and uncoupled cardiomyocytes as well as the amount of MFFR bound were significantly different at a level of $P < 0.05$. In general, energization of cellular mitochondria increased dye binding and change in the fluorescence ($\Delta F/F_0$).

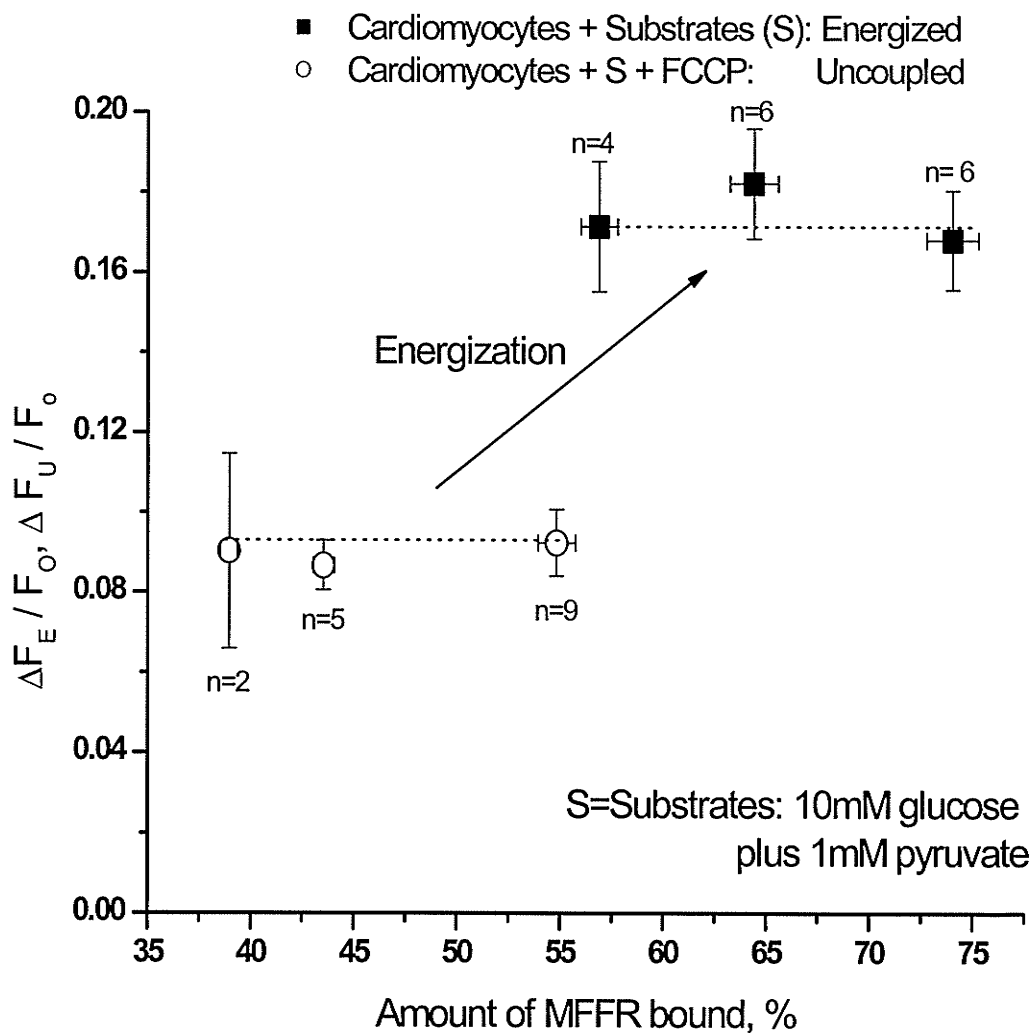


Figure 3-18. Relationship between changes in the fluorescence ratios F_E / F_O and F_U / F_O and amount of MFFR bound. Cardiomyocytes at concentrations of 0.3-0.9 mg/mL protein were used for the experiment. After the fluorescence measurement of MFFR, samples were taken for MFFR binding determination (section 2.2.7 for details). Data are presented as mean \pm S.E.

In cells, MFFR has to pass through the plasma membrane into the cell cytoplasm before it is taken up by mitochondria. Plasma membrane potential can affect the MFFR concentration in the cytoplasm and therefore indirectly dye accumulation in the mitochondria. For this reason studies were performed to investigate the effect of the plasma membrane potential on the fluorescence measurement of MFFR in the cells. In the presence of low K^+ buffer the plasma membrane potential is intact at about -80mV whereas in high K^+ buffer the plasma membrane potential is near zero. Therefore, studies were conducted with cardiomyocytes in high (120mM) and low K^+ (~5mM) buffer to determine the effect of the plasma membrane potential on the fluorescence of MFFR in the cells. Figure 3-19 shows that changes of MFFR fluorescence were dependent mainly on $\Delta\Psi_m$. In the energized cardiomyocytes, $\Delta F/F_0$ values were 0.19 ± 0.01 and 0.16 ± 0.01 , higher in the low K^+ than in the high K^+ buffer, respectively. A similar trend was observed in the uncoupled cardiomyocytes, where the changes of the fluorescence were 0.11 ± 0.01 in the low K^+ and 0.08 ± 0.01 in the high K^+ buffer. However, the mean values of $\Delta F/F_0$ were not significantly different between low K^+ and in the high K^+ buffer ($P>0.05$). These results show that the plasma membrane potential had no significant effect on the fluorescence of MFFR in the cell suspensions in our experiments.

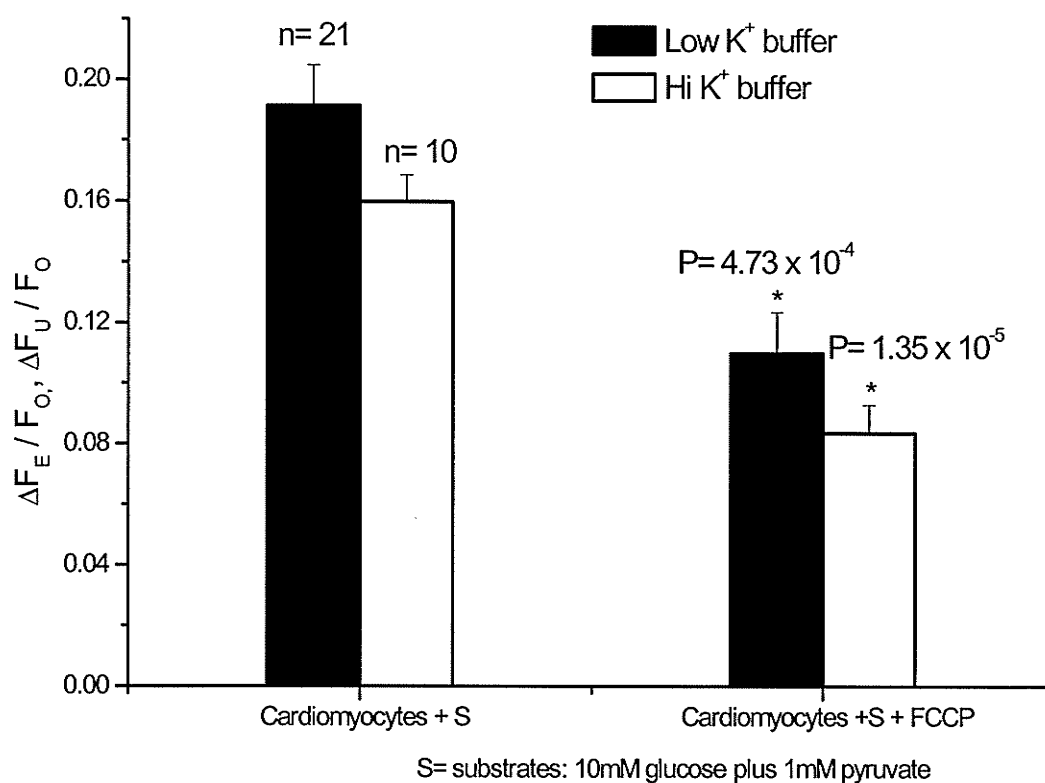


Figure 3-19. The effects of the plasma membrane potential on the fluorescence of MFFR. Cardiomyocytes (0.3-0.9 mg/mL of protein) were incubated in low K⁺ and high K⁺ incubation buffer with MFFR (final concentration of 1 μM). P values are for comparison of cardiomyocytes + FCCP to cardiomyocytes in the same buffer. Data are presented as mean ± S.E.

3.3.4 Changes in MFFR Fluorescence Spectra in Hepatocyte

Suspensions

To determine changes in MFFR fluorescence in suspensions of hepatocytes caused by changes in $\Delta\Psi_m$, the fluorescence intensity of MFFR was measured in energized and FCCP uncoupled hepatocytes. In the absence of hepatocytes, the fluorescence intensity was 337 a.u. at 712 nm in the representative experiment shown in Figure 3- 20. Accumulation of MFFR by energized hepatocytes resulted in a decrease in the fluorescence intensity to 201 a.u.(40 % lower than in the buffer) an indication of changes in optical properties of MFFR upon binding. The addition of FCCP to energized hepatocytes partially restored the MFFR fluorescence intensity to 258 a.u. (28.1 % higher than in the energized hepatocytes). This increase in the fluorescence intensity was presumably caused by release of MFFR from cellular mitochondria.

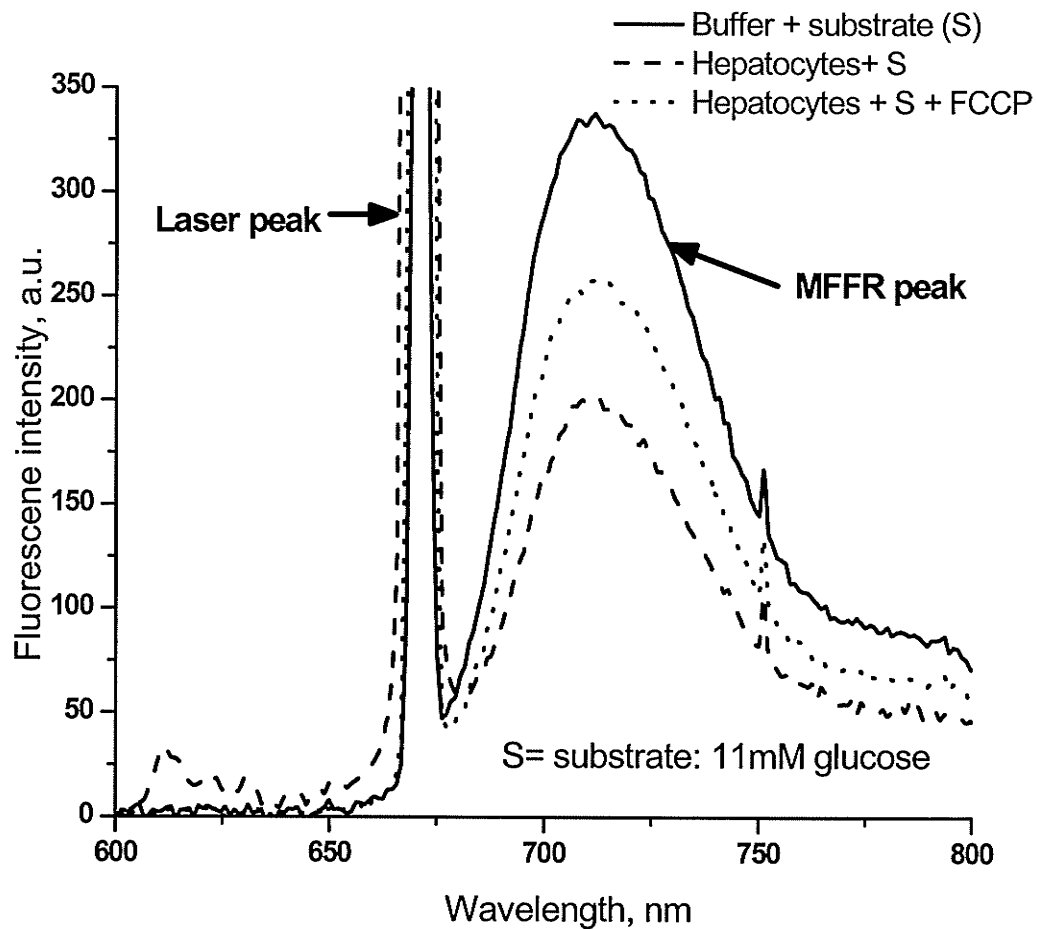


Figure 3-20. MFFR fluorescence spectra of hepatocyte suspension. Isolated rat liver hepatocytes (1.24mg/mL) were added to $1\mu\text{M}$ MFFR in hepatocytes low K^+ incubation buffer (for details see in 2.2.7 of Materials and Methods section) with 11mM glucose. Subsequently FCCP was added to uncouple hepatocytes. The fluorescence maxima were between 708-720nm.

To determine the time course of MFFR fluorescence, the fluorescence intensity of MFFR was measured as a function of time. Figure 3-21 shows changes of MFFR fluorescence intensity induced by hepatocyte addition and subsequent FCCP treatment. Addition of hepatocytes slowly decreased the fluorescence intensity of MFFR within 7 minutes from 311 to 186 a.u. After the fluorescence intensity of MFFR was observed for 5 minutes, $1\mu\text{M}$ FCCP was added, which resulted in a slight increase in the fluorescence intensity within 2 minutes from 216 to 228 and stabilization of its level.

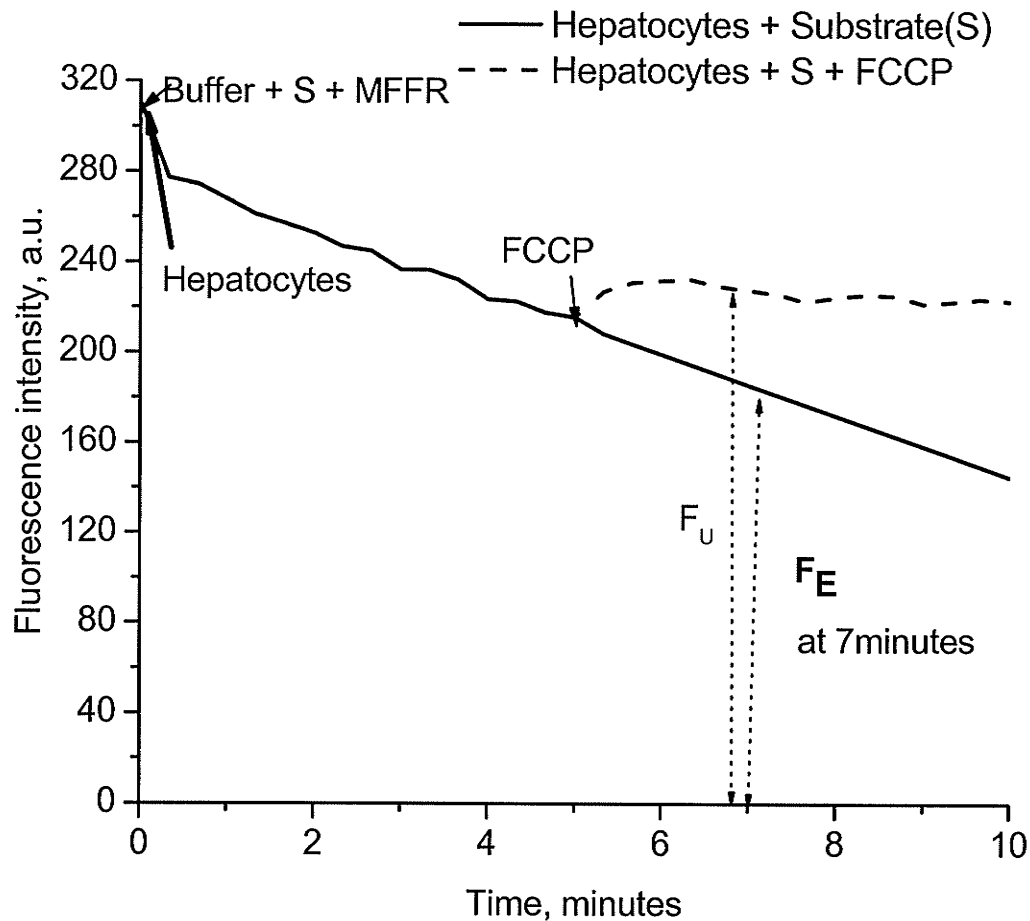


Figure 3-21. Time course of MFFR fluorescence in hepatocyte suspension. Spectra were recorded every 20 seconds for 10 minutes. Hepatocytes were energized by glucose (S, 11mM) for 5 minutes and then $1\mu\text{M}$ FCCP was added to uncouple the cells. The fluorescence intensity was measured between 708 and 720 nm at 7 minutes. F_O is the initial fluorescence intensity before the addition of hepatocytes, F_E is the fluorescence intensity after the addition of hepatocytes (energized), and F_U is the fluorescence intensity after the addition of FCCP (uncoupled).

To determine whether the fluorescence intensity of MFFR is dependent on the concentration of hepatocytes protein, the fluorescence intensity was measured at 7 minutes as a function of hepatocytes concentration (protein, mg/mL). In this experiment, the fluorescence peak was normalized to the initial fluorescence to calculate the change in the F_E/F_O and F_U/F_O ratios. Figure 3-22 shows that the protein concentration (0.06-1.24 mg/mL) did significantly affect F_E/F_O and F_U/F_O values. The values of the changes obtained after the addition of hepatocytes ($1 - F_E/F_O$) as well as the change in ratio upon the addition of FCCP ($1 - F_U/F_O$) to the hepatocytes were plotted against the protein concentration. The value for energized hepatocytes increased from 0.14 ± 0.01 at protein concentration of 0.06 mg/mL to 0.53 ± 0.04 at the concentration of 0.72 mg/mL. However, at protein concentrations above 0.72mg/mL, the value slightly decreased from 0.52 ± 0.1 to 0.41 ± 0.03 with increasing protein concentration to 1.24 mg/mL. Similarly, the value for uncoupled hepatocytes was increased from 0.13 ± 0.01 at protein concentration of 0.06 mg/mL to 0.33 ± 0.01 at the concentration of 0.72 mg/mL. Then, the value was slightly decreased from 0.33 ± 0.01 to 0.22 ± 0.01 with increasing protein concentration to 1.24 mg/mL.

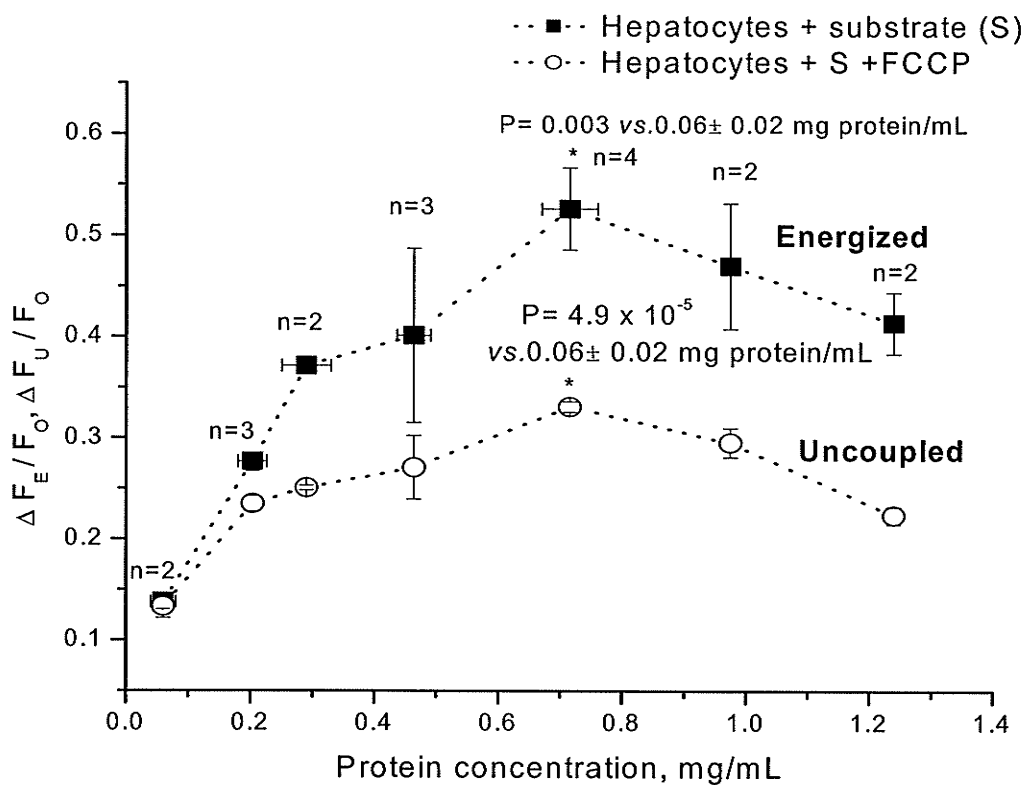


Figure 3-22. $\Delta F/F_0$ for energized (■) and uncoupled hepatocytes (○) as a function of protein concentration (0.06- 1.24mg/mL). Hepatocytes were energized by 11mM glucose and uncoupled with $1\mu\text{M}$ FCCP. Average cell viability was 63%. Data are presented as mean \pm S.E.

The fraction of bound MFFR increased up to 79 and 64 % (% of total bound MFFR plus free MFFR) in the energized and the uncoupled hepatocytes, respectively in response to increase in the protein concentration to 0.87 ± 0.1 mg/mL (Figure 3-23).

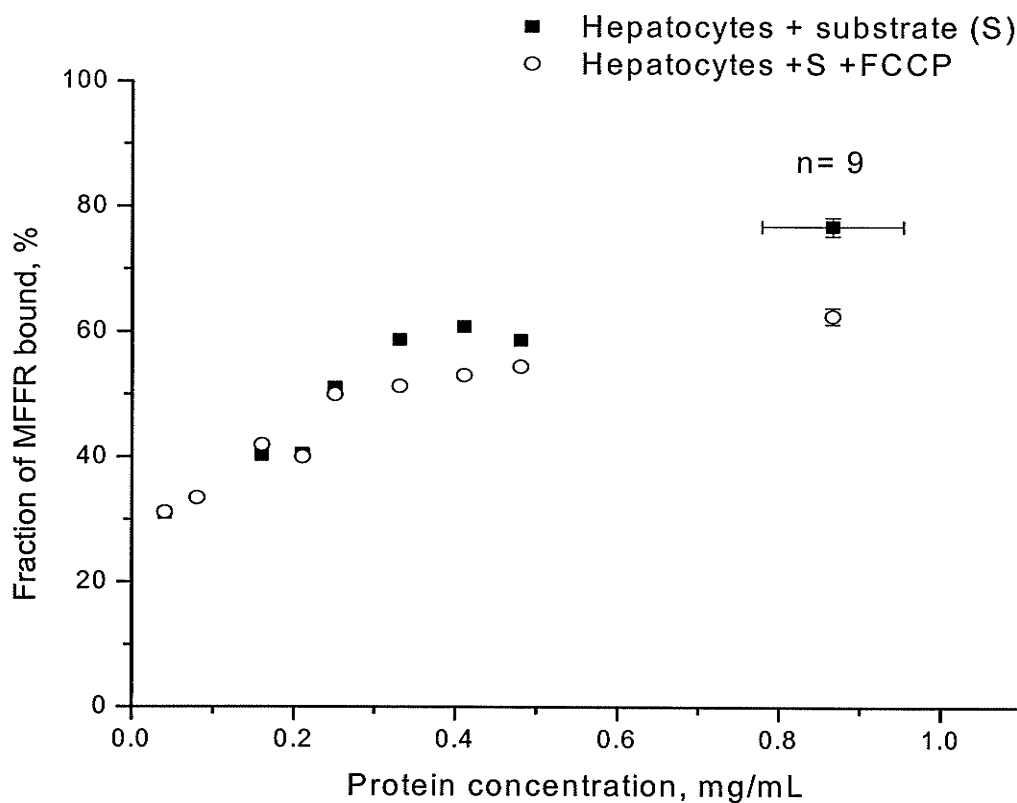


Figure 3-23. The relationship between the amounts of MFFR bound to energized and uncoupled hepatocytes and protein concentrations (0.04 – 1.24 mg/mL). The percentage of bound MFFR was calculated as a ratio of the amount of bound MFFR to the total amount of MFFR (bound plus free). Average cell viability was 63%.

To investigate the relationship between the changes in the fluorescence ratios F_E and F_U to F_O and the amount of MFFR bound, MFFR binding was measured. Subsequently, hepatocytes were separated and the amount of MFFR determined as described in section 2.2.7. Increases in the amount of bound MFFR correlated with an increase in the fluorescence change. A positive correlation ($R^2 = 0.64$) was obtained between the change in the fluorescence ratio and the amount of MFFR bound in the range of 32-80 % binding (Figure 3-24). Mean values of the fluorescence change between energized and uncoupled hepatocytes plotted over the amount of MFFR bound were significantly different at a level of $P < 0.05$. In general, higher MFFR binding to the cells resulted in greater changes in fluorescence.

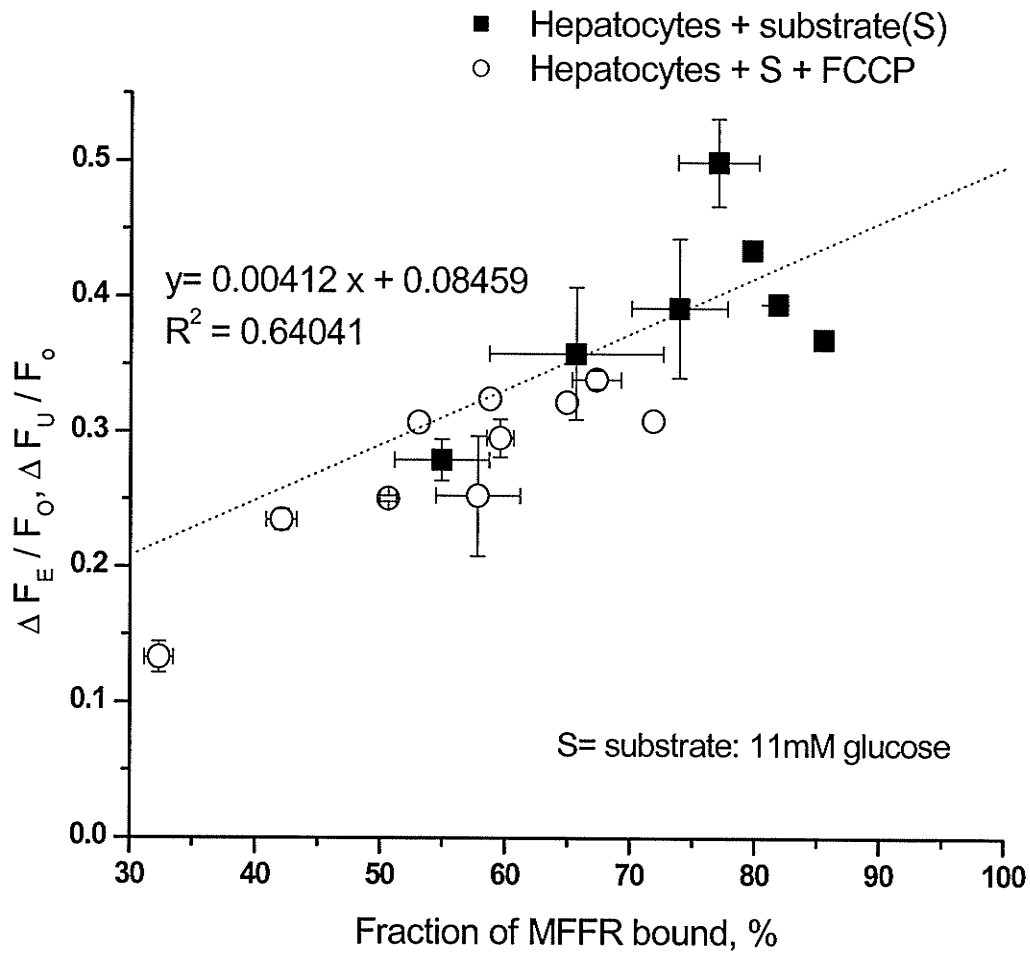


Figure 3-24. The relationship between the amounts of MFFR bound to energized and uncoupled hepatocytes and fluorescence changes. The fraction of MFFR bound was calculated as the percentage of the amount of MFFR bound relative to the total amount of MFFR (bound plus free). Binding and fluorescence were varied by changing cell concentration from 0.06 to 1.24 mg protein / mL. Average cell viability was 63%. Data are presented as mean \pm S.E.

CHAPTER 4

DISCUSSION

4.1 Summary of Major Findings

MFFR binding measurements allowed quantitative estimation of $\Delta\Psi_m$ in isolated mitochondria. In the studies that were undertaken to investigate the relationship between $\Delta\Psi_m$ and MFFR binding in isolated mitochondria, it was shown that MFFR binding was dependent on $\Delta\Psi_m$ (Figure 3-1). The dependence of MFFR binding on $\Delta\Psi_m$ was not affected by two incubation buffers representing the physiological cellular environment (high K^+) and iso-osmotic sucrose buffer. The generation of $\Delta\Psi_m$ in energized mitochondria by substrate oxidation, ATP hydrolysis or both resulted in accumulation of MFFR in the mitochondria. Changes in $\Delta\Psi_m$ induced changes in the magnitude of MFFR binding to the mitochondria. In mitochondria energized by respiration and ATP hydrolysis, FCCP depolarized $\Delta\Psi_m$ by approximately 140 mV (Figure 3-2), which is similar to the literature value (~160mV). In addition, FCCP decreased $\Delta\Psi_m$ by about 104 mV in mitochondria energized by respiration alone and by about 81mV in mitochondria energized by ATP hydrolysis alone (Figure 3-3). These values are lower than those mitochondria energized by both respiration and ATP hydrolysis.

It is recognized that TMRM is the most reliable dye for measurements of $\Delta\Psi_m$ due to its lower toxicity to mitochondria than rhodamine 123 and TMRE [131]. A linear relationship between $\Delta\Psi_m$ and fluorescence of TMRM was demonstrated. Therefore, TMRM was selected as an indicator for comparing with MFFR. We compared the

binding of MFFR and TMRM to mitochondria as a function of $\Delta\Psi_m$ in isolated mitochondria using our protocol of directly measuring the dye content in the mitochondria. The results showed that MFFR is comparable with TMRM because $\Delta\Psi_m$ values determined from MFFR and TMRM binding showed linear correlations with similar slopes (Figure 3-4).

Inhibitory analysis with oligomycin, atractyloside and P-1075 allowed us to estimate changes in $\Delta\Psi_m$ in MFFR binding measurements. Oligomycin, an inhibitor of ATP synthase and atractyloside, an inhibitor of ATP/ADP translocase partially decreased $\Delta\Psi_m$ by approximately 60 and 50 mV, respectively (Fig 3-3). P-1075, a mito- K_{ATP} opener slightly depolarized $\Delta\Psi_m$ by approximately 7 mV. By using these agents we were able to estimate $\Delta\Psi_m$, which allowed us to investigate the relationship of MFFR binding to the membrane potential. Based on the results from these studies we conclude that accumulation of MFFR depends on $\Delta\Psi_m$ in mitochondria. Therefore MFFR binding is useful for the quantitative estimation of $\Delta\Psi_m$ in isolated mitochondria.

MFFR binding measurements allow only qualitative estimation of $\Delta\Psi_m$ in cells. After demonstrating that MFFR binding in isolated mitochondria was dependent on $\Delta\Psi_m$, the experiments were conducted in cardiomyocytes and hepatocytes to determine dependence of MFFR binding on $\Delta\Psi_m$ in the cells. The bound/free ratio of MFFR was lower in cardiomyocytes and hepatocytes than in mitochondrial suspension indicating that there was less MFFR binding in the cells (Table 3-3). Seventy five percent was bound to the cells after correction for cell viability whereas 99% of the total MFFR was bound in the isolated mitochondria (Figure 3-1).

MFFR binding to mitochondria and cells resulted in decreases in its fluorescence. It was demonstrated that the fluorescence intensity decreased upon addition of the mitochondria and cells energized by oxidizable substrates whereas fluorescence intensity increased upon addition of FCCP, which caused release of bound MFFR (Figures 3-10, 3-14, and 3-20). However, the magnitude of changes in fluorescence intensity was different. The MFFR fluorescence intensity decreased by 86 % of that in the buffer (100%) by the addition of mitochondria and recovered to 70% of that in energized mitochondria in response to FCCP. The degree of changes in MFFR fluorescence due to different mitochondrial energy states was similar to that found by Sakanoue et al. 1997. In the cell suspensions, the fluorescence intensity decreased by 24% and 40% of that in the buffer by the addition of cardiomyocytes and hepatocytes, respectively and recovered to 84% and 72% of that in the energized cells in response to FCCP addition, respectively. It showed that more binding corresponds to larger changes in fluorescence.

4.2 MFFR Binding and $\Delta\Psi_m$

Dye binding is determined by two components, $\Delta\Psi_m$ - dependent (matrix accumulation) and $\Delta\Psi_m$ - independent (membrane and non-mitochondrial binding). $\Delta\Psi_m$ - dependent binding is determined by an increase in the matrix dye concentration. In isolated mitochondria, the $\Delta\Psi_m$ - independent component can be expressed through the partition coefficient, $P = [C]_{\text{membrane}} / [C]_{\text{matrix}}$ where $[C]_{\text{membrane}}$ and $[C]_{\text{matrix}}$ are dye concentrations in mitochondrial membrane and matrix, respectively. Since $[C]_{\text{membrane}} = P \times [C]_{\text{matrix}}$, $[C]_{\text{membrane}}$ and $[C]_{\text{matrix}}$ are functions of $\Delta\Psi_m$. Combined with the Nernst equation it gives us: Mitochondrial dye content (MDC) / $[C]_{\text{cytoplasm}} = (V_{\text{matrix}} + P \times$

$V_{\text{membrane}}) \times \exp(-\Delta\Psi_m \times F/RT)$ where $[C]_{\text{cytosol}}$ is an equilibrium cytosol dye concentration, V_{matrix} and V_{membrane} are volumes of matrix and membrane, respectively, F is a Faraday's constant, R , gas constant and T , absolute temperature.

In cells there is truly a $\Delta\Psi_m$ – independent component, which includes binding to non-mitochondrial constituents: cell membranes, DNA/RNA, cytosol and other cell structures. This component comprises a considerable portion of dye binding and remains constant in response to cell de-energization or even increases as the extra-mitochondrial dye concentration increases upon de-energization. In other words, uncoupling causes considerable dye redistribution between mitochondria and other cell structures rather than its significant efflux from the cells. This makes quantitative evaluation of $\Delta\Psi_m$ in cell suspensions extremely difficult.

4.3 Relationships between Dye Binding and Fluorescence

In general, there is a correlation between dye binding to mitochondria and cells and a fluorescence decrease (ΔF). This can be explained by fluorescence quenching (dimer formation and self-quenching) during dye accumulation in mitochondria [117, 118] and lack thereof during diffusion into the cytosol and binding with cell structures. Indeed, the mitochondrial volume fraction in the cells is 10-30%, which inevitably allows binding of only a fraction of cell dye to mitochondria. If dye binding with non-mitochondrial cell structures and its fluorescence remain relatively constant, the response to the uncoupler should be significantly smaller as compared to mitochondria.

4.4 Effects of Mitochondrial and Cell Concentrations on Dye Fluorescence

Theoretically, in the closed system (total dye amount = constant) the dependence of any fluorescence decrease ($\Delta F/F_0$) on mitochondrial/cell concentration should be a bell-shaped function. Indeed, as the cell protein concentration increases from zero, ΔF increases due to an increase in the intra-mitochondrial dye content and concentration that results in net fluorescence quenching. However, at high protein concentrations (high intra-mitochondrial volume), when nearly all dye is already inside mitochondria, matrix dye concentration is low and dimerization and self-quenching are reduced. This should result in a ΔF decrease. At intermediate protein concentrations effects of dye accumulation and dilution in the mitochondrial matrix cancel each other. Experimentally this kind of dependence was observed in hepatocytes (Figure 3-22) and cardiomyocytes (Figure 3-16). However in the isolated mitochondria the dependence was flat (Fig. 3-13), perhaps due to significant dye binding even at the lowest concentration of 0.03 mg/ml.

4.5 Conclusions

MFFR is suitable for quantitative measurements of $\Delta\Psi_m$ in isolated mitochondria. Advantages of this dye are as follows: a) its NIR absorption (~680 nm) and fluorescence (708-720 nm) eliminate interference from endogenous chromophores (myoglobin and cytochromes), which strongly absorb visible light but not the NIR one; b) reduced NIR

light scattering in comparison with visible light, which allows the use of more concentrated cells/mitochondria suspensions. A major disadvantage of MFFR is its high hydrophobicity, which causes its strong binding to mitochondrial membranes and cell structures making $\Delta\Psi_m$ -independent binding dominant.

We conclude that MFFR can be used for evaluation of energetic changes and viability in isolated cells, however quantitative $\Delta\Psi_m$ measurements are problematic. NIR dye(s) with similar optical properties but lower hydrophobicity would be more suitable than MFFR for cellular and tissue applications.

REFERENCES

- [1] Marin-Garcia, J., and Goldenthal, M.J. (2004). Heart mitochondria signaling pathways: appraisal of an emerging field. *J. Mol. Med.*, **82**:565-578.
- [2] Di Lisa, F., and Bernardi, P. (1998). Mitochondrial function as a determinant of recovery or death in cell response to injury. *Mol. Cell Biochem.*, **184**:379-391.
- [3] Kupriyanov, V.V., Lakomkin, V.L., Korchazhkina, O.V., Stepanov, V.A., Steinschneider, A.Ya., and Kapelko, V.I. (1991). Cardiac contractile function, oxygen consumption rate and cytosolic phosphates during inhibition of electron flux by amytal--a ³¹P-NMR study. *Biochim. Biophys. Acta*, **1058**:386-399.
- [4] Jilkina, O., Kuzio, B., Grover, G.J., and Kupriyanov, V.V. (2002). Effects of K(ATP) channel openers, P-1075, pinacidil, and diazoxide, on energetics and contractile function in isolated rat hearts. *J. Mol. Cell Cardiol.*, **34**:427-440.
- [5] Tamura, M., Hazeki, O., Nioka, S., Chance, B. (1989). In vivo study of tissue oxygen metabolism using optical and nuclear magnetic resonance spectroscopies. *Annu. Rev. Physiol.*, **51**:813-834.
- [6] Heineman, F.W., Kupriyanov, V.V., Marshall, R., Fralix, T.A., and Balaban, R.S. (1992). Myocardial oxygenation in the isolated working rabbit heart as a function of work. *Am. J. Physiol.*, **262**:H255-267.
- [7] Nishiki, K., Erecinska, M., and Wilson, D.F. (1978). Energy relationships between cytosolic metabolism and mitochondrial respiration in rat heart. *Am. J. Physiol.*, **234**:73-81.
- [8] Gruwel, M.L., Kuzio, B., Deslauriers, R., and Kupriyanov, V.V. (1998). Observation of two inorganic phosphate NMR resonances in the perfused hypothermic rat heart. *Cryobiology*, **37**:355-361.
- [9] Mitchell, P. (1966). Chemiosmotic coupling in oxidative and photosynthetic phosphorylation. *Biol. Rev. Camb. Philos. Soc.*, **41**:445-502.
- [10] Rottenberg, H. (1970). ATP synthesis and electrical membrane potential in mitochondria. *Eur. J. Biochem.*, **15**:22-28.
- [11] Jacobus, W.E. (1985). Respiratory control and the integration of heart high-energy phosphate metabolism by mitochondrial creatine kinase. *Annu. Rev. Physiol.*, **47**:707-725.
- [12] Harris, D.A., and Das, A.M. (1991). Control of mitochondrial ATP synthesis in the heart. *Biochem. J.*, **280**: 561-573.

- [13] Ventura-Clapier, R., Garnier, A., and Veksler, V. (2004). Energy metabolism in heart failure. *J. Physiol.*, **555**:1-13.
- [14] Burkhoff, D., Weiss, R.G., Schulman, S.P., Kalil-Filho, R., Wannenburg, T., and Gerstenblith, G. (1991). Influence of metabolic substrate on rat heart function and metabolism at different coronary flows. *Am. J. Physiol.*, **261**:H741-750.
- [15] Mallet, R.T., and Bungler, R. (1994). Energetic modulation of cardiac inotropism and sarcoplasmic reticular Ca²⁺ uptake. *Biochim. Biophys. Acta*, **1224**:22-32.
- [16] Berkich, D.A., Williams, G.D., Masiakos, P.T., Smith, M.B., Boyer, P.D., and LaNoue, K.F. (1991). Rates of various reactions catalyzed by ATP synthase as related to the mechanism of ATP synthesis. *J. Biol. Chem.*, **266**:123-129.
- [17] Kingsley-Hickman, P.B., Sako, E.Y., Mohanakrishnan, P., Robitaille, P.M., From, A.H., Foker, J.E., and Ugurbil, K. (1987). ³¹P NMR studies of ATP synthesis and hydrolysis kinetics in the intact myocardium. *Biochemistry*, **26**:7501-7510.
- [18] LaNoue, K.F., Jeffries, F.M., and Radda, G.K. (1986). Kinetic control of mitochondrial ATP synthesis. *Biochemistry*, **25**:7667-7675.
- [19] Wan, B., Doumenm C., Duszynski, J., Salama, G., Vary, T.C., and LaNoue, K.F. (1993). Effects of cardiac work on electrical potential gradient across mitochondrial membrane in perfused rat hearts. *Am. J. Physiol.*, **265**:H453-460.
- [20] Zweier, J.L., and Jacobus, W.E. (1987). Substrate-induced alterations of high energy phosphate metabolism and contractile function in the perfused heart. *J. Biol. Chem.*, **262**:8015-8021.
- [21] Monteiro, P., Duarte, A., Moreno, A., Goncalves, L., and Providencia, L.A. (2003). Pyruvate improves mitochondrial bioenergetics in an ex-vivo animal model of myocardial ischemia. *Rev. Port. Cardiol.*, **22**:79-88.
- [22] Saks, V.A., Rosenshtraukh, L.V., Smirnov, V.N., and Chazov, E.I. (1978). Role of creatine phosphokinase in cellular function and metabolism. *Can. J. Physiol. Pharmacol.*, **56**:691-706.
- [23] Dos Santos, P., Aliev, M.K., Diolez, P., Duclos, F., Besse, P., Bonoron-Adele, S., Sikk, P., Canioni, P., and Saks, V.A. (2000). Metabolic control of contractile performance in isolated perfused rat heart. Analysis of experimental data by reaction:diffusion mathematical model. *J. Mol. Cell Cardiol.*, **32**:1703-1734.
- [24] Opie, L.H. (1965). Coronary flow rate and perfusion pressure as determinants of mechanical function and oxidative metabolism of isolated perfused rat heart. *J. Physiol.*, **180**:529-541.

- [25] Neely, J.R., Liebmeister, H. and Morgan, H. (1967). Effect of pressure development on membrane transport of glucose in isolated rat heart. *Am. J. Physiol.*, **212**:815-822.
- [26] Neely, J.R., Rovetto, M.J. and Oram, J.F. (1972). Myocardial utilization of carbohydrate and lipids. *Prog. Cardiovasc. Dis.*, **15**:289-329.
- [27] Neely, J.R., and Morgan, H.E. (1974). Relationship between carbohydrate and lipid metabolism and the energy balance of heart muscle. *Annu. Rev. Physiol.*, **36**:413-459.
- [28] Williamson, J.R., Ford, C., Kobayashi, K., Illigworth, J. and Safer, B. (1976). Coordination of citric acid cycle activity with electron transport flux. *Circ. Res.*, **38**:39-48.
- [29] Kobayahi, K., and J.R. Neely. (1979). Control of maximal glycolysis in rat cardiac muscle. *Circ. Res.*, **44**: 166-175.
- [30] Bungler, R., and Soboll, S. (1986). Cytosolic adenylates and adenosine release in perfused working heart. Comparison of whole tissue with cytosolic non-aqueous fractionation analyses. *Eur. J. Biochem.*, **159**:203-213.
- [31] Katz, L.A., Swain, J.A., Portman, M.A., and Balaban, R.S. (1989). Relation between phosphate metabolites and oxygen consumption of heart in vivo. *Am. J. Physiol.*, **256**:H265-274.
- [32] Koretsky, A.P., Katz, L.A., and Balaban, R.S. (1989). The mechanism of respiratory control in the in vivo heart. *J. Mol. Cell Cardiol.*, **21**:59-66.
- [33] Jeffrey, F.M., and Malloy, C.R. (1992). Respiratory control and substrate effects in the working rat heart. *Biochem. J.*, **287**:117-123.
- [34] From, A.H., Petein, M.A., Michurski, S.P., Zimmer, S.D., and Ugurbil, K. (1986). ³¹P-NMR studies of respiratory regulation in the intact myocardium. *FEBS Lett.*, **206**:257-261.
- [35] From, A.H., Zimmer, S.D., Michurski, S.P., Mohanakrishnan, P., Ulstad, V.K., Thoma, W.J., and Ugurbil, K. (1990). Regulation of the oxidative phosphorylation rate in the intact cell. *Biochemistry*, **29**:3731-3743.
- [36] Neely, J.R., Denton, R.M., England, P.J., and Randle, P.J. (1972). The effects of increased heart work on the tricarboxylate cycle and its interactions with glycolysis in the perfused rat heart. *Biochem. J.*, **128**:147-159.

- [37] Chance, B., and Williams, G. (1956). The respiratory chain and oxidative phosphorylation. *Adv. Enzymol. Relat. Subj. Biochem.*, **17**:65-134.
- [38] Alberts, B., Bray, D., Lweis, J., Raff, M., Roberts, K., and Watson, J.D. (eds.) (1994). *Molecular Biology of the Cell*. Garland, New York and London.
- [39] Granville, D.J., and Gottlieb, R.A. (2002). Mitochondria: regulators of cell death and survival. *Scientific WorldJournal*, **2**:1569-1578.
- [40] Crompton, M., Andreeva, L. (1993). On the involvement of a mitochondrial pore in reperfusion injury. *Basic Res. Cardiol.*, **88**:513-523.
- [41] Cortese, J.D., Voglino, A.L., and Hackenbrock, C.R. (1992). The ionic strength of the intermembrane space of intact mitochondria is not affected by the pH or volume of the intermembrane space. *Biochim. Biophys. Acta*, **1100**:189-197.
- [42] Hoch, F.L. (1992). Cardiolipins and biomembrane function. *Biochim. Biophys. Acta*, **1113**:71-133.
- [43] Araki, R., Tamura, M., and Yamazaki, I. (1983). The effect of intracellular oxygen concentration on lactate release, pyridine nucleotide reduction, and respiration rate in the rat cardiac tissue. *Circ. Res.*, **53**:448-455.
- [44] Carvajal, K., and Moreno-Sanchez, R. (2003). Heart metabolic disturbances in cardiovascular diseases. *Arch. Med. Res.*, **34**:89-99.
- [45] Zierler, K.L. (1976). Fatty acids as substrates for heart and skeletal muscle. *Circ. Res.*, **38**:459-463.
- [46] Heales, S.J, Gegg, M.E., and Clark, J.B. (2002). Oxidative phosphorylation: structure, function, and intermediary metabolism. *Int. Rev. Neurobiol.*, **53**:25-56.
- [47] Nelson, D.L., and Cox, M.M. (eds.) (2000). *Lehninger Principles of Biochemistry*. Worth Publishers, New York, 184-215.
- [48] Lenaz, G., Bovina, C., Castelluccio, C., Fato, R., Formiggini, G., Genova, M.L., Marchetti, M., Pich, M.M., Pallotti, F., Parenti Castelli, G., and Biagini, G. (1997). Mitochondrial complex I defects in aging. *Mol. Cell Biochem.*, **174**:329-333.
- [49] Inomoto, T., Tanaka, A., Mori, S., Jin, M.B., Sato, B., Yanabu, N., Tokuka, A., Kitai T., Ozawa, K., and Yamaoka, Y. (1994). Changes in the distribution of the control of the mitochondrial oxidative phosphorylation in regenerating rabbit liver. *Biochim. Biophys. Acta*, **1188**:311-317.

- [50] Kuznetsov, A.V., Winkler, K., Kirches, E., Lins, H., Feistner, H., and Kunz, W.S. (1997). Application of inhibitor titrations for the detection of oxidative phosphorylation defects in saponin-skinned muscle fibers of patients with mitochondrial diseases. *Biochim. Biophys. Acta*, **1360**:142-150.
- [51] Mitchell, P., and Moyle, J. (1976). Chemiosmotic hypothesis of oxidative phosphorylation. *Nature*, **213**:137-139.
- [52] Nicholls, D.G., and Budd, S.L. (2000). Mitochondria and neuronal survival. *Physiol. Rev.*, **80**: 315-360.
- [53] Nishiki, K., Erecinska, M., and Wilson, D.F. (1979). Effect of Amytal on metabolism of perfused rat heart: relationship between glycolysis and oxidative phosphorylation. *Am. J. Physiol.*, **237**:C221-230.
- [54] Li, N., Ragheb, K., Lawler, G., Sturgis, J., Rajwa, B., Melendez, J.A., and Robinson, J.P. (2003). Mitochondrial complex I inhibitor rotenone induces apoptosis through enhancing mitochondrial reactive oxygen species production. *J. Biol. Chem.*, **278**:8516-8525.
- [55] Huang, L.S., Cobessi, D., Tung, E.Y., and Berry, E.A. (2005). Binding of the respiratory chain inhibitor antimycin to the mitochondrial bc₁ complex: a new crystal structure reveals an altered intramolecular hydrogen-bonding pattern. *J. Mol. Biol.*, **351**:573-597.
- [56] Zhang, J.G., Tirmenstein, M.A., Nicholls-Grzemeski, F.A., and Fariss, M.W. (2001). Mitochondrial electron transport inhibitors cause lipid peroxidation-dependent and -independent cell death: protective role of antioxidants. *Arch. Biochem. Biophys.*, **393**:87-96.
- [57] Bertina, R.M., Steenstra, J.A., and Slater, E.C. (1974). The mechanism of inhibition by oligomycin of oxidative phosphorylation in mitochondria. *Biochim. Biophys. Acta*, **368**:279-297.
- [58] Davis, E.J., and Davis-Van Thienen, W.I. (1984). Rate control of phosphorylation-coupled respiration by rat liver mitochondria. *Arch. Biochem. Biophys.*, **233**:573-581.
- [59] Mokhova, E.N., and Rozovskaya, I.A. (1986). The effects of mitochondrial energetics inhibitors on the fluorescence of potential-sensitive dyes rhodamine 123 and diS-C3-(5) in lymphocyte suspensions. *J. Bioenerg. Biomembr.*, **18**:265-276.

- [60] Jilkina, O., Kuzio, B., Grover, G.J., Folmes, C.D., Kong, H.J., and Kupriyanov, V.V. (2003). Sarcolemmal and mitochondrial effects of a KATP opener, P-1075, in "polarized" and "depolarized" Langendorff-perfused rat hearts. *Biochim. Biophys. Acta*, **1618**:39-50.
- [61] Pompermayer, K., Souza, D.G., Lara, G.G., Silveira, K.D., Cassali, G.D., Andrade, A.A., Bonjardim, C.A., Passaglio, K.T., Assreuy, J., Cunha, F.Q., Vieira, M.A., and Teixeira, M.M. (2005). The ATP-sensitive potassium channel blocker glibenclamide prevents renal ischemia/reperfusion injury in rats. *Kidney Int.*, **67**:1785-1796.
- [62] Garlid, K.D. (1996). Cation transport in mitochondria--the potassium cycle. *Biochim. Biophys. Acta*, **1275**:123-126.
- [63] Campos, Y., Martin, M.A., Garcia-Silva, T., del Hoyo, P., Rubio, J.C., Castro-Gago, M., Garcia-Penas, J., Casas, J., Cabello, A., Ricoy, J.R., and Arenas, J. (1998). Clinical heterogeneity associated with mitochondrial DNA depletion in muscle. *Neuromuscul. Disord.*, **8**:568-573.
- [64] Regitz, V., Paulson, D.J., Hodach, R.J., Little, S.E., Schaper, W., and Shug, A.L. (1984). Mitochondrial damage during myocardial ischemia. *Basic Res. Cardiol.*, **79**:207-217.
- [65] Piper, H.M., Noll, T., and Siegmund, B. (1994). Mitochondrial function in the oxygen depleted and reoxygenated myocardial cell. *Cardiovasc. Res.*, **28**:1-15.
- [66] Borutaite, V., Morkuniene, R., Budriunaite, A., Krasauskaite, D., Ryselis, S., Toleikis, A., and Brown, G.C. (1996). Kinetic analysis of changes in activity of heart mitochondrial oxidative phosphorylation system induced by ischemia. *J. Mol. Cell Cardiol.*, **28**:2195-2201.
- [67] Lesnefsky, E.J., Tandler, B., Ye, J., Slabe, T.J., Turkaly, J., and Hoppel, C.L. (1997). Myocardial ischemia decreases oxidative phosphorylation through cytochrome oxidase in subsarcolemmal mitochondria. *Am. J. Physiol.*, **273**:H1544-554.
- [68] Piper, H.M., Sezer, O., Schleyer, M., Schwartz, P., Hutter, J.F., and Spieckermann, P.G. (1985). Development of ischemia-induced damage in defined mitochondrial subpopulations. *J. Mol. Cell Cardiol.*, **17**:885-896.
- [69] Rouslin, W. (1983). Mitochondrial complexes I, II, III, IV, and V in myocardial ischemia and autolysis. *Am. J. Physiol.*, **244**:H743-748.
- [70] Flameng, W., Andres, J., Ferdinande, P., Mattheussen, M., and Van Belle, H. (1991). Mitochondrial function in myocardial stunning. *J. Mol. Cell Cardiol.*, **23**:1-11.

- [71] Iwai, T., Tanonaka, K., Inoue, R., Kasahara, S., Kamo, N., and Takeo, S. (2002). Mitochondrial damage during ischemia determines post-ischemic contractile dysfunction in perfused rat heart. *J. Mol. Cell Cardiol.*, **34**:725-738.
- [72] Duan, J., Karmazyn, M. (1989). Relationship between oxidative phosphorylation and adenine nucleotide translocase activity of two populations of cardiac mitochondria and mechanical recovery of ischemic hearts following reperfusion. *Can. J. Physiol. Pharmacol.*, **67**:704-709.
- [73] Asimakis, G.K., Conti, V.R. (1984). Myocardial ischemia: correlation of mitochondrial adenine nucleotide and respiratory function. *J. Mol. Cell Cardiol.*, **16**:439-447.
- [74] Berkich, D.A., Salama, G., and LaNoue, K.F. (2003). Mitochondrial membrane potentials in ischemic hearts. *Arch. Biochem. Biophys.*, **420**:279-286.
- [75] Murfitt, R.R., Stiles, J.W., Powell, W.J.Jr., Sanadi, D.R. (1978). Experimental myocardial ischemia characteristics of isolated mitochondrial subpopulations. *J. Mol. Cell Cardiol.*, **10**:109-123.
- [76] Lesnefsky, E.J., Slabe, T.J., Stoll, M.S., Minkler, P.E., and Hoppel, C.L. (2001). Myocardial ischemia selectively depletes cardiolipin in rabbit heart subsarcolemmal mitochondria. *Am. J. Physiol. Heart Circ. Physiol.*, **280**:H2770-2778.
- [77] Paradies, G., Petrosillo, G., Pistolese, M., Di Venosa, N., Serena, D., and Ruggiero, F.M. (1999). Lipid peroxidation and alterations to oxidative metabolism in mitochondria isolated from rat heart subjected to ischemia and reperfusion. *Free Radic. Biol. Med.*, **27**:42-50.
- [78] Shidoji, Y., Hayashi, K., Komura, S., Ohishi, N., and Yagi, K. (1999). Loss of molecular interaction between cytochrome c and cardiolipin due to lipid peroxidation. *Biochem. Biophys. Res. Commun.*, **264**:343-347.
- [79] Rytomaa, M., and Kinnunen, P.K. (1994). Evidence for two distinct acidic phospholipid-binding sites in cytochrome c. *J. Biol. Chem.*, **269**:1770-1774.
- [80] Lesnefsky, E.J., Chen, Q., Slabe, T.J., Stoll, M.S., Minkler, P.E., Hassan, M.O., Tandler, B., and Hoppel, C.L. (2004). Ischemia, rather than reperfusion, inhibits respiration through cytochrome oxidase in the isolated, perfused rabbit heart: role of cardiolipin. *Am. J. Physiol. Heart Circ. Physiol.*, **287**:H258-267.
- [81] Turrens, J.F., and Boveris, A. (1980). Generation of superoxide anion by the NADH dehydrogenase of bovine heart mitochondria. *Biochem. J.*, **191**:421-427.

- [82] Turrens, J.F. (1997). Superoxide production by the mitochondrial respiratory chain. *Biosci. Rep.*, **17**:3-8.
- [83] Davies, M.J. (1989). Direct detection of radical production in the ischaemic and reperfused myocardium: current status. *Free Radic. Res. Commun.*, **7**:275-284.
- [84] Becker, L.B., vanden Hoek, T.L., Shao, Z.H., Li, C.Q., and Schumacker, P.T. (1999). Generation of superoxide in cardiomyocytes during ischemia before reperfusion. *Am. J. Physiol.*, **277**:H2240-2246.
- [85] Sugioka, K., Nakano, M., Totsune-Nakano, H., Minakami, H., Tero-Kubota, S., and Ikegami, Y. (1988). Mechanism of O₂⁻ generation in reduction and oxidation cycle of ubiquinones in a model of mitochondrial electron transport systems. *Biochim. Biophys. Acta*, **936**:377-385.
- [86] Turrens, J.F., Alexandre, A., and Lehninger, A.L. (1985). Ubisemiquinone is the electron donor for superoxide formation by complex III of heart mitochondria. *Arch. Biochem. Biophys.*, **237**:408-14.
- [87] Radi, R., Rodriguez, M., Castro, L., and Telleri, R. (1994). Inhibition of mitochondrial electron transport by peroxynitrite. *Arch. Biochem. Biophys.*, **308**:89-95.
- [88] Pepe, S. (2000). Mitochondrial function in ischaemia and reperfusion of the ageing heart. *Clin Exp. Pharmacol. Physiol.*, **27**:745-750.
- [89] Griffiths, E.J., and Halestrap, A.P. (1995). Mitochondrial non-specific pores remain closed during cardiac ischaemia, but open upon reperfusion. *Biochem. J.*, **307**:93-98.
- [90] Li, P., Nijhawan, D., Budihardjo, I., Srinivasula, S.M., Ahmad, M., Alnemri, E.S., and Wang, X. (1997). Cytochrome c and dATP-dependent formation of Apaf-1/caspase-9 complex initiates an apoptotic protease cascade. *Cell*, **91**:479-489.
- [91] Nicholls, D.G., and Budd, S.L. (2000). Mitochondria and neuronal survival. *Physiol. Rev.*, **80**:315-360.
- [92] Kroemer, G., Dallaporta, B., and Resche-Rigon, M. (1998). The mitochondrial death/life regulator in apoptosis and necrosis. *Annu. Rev. Physiol.*, **60**:619-642.
- [93] Bernardi, P. (1999). Mitochondrial transport of cations: channels, exchangers, and permeability transition. *Physiol. Rev.*, **79**:1127-1155.
- [94] Szewczyk, A., and Wojtczak, L. (2002). Mitochondria as a pharmacological target. *Pharmacol. Rev.*, **54**:101-127.

- [95] Lipton, P. (1999). Ischemic cell death in brain neurons. *Physiol. Rev.*, **79**:1431-1568.
- [96] Norbury, C.J., and Hickson, I.D. (2001). Cellular responses to DNA damage. *Annu. Rev. Pharmacol. Toxicol.*, **41**:367-401.
- [97] Bortner, C.D., and Cidlowski, J.A. (2002). Cellular mechanisms for the repression of apoptosis. *Annu. Rev. Pharmacol. Toxicol.*, **42**:259-281.
- [98] Gottlieb, R.A., and Granville, D.J. (2002). Analyzing mitochondrial changes during apoptosis. *Methods*, **26**:341-347.
- [99] Griffiths, E.J. (2000). Mitochondria--potential role in cell life and death. *Cardiovasc. Res.*, **46**:24-27.
- [100] Bernardi, P., Scorrano, L., Colonna, R., Petronilli, V., and Di Lisa, F. (1999). Mitochondria and cell death. Mechanistic aspects and methodological issues. *Eur. J. Biochem.*, **264**:687-701.
- [101] Scorrano, L., Petronilli, V., Colonna, R., Di Lisa, F., and Bernardi, P. (1999). Chloromethyltetramethylrosamine (Mitotracker Orange) induces the mitochondrial permeability transition and inhibits respiratory complex I. Implications for the mechanism of cytochrome c release. *J. Biol. Chem.*, **274**:24657-24663.
- [102] Jacobs, H.T., and Turnbull, D.M. (2005). Nuclear genes and mitochondrial translation: a new class of genetic disease. *Trends Genet.*, **21**:312-314.
- [103] DiMauro, S. (2004). Mitochondrial diseases. *Biochim. Biophys. Acta*, **1658**:80-88.
- [104] Janssen, R.J., Van Den Heuvel, L.P., and Smeitink, J.A. (2004). Genetic defects in the oxidative phosphorylation (OXPHOS) system. *Expert Rev. Mol. Diagn.*, **4**:143-156.
- [105] Shapiro, H.M. (2001). Optical measurements in cytometry: light scattering, extinction, absorption, and fluorescence. *Methods Cell Biol.*, **63**:107-129.
- [106] Haugland, R.P. (ed.) (2002). *Handbook of Fluorescent Probes and Research Products*. Molecular Probes, Inc., USA, 1-5.
- [107] Morad, M., and Salama, G. (1979). Optical probes of membrane potential in heart muscle. *J. Physiol.*, **292**:267-295.
- [108] Loew, L.M., Tuft, R.A., Carrington, W., and Fay, F.S. (1993). Imaging in five dimensions: time-dependent membrane potentials in individual mitochondria. *Biophys. J.*, **65**:2396-2407.

- [109] Fink, C., Morgan, F., and Loew, L.M. (1998). Intracellular fluorescent probe concentrations by confocal microscopy. *Biophys. J.*, **75**:1648-1658.
- [110] Dykens, J.A., and Stout, A.K. (2001). Assessment of mitochondrial membrane potential in situ using single potentiometric dyes and a novel fluorescence resonance energy transfer technique. *Methods Cell Biol.*, **65**:285-309.
- [111] Rottenberg, H. (1984). Membrane potential and surface potential in mitochondria: uptake and binding of lipophilic cations. *J. Membr. Biol.*, **81**:127-138.
- [112] Vergun, O., Votyakova, T.V., and Reynolds, I.J. (2003). Spontaneous changes in mitochondrial membrane potential in single isolated brain mitochondria. *Biophys. J.*, **85**:3358-3366.
- [113] Duchen, M.R., Leyssens, A., and Crompton, M. (1998). Transient mitochondrial depolarizations reflect focal sarcoplasmic reticular calcium release in single rat cardiomyocytes. *J. Cell Biol.*, **142**:975-988.
- [114] Emaus, R.K., Grunwald, R., and Lemasters, J.J. (1986). Rhodamine 123 as a probe of transmembrane potential in isolated rat-liver mitochondria: spectral and metabolic properties. *Biochim. Biophys. Acta*, **850**:436-448.
- [115] Johnson, L.V., Walsh, M.L., and Chen, L.B. (1980). Localization of mitochondria in living cells with rhodamine 123. *Proc. Natl. Acad. Sci. U S A*, **77**:990-994.
- [116] Smiley, S.T., Reers, M., Mottola-Hartshorn, C., Lin, M., Chen, A., Smith, T.W., Steele, G.D. Jr., and Chen, L.B. (1991). Intracellular heterogeneity in mitochondrial membrane potentials revealed by a J-aggregate-forming lipophilic cation JC-1. *Proc. Natl. Acad. Sci. U S A*, **88**:3671-3675.
- [117] Tomov, T.C. (1986). Pyronin G as a fluorescent probe for quantitative determination of the membrane potential of mitochondria. *J. Biochem. Biophys. Methods*, **13**:29-38.
- [118] MacDonald, R.I. (1990). Characteristics of self-quenching of the fluorescence of lipid-conjugated rhodamine in membranes. *J. Biol. Chem.*, **265**:13533-13539.
- [119] Smith, J.C. (1990). Potential-sensitive molecular probes in membranes of bioenergetic relevance. *Biochim. Biophys. Acta*, **1016**:1-28.
- [120] Zamzami, N., Metivier, D., and Kroemer, G. (2000). Quantitation of mitochondrial transmembrane potential in cells and in isolated mitochondria. *Methods Enzymol.*, **322**:208-213.

- [121] Zamzami, N., Maise, C., Metivier, D., and Kroemer, G. (2001). Measurement of membrane permeability and permeability transition of mitochondria. *Methods Cell Biol.*, **65**:147-158.
- [122] Zamzami, N., and Kroemer, G. (2004). Methods to measure membrane potential and permeability transition in the mitochondria during apoptosis. *Methods Mol. Biol.*, **282**:103-115.
- [123] Shapiro, H.M. (1994). Cell membrane potential analysis. *Methods Cell Biol.*, **41**:121-133.
- [124] Shapiro, H.M. (2000). Membrane potential estimation by flow cytometry. *Methods*, **21**:271-279.
- [125] Sugrue, M.M., and Tatton, W.G. (2001). Mitochondrial membrane potential in aging cells. *Biol. Signals Recept.*, **10**:176-188.
- [126] Chen, L.B. (1988). Mitochondrial membrane potential in living cells. *Annu. Rev. Cell Biol.*, **4**:155-181.
- [127] Fuchs, J., Zimmer, G., and Bereiter-Hahn, J. (1987). A multiparameter analysis of the perfused rat heart: responses to ischemia, uncouplers and drugs. *Cell Biochem. Funct.*, **5**:245-253.
- [128] Fuchs, J., Zimmer, G., Thurich, T., Bereiter-Hahn, J., and Packer, L. (1990). Noninvasive fluorometric measurement of mitochondrial membrane potential in isolated working rat hearts during ischemia and reperfusion. *Methods Enzymol.*, **186**:723-729.
- [129] Scott, D.A., Grotyohann, L.W., Cheung, J.Y., and Scaduto, R.C. Jr. (1994). Ratiometric methodology for NAD(P)H measurement in the perfused rat heart using surface fluorescence. *Am. J. Physiol.*, **267**:H636-644.
- [130] Palmeira, C.M., Moreno, A.J., Madeira, V.M., and Wallace, K.B. (1996). Continuous monitoring of mitochondrial membrane potential in hepatocyte cell suspensions. *J. Pharmacol. Toxicol. Methods*, **35**:35-43.
- [131] Scaduto, R.C. Jr., and Grotyohann, L.W. (1999). Measurement of mitochondrial membrane potential using fluorescent rhodamine derivatives. *Biophys. J.*, **76**:469-477.
- [132] Vergun, O., and Reynolds, I.J. (2004). Fluctuations in mitochondrial membrane potential in single isolated brain mitochondria: modulation by adenine nucleotides and Ca²⁺. *Biophys. J.*, **87**:3585-3593.

- [133] Zhang, H., Huang, H.M., Carson, R.C., Mahmood, J., Thomas, H.M., and Gibson, G.E. (2001). Assessment of membrane potentials of mitochondrial populations in living cells. *Anal. Biochem.*, **298**:170-180.
- [134] Huang, S.G. (2002). Development of a high throughput screening assay for mitochondrial membrane potential in living cells. *J. Biomol. Screen*, **7**:383-389.
- [135] Wong, A., and Cortopassi, G.A. (2002). High-throughput measurement of mitochondrial membrane potential in a neural cell line using a fluorescence plate reader. *Biochem. Biophys. Res. Commun.*, **298**:750-754.
- [136] O'Reilly, C.M., Fogarty, K.E., Drummond, R.M., Tuft, R.A., and Walsh, J.V. Jr. (2003). Quantitative analysis of spontaneous mitochondrial depolarizations. *Biophys. J.*, **85**:3350-3357.
- [137] Nakayama, S., Sakuyama, T., Mitaku, S., and Ohta, Y. (2002). Fluorescence imaging of metabolic responses in single mitochondria. *Biochem. Biophys. Res. Commun.*, **290**:23-28.
- [138] Ehrenberg, B., Montana, V., Wei, M.D., Wuskell, J.P., and Loew, L.M. (1988). Membrane potential can be determined in individual cells from the nernstian distribution of cationic dyes. *Biophys. J.*, **53**:785-94.
- [139] Davis, S., Weiss, M.J., Wong, J.R., Lampidis, T.J., and Chen, L.B. (1985). Mitochondrial and plasma membrane potentials cause unusual accumulation and retention of rhodamine 123 by human breast adenocarcinoma-derived MCF-7 cells. *J. Biol. Chem.*, **260**:13844-13850.
- [140] Nicholls, D.G., and Budd, S.L. (2000). Mitochondria and neuronal survival. *Physiol. Rev.*, **80**:315-360.
- [141] Nicholls, D.G., and Ward, M.W. (2000). Mitochondrial membrane potential and neuronal glutamate excitotoxicity: mortality and millivolts. *Trends Neurosci.*, **23**:166-174.
- [142] Huser, J., Rechenmacher, C.E., and Blatter, L.A. (1998). Imaging the permeability pore transition in single mitochondria. *Biophys. J.*, **74**:2129-2137.
- [143] Bunting, J.R., Phan, T.V., Kamali, E., and Dowben, R.M. (1989). Fluorescent cationic probes of mitochondria. Metrics and mechanism of interaction. *Biophys. J.*, **56**:979-93.
- [144] Toescu, E.C., and Verkhatsky, A. (2000). Assessment of mitochondrial polarization status in living cells based on analysis of the spatial heterogeneity of rhodamine 123 fluorescence staining. *Pflugers Arch.*, **440**:941-947.

- [145] Reers, M., Smiley S.T., Mottola-Hartshorn, C., Chen, A., Lin, M., and Chen, L.B. (1995). Mitochondrial membrane potential monitored by JC-1 dye. *Methods Enzymol.*, **260**:406-417.
- [146] Scanlon, J.M., and Reynolds, I.J. (1998). Effects of oxidants and glutamate receptor activation on mitochondrial membrane potential in rat forebrain neurons. *J. Neurochem.*, **71**:2392-2400.
- [147] Salvioli, S., Ardizzoni, A., Franceschi, C., and Cossarizza, A. (1997). JC-1, but not DiOC6(3) or rhodamine 123, is a reliable fluorescent probe to assess delta psi changes in intact cells: implications for studies on mitochondrial functionality during apoptosis. *FEBS Lett.*, **411**:77-82.
- [148] Kauppinen, R.A., and Hassinen, I.E. (1984). Monitoring of mitochondrial membrane potential in isolated perfused rat heart. *Am. J. Physiol.*, **247**:H508-16.
- [149] Akerman, K.E., and Jarvisalo, J.O. (1980). Effects of ionophores and metabolic inhibitors on the mitochondrial membrane potential within isolated hepatocytes as measured with the safranine method. *Biochem. J.*, **192**:183-90.
- [150] Zanotti, A., and Azzone, G.F. (1980). Safranine as membrane potential probe in rat liver mitochondria. *Arch. Biochem. Biophys.*, **201**:255-265.
- [151] Akerman, K.E., and Saris, N.E. (1976). Stacking of safranine in liposomes during valinomycin-induced efflux of potassium ions. *Biochim. Biophys. Acta*, **426**:624-629.
- [152] Bereiter-Hahn, J. (1976). Dimethylaminostyrylmethylpyridiniumiodine (daspmi) as a fluorescent probe for mitochondria in situ. *Biochim. Biophys. Acta*, **423**:1-14.
- [153] Mai, M.S., and Allison, W.S. (1983). Inhibition of an oligomycin-sensitive ATPase by cationic dyes, some of which are atypical uncouplers of intact mitochondria. *Arch. Biochem. Biophys.*, **221**:467-476.
- [154] Haugland, R.P. (ed.) (2002). *Handbook of Fluorescent Probes and Research Products*. Molecular Probes, Inc., USA, 473-488.
- [155] Abugo, O.O., Nair, R., and Lakowicz, J.R. (2000). Fluorescence properties of rhodamine 800 in whole blood and plasma. *Anal. Biochem.*, **279**:142-150.
- [156] Gryczynski, Z., Abugo, O.O., and Lakowicz, J.R. (1999). Polarization sensing of fluorophores in tissues for drug compliance monitoring. *Anal. Biochem.*, **273**:204-211.
- [157] Shapiro, H.M., and Stephens, S. (1986). Flow cytometry of DNA content using oxazine 750 or related laser dyes with 633nm excitation. *Cytometry*, **7**:107-110.

- [158] Sakanoue, J., Ichikawa, K., Nomura, Y., and Tamura, M. (1997). Rhodamine 800 as a probe of energization of cells and tissues in the near-infrared region: a study with isolated rat liver mitochondria and hepatocytes. *J. Biochem.*, **121**:29-37.
- [159] Rossi, E., and Azzone, G.F. (1968). Ion transport in liver mitochondria. IV. The relationship between ion translocation and electron transport. *J. Biol. Chem.*, **243**:1514-1522.
- [160] Jilkina, O., Kong, H.J., Hwi, L., Kuzio, B., Xiang, B., Manley, D., Jackson, M., and Kupriyanov, V.V. (2006). Interaction of a mitochondrial membrane potential-sensitive dye, rhodamine 800, with rat mitochondria, cells, and perfused hearts. *J. Biomed. Opt.*, **11**:14009.
- [161] Sordahl, L.A., Johnson, C., Bladilock, Z.R., and Schwartz, A. (1971). The mitochondrion In: A. Schwartz (ed) *Methods in Pharmacol.*, V. 1, Appleton-Centruy-Crofts, Educational Division, Meredith Corporation, New York, 247-286.
- [162] Thum, T., and Borlak, J. (2001). Butanedione monoxime increases the viability and yield of adult cardiomyocytes in primary cultures. *Cardiovasc. Toxicol.*, **1**:61-72.
- [163] Viko, H., Osnes, J.B., Sjetnan, A.E., and Skomedal, J. (1995). Improved isolation of cardiomyocytes by trypsination in addition to collagenase treatment. *Pharmacol. Toxicol.*, **76**:68-71.
- [164] Woodcock, E.A., and Lambert, K.A. (1997). Acute effects of cell isolation on InsP profiles in adult rat cardiomyocytes. *J. Mol. Cell Cardiol.*, **29**:3275-3283.
- [165] Seglen, P.O. (1976). Preparation of isolated rat liver cells. *Methods in Cell Biology*, **13**:29-83.
- [166] Aiken, J., Cima, L., Schloo, B., Mooney, D., Johnson, L., Lange, R., and Vacanti, J. P. (1990). Studies in rat liver perfusion for optimal harvest of hepatocytes. *J. Pediatric. Surgery*, **25**:140-145.
- [167] Berry, M. N., and Friend, D. S. (1969). High-yield preparation of isolated rat liver parenchymal cells: a biochemical and fine structural study. *J. Cell Biology*, **43**:506-520.